MOLECULAR INTERACTION ANALYSES OF SELECTED DRUGS AS DENGUE VIRUS TYPE-2 PROTEASE INHIBITORS

RUFAIDAH BINTI OTHMAN

FACULTY OF SCIENCE
UNIVERSITY OF MALAYA
KUALA LUMPUR

2017

MOLECULAR INTERACTION ANALYSES OF SELECTED DRUGS AS DENGUE VIRUS TYPE-2 PROTEASE INHIBITORS

RUFAIDAH BINTI OTHMAN

DISSERTATION SUBMITTED IN FULFILMENT OF THE REQUIREMENTS FOR THE DEGREE OF MASTER OF SCIENCE

INSTITUTE OF BIOLOGICAL SCIENCES
FACULTY OF SCIENCE
UNIVERSITY OF MALAYA
KUALA LUMPUR

2017

UNIVERSITY OF MALAYA

ORIGINAL LITERARY WORK DECLARATION

Name of Candidate: **Rufaidah Binti Othman** [redacted]

120012

Name of Degree: **Master of Science**

Title of Dissertation ("this Work"): **Molecular Interaction Analyses of Selected Drugs as Dengue Virus Type-2 Protease Inhibitors**

Field of Study: **Biochemistry**

I do solemnly and sincerely declare that:

(1) I am the sole author/writer of this Work;
(2) This Work is original;
(3) Any use of any work in which copyright exists was done by way of fair dealing and for permitted purposes and any excerpt or extract from, or reference to or reproduction of any copyright work has been disclosed expressly and sufficiently and the title of the Work and its authorship have been acknowledged in this Work;
(4) I do not have any actual knowledge nor do I ought reasonably to know that the making of this work constitutes an infringement of any copyright work;
(5) I hereby assign all and every rights in the copyright to this Work to the University of Malaya ("UM"), who henceforth shall be owner of the copyright in this Work and that any reproduction or use in any form or by any means whatsoever is prohibited without the written consent of UM having been first had and obtained;
(6) I am fully aware that if in the course of making this Work I have infringed any copyright whether intentionally or otherwise, I may be subject to legal action or any other action as may be determined by UM.

Candidate's Signature Date:

Subscribed and solemnly declared before,

Witness's Signature Date:

Name:

Designation:

ABSTRACT

Dengue is a disease that is endemic to the tropical and subtropical regions of the world. It is a potentially deadly disease with no available effective drug. Thus, it is becoming increasingly important to develop therapeutics/drugs to combat the dengue virus. Compounds able to inhibit the NS2B-NS3 DENV-2 protease (NS2B-NS3pro) have potential anti-dengue activity. As such, we investigated several compounds that have previously been shown to inhibit the NS2B-NS3 protease of the dengue virus-2 (DENV-2). These compounds are antibiotic derivatives: doxycycline and rolitetracycline, and a non-steroidal anti-inflammatory drug (NSAID) - meclofenamic acid. Our focus was on the interaction between these compounds and NS2B-NS3pro where better interaction would suggest better inhibitory action. We used a combination of surface plasmon resonance (SPR) technology (Biacore 3000) and molecular docking simulations (Autodock 4.2.6). To the best of our knowledge, there are no studies investigating the molecular interactions of these inhibitors using a combination of these two approaches. In the initial part of the study, NS2B-NS3pro was expressed, and purified (to >90% purity) using Ni-IMAC and size exclusion chromatography (SEC). The protease complex was then bound to an NTA chip and interaction studies were performed. The resulting sensorgrams showed high reproducibility based on the overlaid replicates. However, the sensorgrams were not a fit to the 1:1 Langmuir model. The association phase showed significant deviation from pseudo-first order kinetic behavior. An attempt to fit to the heterogenous ligand-parallel reaction models was also unsuccessful. The Chi^2 values were relatively optimal for doxycycline and meclofenamic acid (<10 RU), however, for rolitetracycline the values were beyond the limit value (>10 RU). Nevertheless, the residual values for all compounds were more than the optimal level of ± 2 RU. An *in silico* molecular docking approach was then performed. The results predicted that doxycycline to posses the highest binding affinity

to the protease complex based on its binding energy of -5.15 kcal/mol followed by meclofenamic acid -3.64 kcal/mol and rolitetracycline -3.21 kcal/mol. It also suggested that doxycycline binds via a specific allosteric site involving interaction with Lys74, suggesting that it was a non-competitive inhibitor. On the other hand, meclofenamic acid and rolitetracycline was predicted to have a direct interaction with His51 and Ser135, suggesting that they were competitive inhibitors. In conclusion, this study has demonstrated the use of SPR and in silico approaches to study the potential interactions between drugs and its potential targets. The information obtained may eventually be used in the development of anti-dengue therapeutics.

ABSTRAK

Denggi adalah suatu penyakit yang endemik di kawasan tropika dan subtropika. Ia adalah sejenis penyakit yang boleh membawa maut dan sehingga kini tiada sebarang ubat yang berkesan untuk merawat penyakit tersebut. Oleh itu, penghasilan ubat terapeutik/dadah adalah amat penting dalam usaha untuk menangani denggi. Sebatian yang dapat menghalang aktiviti NS2B-NS3 DENV-2 protease (NS2B-NS3pro) mempunyai potensi yang tinggi sebagai sebatian anti-denggi. Justeru itu, beberapa penyelidikan telah dijalankan terhadap segelintir sebatian yang mempunyai potensi untuk merencat NS2B-NS3 protease dari denggi virus-2 (DENV-2). Sebatian yang dikaji adalah terdiri dari derivatif antibiotik: doxycycline dan rolitetracycline serta dadah anti-radang bukan steroid (NSAID) - asid meclofenamic. Tumpuan kami adalah untuk mengkaji interaksi antara ketiga-tiga sebatian tersebut, di mana lebih baik interaksi dengan NS2B-NS3pro menunjukkan aktiviti perencatan yang lebih baik. Untuk mencapai objektif ini, kami telah menggunakan kombinasi teknologi "surface plasmon resonance" (SPR) (Biacore 3000) dan simulasi doking molekul (Autodock 4.2.6). Sepanjang pengetahuan kami, tidak terdapat lagi kajian interaksi pada tahap molekular yang dijalankan terhadap molekul perencat tersebut yang mana gabungan kedua-dua kaedah seperti yang dinyatakan digunakan. Pada peringkat awal kajian, NS2B-NS3pro telah diekspres dan ditulinkan (kepada >90% ketulinan) menggunakan kolum Ni-IMAC dan kromatografi pengecualian saiz (SEC). Kompleks protease tersebut kemudiannya 'dilekatkan' pada permukaan cip NTA bagi membolehkan kajian interaksi dijalankan. Rajah sensorgram yang terhasil menunjukkan kebolehulangan yang tinggi berdasarkan corak replikasi yang bertindih. Walau bagaimanapun, sensorgram-sensorgram tersebut menunjukkan ketidaksesuaian terhadap model 1:1 Langmuir. Fasa assosiasi menunjukkan penyimpangan ketara daripada sistem kinetik pseudo-pertama. Cubaan untuk dimuatkan kepada model ligan heterogenus-reaksi selari

juga tidak berjaya dilakukan. Secara relatifnya, nilai Chi^2 adalah optimum untuk doxycycline dan asid meclofenamic (<10 RU), walaubagaimanapun, nilainya adalah di luar nilai had (> 10 RU) bagi rolitetracycline. Meskipun demikian, nilai residual untuk ketiga-tiga sebatian adalah melebihi dari tahap optimum, ± 2 RU. Pendekatan secara *in silico* kemudiannya dilakukan, di mana doxycycline diramalkan memiliki interaksi yang paling kuat terhadap kompleks protease tersebut berdasarkan pada nilai tenaga ikatan, -5.15 kcal/mol. Ini diikuti dengan asid meclofenamic -3.64 kcal/mol dan rolitetracycline -3.21 kcal/mol. Kajian ini juga meramalkan bahawa doxycycline mempunyai interaksi di dalam kawasan alosterik yang melibatkan Lys74, dan secara langsung menunjukkan bahawa ianya adalah perencat yang tidak kompetitif. Sebaliknya, asid meclofenamic dan rolitetracycline diramalkan mempunyai interaksi secara langsung dengan His51 dan Ser135, yang menunjukkan bahawa kedua-dua sebatian tersebut bertindak sebagai perencat kompetitif. Kesimpulannya, kajian ini dapat memberi penjelasan terhadap penggunaan kaedah SPR dan *in silico* dalam mengkaji potensi interaksi antara ubat-ubatan dan sasaran potensinya. Maklumat yang diperoleh juga boleh digunakan dalam usaha untuk perkembangan dan penghasilan anti-denggi secara terapeutik.

ACKNOWLEDGEMENT

First and foremost, I would like to share my deepest gratitude to Prof. Datuk Dr. Rohana Yusof that has given me the opportunity to work with her and utilize all the facilities and equipments provided in the laboratory of Molecular Biology. A heartfelt appreciation goes to Assoc. Prof. Dr. Saiful Anuar Karsani that has always been given me ideas and thoughtful support throughout the wonder years working with him. To Prof. Dr. Noorsaadah Abd. Rahman, it is such a huge privilege to be able to collaborate with her and to gain new ideas and support. To the dearest Dr. Rozana Othman, I thank her for her great advice and support in the docking work. Her involvement has given a huge impact towards the success of this master project. My deepest appreciation also goes to Dr. R. Nagasundara Ramanan (Monash University), who has been very dedicated and determine to share and guide me on the theoretical and practical parts of SPR assay, and to Dr. Aida Baharuddin, a great post-doc which has always been my backbone and given me encouragement and advice.

To the most important individuals in my life, my beloved parents, Hjh. Jamilah and Hj. Othman. This master project is dedicated to them for their moral support, financial contribution, patience, doa' and prayers. I would also like to thank Episentec (Sweden); for their thorough insights into the SPR assay, to all my brothers and sisters that have been providing me constant support; emotionally and financially. To the DDDRG (Drug Design and Development Research Group) members, dearest friends and lab mates of the Dep. of Molecular Medicine, thank you for being there when help was needed. And thank you to Allah S.W.T for bestowing me the strength to complete this project.

Alhamdulillah. Jazakumullah khairan.

TABLE OF CONTENTS

LIST OF FIGURES

LIST OF TABLES

LIST OF ABBREVIATIONS

2D	Two-dimensional structure
3D	Three-dimensional structure
~	Approximately
Ø	Diameter
% v/v	Percent by volume of solute in the total volume of solution
% w/v	Percent by weight of solute in the total volume of solution
% w/w	Percent by weight of solute in the total weight of solution
β	Beta
µl	Microliter
µM	Micromolar
µM	Microgram
AbsResp	Absolute response
ACN	Acetonitrile
ADE	Antibody-dependent enhancement
Ala	Alanine
Arg	Arginine
APS	Ammonium persulfate
Asp75	Aspartic acid at position number 75 from the N-terminal
Au	Absorbance unit
bp	Base pair
BSA	Bovine serum albumin
C	Capsid protein
CA	Cellulose acetate
CBB R-250	Coomassie brilliant blue R-250
Chi^2	Chi-square

CM	Carboxymethyl
COOH	Carboxyl group
Cryo-EM	Cryo-electron microscopy
CV	Column volume
DENV	Dengue virus
dH_2O	Distilled water
DHF	Dengue hemorrhagic fever
DMSO	Dimethyl sulfoxide
DNA	Deoxyribonucleic acid
dsRNA	Double-stranded RNA
DSS	Dengue shock syndrome
DTT	Dithiothreitol
E	Envelope protein
E_{bind}	Free binding energy
EC_{50}	Half maximal effective concentration
E.coli	Escherichia coli
EDC	1-ethyl-3-(3-dimethylamino-propyl)carbodiimide hydrochloride
EDTA	Ethylenediaminetetraacetic acid
ER	Endoplasmic reticulum
FA	Formic acid
Fc	Flow cell
g	Gram
Gln	Glutamine
Gly	Glycine
HBA	Hydrogen bond acceptors
HBS	Hydrogen bond donors

HBS-EP	HEPES buffered saline with EDTA and surfactant
HBS-P	HEPES buffered saline with surfactant
HCl	Hydrochloric acid
HEPES	4-(2-hydroxyethyl)-1-piperazineethanesulfonic acid
HIC	Hydrophobic interaction chromatography
His51	Histidine at position number 51 from the N-terminal
IAA	Iodoacetamide
IC_{50}	Half maximal inhibitory concentration
IEC	Ion exchange chromatography
IFC	Integrated μ-fluidic cartridge
IPTG	Isopropyl-β-D-thiogalactopyranoside
k_a	Association rate constant
K_A	Equilibrium association constant
K_d	Dissociation rate constant
k_D	Equilibrium dissociation constant
kDa	Kilodalton
K_i	Equilibrium inhibitor dissociation constant
K_{obs}	Observed (fitted) association rate constant
L	Litre
LAV	Live attenuated virus
LB medium	Luria-bertani medium
Lys	Lysine
M	Molar
M	Membrane protein
mA	Miliampere
MD	Molecular dynamics

mg	Miligram
ml	Mililitre
mM	Milimolar
mRNA	Messenger ribonucleic acid
MS	Mass spectrometry
MW	Molecular weight
MWCO	Molecular weight cut off
NaCl	Sodium chloride
NaEDTA	Disodium ethylenediaminetetraacetic acid
NaOH	Sodium hydroxide
ng	Nanogram
NH_4HCO_3	Ammoum bicarbonate
NHS	N-hydroxysuccinimide
Ni	Nickel
$NiCl_2$	Nickel chloride
Ni-IMAC	Nickel-immobilized metal affinity chromatography
Ni-NTA	Nickel-nitrilotriacetic acid
nM	Nanomolar
NMR	Nuclear magnetic resonance
NS	Nonstructural
NS2B-NS3pro	NS2B-NS3 protease complex
NS3pro	NS3 protease
NTA	Nitrilotriacetic acid
OD	Optical density
ORF	Open reading frame
P	Amino acid residue from substrate

PAGE	Polyacrylamide gel electrophoresis
PBS	Phosphate buffer saline
pg	Prep grade
pI	Isoeletric point
PIV	Purified inactivated virus
prM	Pre-membrane protein
prM-E	Premembrane-heterodimeric complex
QSAR	Quantitative structure activity relationships
RelResp	Relative response
RI	Refractive index
RNA	Ribonucleic acid
rpm	Revolutions per minute
RU	Resonance unit
S	Subsites from active site of protein
SDS	Sodium dodecyl sulfate
SDS-PAGE	Sodium dodecyl sulfate–polyacrylamide gel electrophoresis
SEC	Size exclusion chromatography
Ser135	Serine at position number 135 from the N-terminal
siRNA	Small interfering RNA
SPR	Surface plasmon resonance
sRNA	Single-stranded RNA
TBE	Tris-Borate-EDTA
TBS	Tris buffered saline
TBST	Tris buffered saline with Tween 20
TEMED	N,N,N’,N’-tetramethylethyldiamine
TGN	Trans-golgi network

UV	Ultraviolet light
V	Voltage
VDW	Van der Waals
V_e	Elution volume
VLP	Virus-like particle
V_o	Void volume
WHO	World Health Organization
YFV	Yellow fever virus

LIST OF APPENDICES

CHAPTER 1: INTRODUCTION

1.1 General introduction

Dengue (DEN) is a neglected and most significant arboviral disease in the 21st century that mainly infected the tropical and sub-tropical countries. This diesease is a potentially deadly disease as it can cause life threatening dengue hemorrhagic fever (DHF) or dengue shock syndrome (DSS) especially in children. This has led dengue to be categorized as a "category A" priority bio threat pathogen by the US National Institute of Allergy and Infectious Diseases. Approximately 4 billion people worldwide are at risk and this status is exacerbated, as there are no antiviral drugs to treat DEN infections (Brady *et al*., 2012). The aggressive spreading and distribution of infection brought by the dengue virus (DENV) have caused the entire world as a whole to be more precautious before this infection kills more people and not being able to treat it. There are four DEN serotypes and dengue virus type-2 (DENV-2) is the most prevalent type (Roberts *et al*., 2013). The nonstructural protein of DENV-2; the NS2B-NS3 protease complex (NS2B-NS3pro), is responsible for proteolytic processing of the DENV polyprotein. It is currently one of the prime targets for rational drug design as it affects the dengue viral replication (Chernov *et al*., 2008).

Several small molecule antibiotics have been shown to inhibit DEN viruses *in vitro* (Kaptein *et al*., 2010; Low *et al*., 2011; Rothan *et al*., 2014a; Zhang *et al*., 2009). These include antibiotics such as doxycycline and rolitetracycline that are proven to show inhibitory effect against NS2B-NS3pro of DENV-2 or also termed as the DENV-2 NS2B-NS3pro (Rothan *et al*., 2013; Rothan *et al*., 2014b). Recently, a study has showed that Non-Steroidal Anti-Inflammatory drugs (NSAIDs) are used not only to treat symptoms of dengue infections (Kumar *et al*., 2015), but also to inhibit the protease complex. Relating to this issue, an NSAID namely meclofenamic acid has

recently been shown to inhibit DENV-2 NS2B-NS3pro (Rothan *et al*., 2013).

Therefore, these protease inhibitors; doxycycline, meclofenamic acid and rolitetracycline were further used in this study to explore its kinetics, affinities and mechanisms as potential drug targets against the DENV-2 NS2B-NS3pro. An optical biosensor based study using Surface Plasmon Resonance (SPR) was implemented to investigate the binding interaction of the small molecule medicinal drugs and the DENV-2 NS2B-NS3pro in hope to determine the association and dissociation rate constants separately. A complementary analysis using the computational (*in silico*) molecular docking was performed to predict the binding sites, the specific residues, type of bonding interactions and binding energy involved.

In general, most kinetic studies are only able to measure the equilibrium constant (the affinity; how strong the binding interaction), which is the quotient of the association and dissociation rate constants (the kinetic; how fast the binding interaction). Relying solely only on equilibrium constant is not advisable since the same equilibrium constants may constitute of a different value of association and dissociation rate constants (GE Healthcare, 2012). Therefore, we chose SPR assay using the Biacore 3000 system in hope to generate these two rate constants. Biacore 3000 is one of the highly sensitive SPR biosensor tools that monitor binding interaction in real time. It requires no label such as fluorescent or radiolabeling. It is also an efficient tool for fast screening of active lead compounds, allows simultaneous binding analysis with multiple compounds, requires short time screening and deceptively easy to generate kinetic data compared to other label-free technologies such as Isothermal titration calorimetry (ITC). Additionally, SPR biosensor such as Biacore 3000 offers a cost effective assay in terms of less compound and protein sample consumption (Navratilova

& Hopkins, 2011; Tanious *et al*., 2008). In this study, SPR assay involved the immobilization of NS2B-NS3pro (the ligand) to both CM5 and NTA chips. The small molecule compounds (the analyte) is injected onto NS2B-NS3pro to measure the binding rate constants trough the assessment of binding affinity and kinetic analysis.

On the other hand, molecular docking is a computational tool that is complementary to the SPR assay, in that it goes into the structure and function of biomolecules. Molecular docking is a common tool used in structure-based rational drug design and also the development of drug candidates that advanced to clinical trials (Rudnitskaya *et al*., 2010). In this study, molecular docking was used to evaluate the complex formation of small molecule compounds with biomolecule, finding the best geometrical arrangements and predicts the efficacy of binding by calculating the strength of the bonding forces (Rudnitskaya *et al*., 2010). The docking process involved the simulation of NS2B-NS3pro that acts as the target macromolecule or the receptor to the small molecule compounds (which unlike in SPR assay are termed as ligands). NS2B-NS3pro and its ligands were modeled based on the three-dimensional (3D) structures and superimposed until a fit is developed between the key sites of the target molecule. By using a program that adopts molecular mechanical calculations such as Autodock 4.2.6, this program could predict the efficacy of interaction can be predicted by calculating the binding energy between NS2B-NS3pro and the ligands (Raschka, 2014). It is hoped that the combination of SPR assay and the computational study using molecular docking will provide insights into the binding mechanism that is involved in creating the compounds' inhibitory effects against the DENV-2 NS2B-NS3pro.

1.2 Problem statements

The threatening and the fatality that a dengue infection imposes causes a huge siren to the global population that this disease must be treated fast as it has been an epidemic since 1779 (Heilman *et al*., 2014). A few clinical trials have been tested over the last 50 years with minimal success. Several preventive and therapeutic measures have been explored, and numerous antiviral studies have shown that NS2B-NS3pro is an interesting site for viral inhibition as it plays a significant role in the DENV-2 replication (Oliveira *et al*., 2014; Sampath & Padmanabhan, 2009). Hence, we are focusing on finding therapeutic action against DENV-2 NS2B-NS3pro implying three types of medicinal drugs (doxycycline, rolitetracycline and meclofenamic acid).

To our knowledge, there have been no studies using SPR technique investigated on these three drugs that could provide kinetic analysis on biomolecular interactions in real time and label-free. With SPR study using Biacore 3000, we attempt to find the kinetic constants (association and dissociation rate constant), which can be determined separately, exceeding the standard steady-state kinetic analysis (Hahnefeld *et al*., 2004). Nearly three decades after its creation in 1984 in Sweden (Gopinath, 2010), SPR studies started to develop in Malaysia and begin its earliest publications emphasizing on the detection of mercury and sugar content (Abdi *et al*., 2011; Yusmawati *et al*., 2007). More studies are being developed focusing on the immobilization, regeneration and concentration analyses, instrumentation application and the development of sensor surface (Fen & Yunus, 2011; Honari *et al*., 2011; Kqueen & Son, 2010; Ramanan *et al*., 2010; Sadrolhosseini *et al*., 2012). In 2013, a kinetic study of the antigen-antibody interaction was reported using the CM5 chip. Opposite to this finding, our study focuses on the kinetic analysis of small molecule compound-protein interaction using NTA chip. Looking at the history of Biacore development, it shows that kinetic analysis

using Biacore SPR technology is still relatively new in Malaysia.

On the other hand, computational docking is a well-known method to study the various properties associated with small molecule-protein interactions. Although docking studies on doxycycline and rolitetracycline have been reported, the interaction analysis involved docking to the envelope (E) protein and not to the NS2B-NS3pro of DENV2 (Yang *et al*., 2007). Furthermore, to date, no related computational docking studies have been found for meclofenamic acid. Thus, in this study, we are focusing on exploring the molecular interaction highlighting on the kinetic analysis *in vitro* (SPR assay) combined with *in silico* docking to identify the binding site of NS2B-NS3pro to where the small molecule binds and the identification of its energetically most favorable binding pose.

1.3 Aims and objectives

The aims of the present study are to determine the kinetic binding of compounds with the DENV-2 NS2B-NS3pro using SPR method and its mechanism of interaction with computational (*in silico*) molecular docking. The objectives of the this study are:

i. To express, purify and characterize the DENV-2 NS2B-NS3pro
ii. To optimize parameters involving binding interaction between compounds and the DENV-2 NS2B-NS3pro using SPR assay
iii. To determine the compound's kinetic rate constants towards the DENV-2 NS2B-NS3pro using SPR assay
iv. To interpret and analyze the conformations and binding energy and interactions between compounds and the DENV-2 NS2B-NS3pro using *in silico* molecular docking

CHAPTER 2 : LITERATURE REVIEW

2.1 Dengue

2.1.1 Dengue disease

Dengue is a viral infection caused by the dengue virus (DENV), a single stranded RNA virus classified under the *Flaviviridae* family (Sukupolvi-Petty *et al*., 2007; Sun & Kochel, 2013). DENV is transmitted by the bite of an infected female Aedes mosquito, principally *Aedes aegypti* (Bhatt *et al*., 2013; Kyle & Harris, 2008). It is the world's most rapidly spreading mosquito-borne viral disease, and has been classified in the Guinness World records of 2002 as the world's most epidemiologically and geographically prevalent arboviral disease (Halstead, 2005). There are four antigenically distinct DENV (DENV-1 to -4), but each DENV serotype share approximately 65% similarity in genetic organization (Mustafa *et al*., 2015; Roberts *et al*., 2013). In 2013, a new serotype of DENV-5 was discovered. The viral sample was originated from a patient living in Sarawak, Malaysia. Like the other four serotypes, DENV-5 is not transmitted through the human cycle, but instead it follows the sylvatic cycle that affects only wild animals. However, despite the occurrence of the new DENV-5, DENV-2 is still classified as the world's most infectious serotype that causes severe illness throughout the world population (American Association for the Advancement of Science, 2015; Panhuis *et al*., 2010).

2.1.2 Epidemiology of dengue

Dengue is transmitted in more than 100 tropical and subtropical countries such as America, Africa, Western Pacific and the South-East Asia. There are approximately 390 million DEN infections annually with 96 million that are clinically manifested (Brady *et al*., 2012). Epidemics of dengue fever were first reported in 1779-1780 in Asia, Africa, and North America. And dengue has become a global problem since the Second World

War, with dramatic increment of dengue fever cases since 1960 (Heilman *et al*., 2014).

The Western Pacific and SEA regions have attributed to 75% of the global dengue disease. Cases of dengue are reported to increase continuously along with the severity of the case, which is 18 times higher than in the Americas. In America, despite the absence of dengue transmission in the middle of the 20th century, almost all of its countries are now manifesting hyperendemicity. Meanwhile, in Africa, all four DENV serotypes have been seen, with DENV-2 to be the cause of most epidemics. Since the last incident during 1926 to 1928, there was no report on dengue transmission in Europe, until in the 1990s, where *A. albopictus* became established due to increasing global trade of used tires. Back in 1994, Pakistan was the first country to have Dengue hemorrhagic fever (DHF) outbreak, and since then the expansion of dengue infections with increasing severity has been reported for other countries in the Eastern Mediterranean (Murray *et al*., 2013). Figure 2.1 shows the world distribution of dengue-transmitted countries.

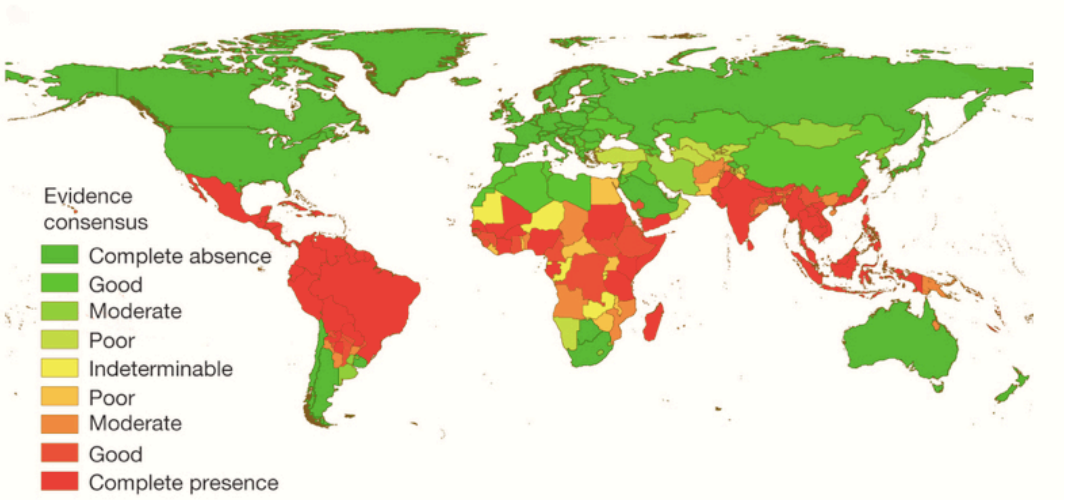

Figure 2.1: Evidence-based global consensus on distribution of dengue. Country highlighted with red representing a complete consensus on the presence of dengue, and green; a complete consensus on the absence of dengue (Brady *et al*., 2012).

2.1.3 Symptoms of dengue infection

Illnesses caused by DENV infection include undifferentiated fever, dengue fever, dengue hemorrhagic fever (DHF), and dengue shock syndrome (DSS). Dengue fever, also known as '*break bone fever*', is an acute febrile with two or more symptoms of body aches, joint pains, retro-orbital pain, frontal headache, weakness, nausea, vomiting, or rash. Dengue fever develops 4-10 days after being infected by the DENV**.** DHF is manifested by persistent high fever, hemorrhagic tendency, thrombocytopaenia and plasma leakage. DSS is defined by all the criteria demonstrated for DHF with the addition of circulatory failure. Figure 2.2 shows the classification of symptomatic dengue infection according to WHO guidelines. Dengue fever constitutes mostly 95 % of cases, while DHF and DSS cause 5% of cases. Recovery from the first type of infection provides lifelong immunity. However, it affords only half protection from subsequent viral infection that ultimately results in the risk of DHF (Kadir *et al*., 2013; Sun & Kochel, 2013; World Health Organization, 2005).

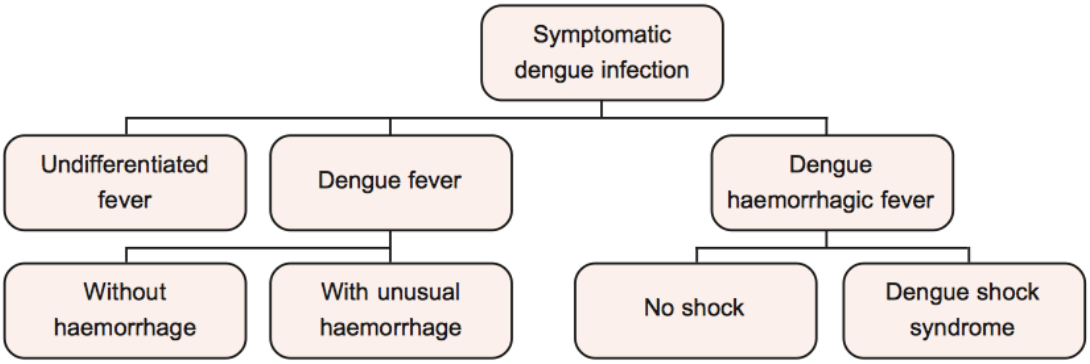

Figure 2.2: The WHO classifications for symptomatic dengue infection (World Health Organization, 2005).

2.1.4 The DENV structure and its polyprotein

The DENV is spherical in shape and has a diameter of approximately 500 Å. The surface is relatively smooth and inside the virus is the nucleocapsid, which contains the positive single-stranded genomic RNA. The envelope is a glycoprotein-embedded lipid bilayer that surrounds the nucleocapsid (Kuhn *et al*., 2002). Figure 2.3 shows the cryo-electron microscopy (cryo-EM) of a DENV undergoing the maturation process.

The DENV possess single positive-sense RNA genome of approximately ~11kb. The RNA encodes single open reading frame (ORF) with a gene order of 5′-C-prM-E-NS1-NS2A-NS2B-NS3-NS4A-NS4B-NS5-3′, which is translated as a single polyprotein (Gruenberg & Wright, 1992; Kapoor *et al*., 1995; Leung *et al*., 2001). Figure 2.4 illustrates the schematic diagram of the DENV polyprotein and the individual function of each protein. There are three structural proteins namely as capsid (C), membrane (M), and envelope (E), and seven nonstructural (NS) proteins (NS1, NS2A, NS2B, NS3, NS4A, NS4B, and NS5) (Chiu *et al*., 2007). Gene expression achieved by a combination of activities from the host proteases and the cytoplasmic viral protease complex, which involves both co- and post-translational proteolytic processing of the large polyprotein precursor. The host signal peptidase in the lumen of the endoplasmic reticulum (ER) is essential in cleaving to generate the amino termini of prM, E, NS1, and NS4B. Whereas the NS2B-NS3 protease complex (NS2B-NS3pro) of the DENV involves the processing of most of the other NS proteins and the COOH terminus of the C protein that takes place in the cytoplasm of the host (Chiu *et al*., 2007; Miller *et al*., 2006).

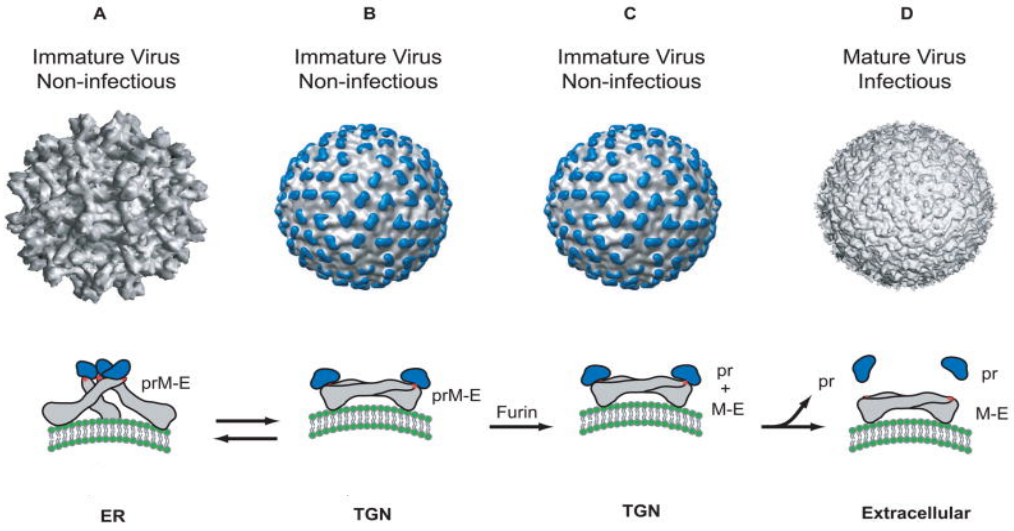

Figure 2.3: The maturation process of the DENV; an electron cryomicroscopy structure of the DENV and the conformations of E protein. **(A)** A 'spiky' immature DENV with the prM-E heterodimer extends as trimeric spikes. This immature virus is the initial phase that enters the endoplasmic reticulum (ER) of the host cell. Below the virus is the conformation of the E protein (gray) and the 'pr' peptide (blue), protecting the fusion peptide (red star) on E protein. **(B)** The immature DENV is undergoing a transition phase in the Trans-Golgi Network (TGN) where the prM-E heterodimers dissociate and form dimers that lie flat forming a 'smooth' surface. **(C)** While in the TGN, the host endoprotease known as furin cleaved the prM protein into the individual 'pr' peptide and M protein. But the cleaved 'pr' peptide still maintains its position as a 'cap' on E and the E proteins remain as homodimers lying parallel to the virion surface. The M protein (not shown in this figure) lies embedded in the viral membrane beneath the E protein. **(D)** The mature virion will be secreted into the extracellular site, and the 'pr' peptide is released from the mature particle, while M protein remains as a transmembrane protein (Perera & Kuhn, 2008)**.**

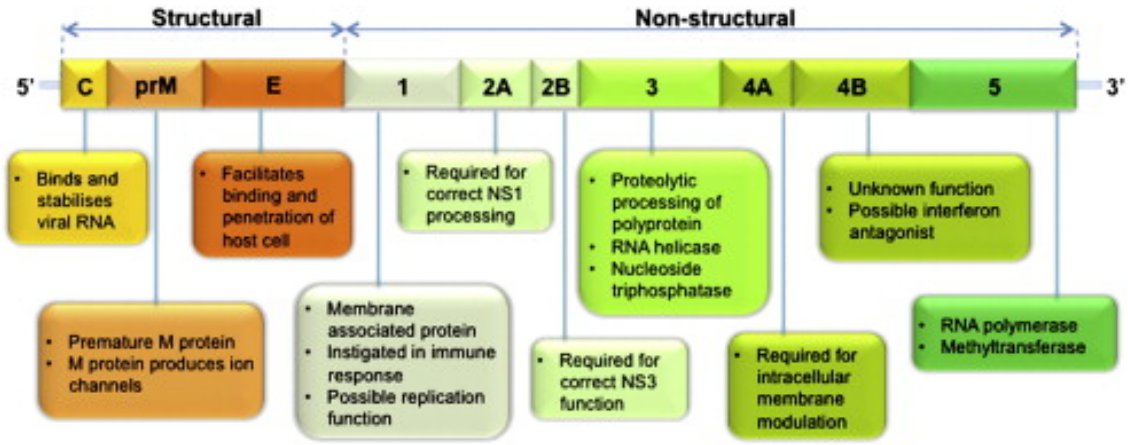

Figure 2.4: Schematic diagram of the DENV polyprotein and its individual function (Herreroa *et al*., 2013).

2.1.5 Current vaccination and antiviral drug development

Several initiatives have been taken to combat dengue including the dengue therapeutic interventions and its preventions involving vector control measures and disease surveillance. However, preventive measures taken over the last decades in many Asian countries have not reduced the mosquito population nor the disease burden. In the meantime, therapeutic interventions such as the development of vaccines and antiviral drugs have been actively conducted (Pasteur, 2012).

Vaccine development for dengue has started since the 1970s. For the past decades, full range studies have been performed to develop the dengue vaccine. These includes the live attenuated virus (LAV), inactivated virus (PIV), recombinant subunits, virus-like particles (VLPs), DNA vaccines and viral vectors (Schmitza *et al*., 2011; Simmons *et al*., 2012). The observation of the Antibody-Dependent Enhancement (ADE) phenomenon, where severe DHF/DSS associated with secondary infection with other DENV serotypes, has posed a significant dilemma in the vaccine development. The lack of an adequate animal model for the DHF effect, immunological complexity, and only partially informative immunogenicity assays are the prevailing challenges in the development of dengue vaccine (Thomas & Endy, 2013).

A tetravalent dengue vaccine targeting all four dengue serotypes, Dengvaxia, developed by Sanofi-Pasteur has completed phase III clinical trials and has become the world's first dengue vaccine (Capeding *et al*., 2014; Guy *et al*., 2015; Villar *et al*., 2015). Its efficacy against DENV-1, DENV-3, and DENV-4 is moderate: approximately 50–55%, 65–78%, and 72–80% respectively, while that to DENV-2 is still poor (about 35–50%) (Capeding *et al*., 2014; Villar *et al*., 2015). For that reason, this vaccine has been licensed only in Mexico, the Philippines, and Brazil, but not in

Malaysia as this country is more prevalent with DENV-2. In spite of this, Dengvaxia is useful in battling the deadly DHF by 88% and reduce hospitalization for vaccinees above 9 years old. Nevertheless, Dengvaxia is not recommended for children under this age as it can increase the severity of the disease when the body infected with DENV.

Other than vaccines, efforts are also being made to develop antiviral drugs. There were several antibodies, compounds from natural plants and synthetic analogs discovered as antiviral agents. Manipulation of the dengue viral structure is one of the strategic methods for the antiviral target. A synthetic compound, ST-148 was found to induce a conformational change of the C protein and therefore blocks its normal function in the encapsidation of the viral genome (Byrd *et al*., 2013; Ma *et al*., 2004). Exploiting the E protein found on the surface of the DENV is one of the strategies to prevent the virus from entering host cells (Julander *et al*., 2011). Previous studies showed that antibiotics from tetracycline derivatives could prevent conformational rearrangements of the E protein, while a compound namely, α-glycosidase inhibitor, was found to inhibit the E protein folding during the glycosylation (Alen & Schols, 2012).

Another approach of antiviral strategy is by targeting the NS protein of DENV. A compound known as 6-O-butanoyl castanospermine was reported to interfere the N-glycosylation of the NS1 protein (Amorim *et al*., 2014). Another study has found a novel synthetic inhibitor, NITD-618, that could interfere with the NS3-NS4B complex formation, and lead to a reduction of viral RNA synthesis and suppresses all four DENV serotypes with EC_{50} = 1-4 μM and CC_{50} >40 μM (Xie *et al*., 2011). Among the NS proteins, NS3 and NS5 are highly conserved proteins in all four DENV serotypes. These proteins exhibit enzymatic activities and involve in viral replication, and

therefore, have been considered as strategic antiviral chemotherapeutics for DENV (Heilman *et al*., 2014). Previously, peptide inhibitor with electrophilic warheads such as boronic acid was found to inhibit DENV NS3 with K_i of 43 nM (Yin *et al*., 2006). Meanwhile, for NS2B-NS3pro, the first finding on synthetic peptide inhibitor based on peptidic α-keto amide was made by Leung *et al*. (2001). Recently, betulinic acid, a flavonoid isolated from *Carpolepis laurifolia* leaf, was shown to inhibit DENV NS5 RNA polymerase with IC_{50} of 1.7 μM (Coulerie *et al*., 2014).

An alternative therapeutic approach against DENV is to utilize the small interfering RNA (siRNA). sRNAi plays an important role as a defense against viruses of invertebrates. Once the virus invades, the dsRNA triggered the mechanism of sRNAi, which causes the targeted gene's mRNA to be catalytically degraded. Previous investigation showed an increased cell survival rate by 2.2 fold and reduction of DENV by 97.54% when the C6/36 cells transfected with the siRNA. siRNA mediate silencing of attachment receptor and therefore inhibit DENV entry and multiplication in HepG2 cells, which ultimately reducing the viral load. With this, dengue fever can be prevented from developing into more severe forms (DHF/DSS) (Idrees & Ashfaq, 2013).

Currently, the antiviral repertoire is more than 30 drugs. But effective therapies against the viral infection have yet to be established (Clercq, 2002). Therefore, more effort has to be allocated towards the search for specific and effective antivirals. Nevertheless, with the findings of several potential candidates and support from the government and private sector, the potential to discover for effective antiviral compound against the dengue disease is seen to be encouraging.

2.1.6 NS2B-NS3pro as therapeutic target

The genetic idiosyncrasy across all four serotypes genotypes makes NS2B-NS3pro as an ideal drug target for DENV therapeutics (Choksupmanee *et al*., 2012). The catalytic triad (His51, Asp75, and Ser135) found within the NS3pro domain, is typical for serine proteases and is responsible for the post-translational proteolytic processing of the polyprotein precursor (Tambunan & Alamudi, 2010). NS2B-NS3pro is required for the *cis* cleavage of the NS2A-NS2B and NS2B-NS3 sites as well as for the *trans* cleavage of the NS3-NS4A and NS4B-NS5 sites (Figure 2.5A). Also, NS3pro mediates cleavages within the C, NS2A, NS3 and NS4A proteins (Clum *et al*., 1997). Cleavages occurred between residues Arg-Arg, Arg-Lys, Lys-Arg and occasionally Gln-Arg at the P1 and P2 positions, respectively, followed by a Gly, Ala, or Ser at the P1' position (Yusof *et al*., 2000). Figure 2.6 shows the nomenclature of the substrate specificity of the protease.

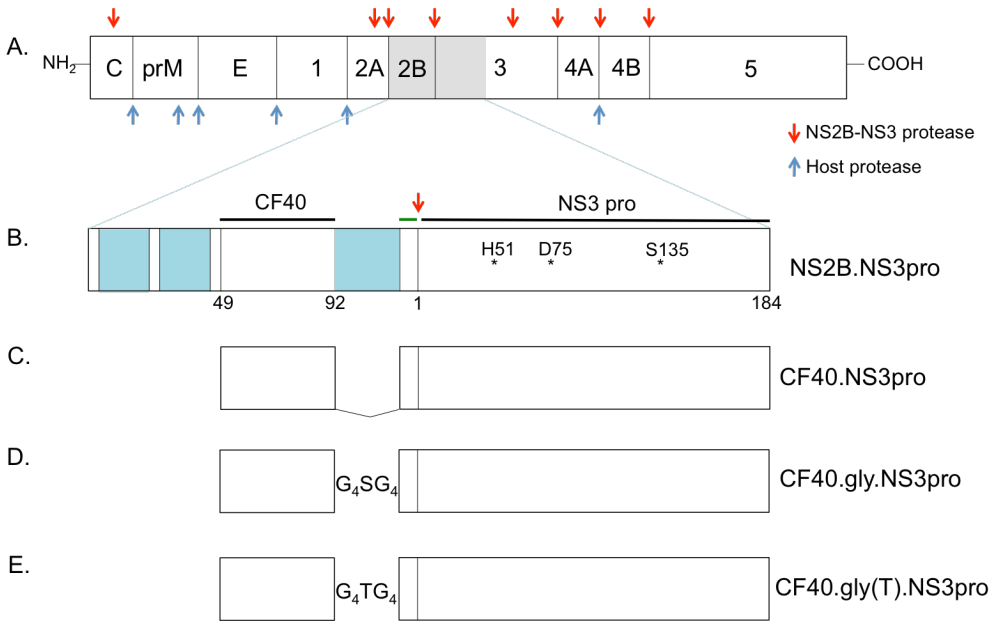

Figure 2.5: Schematic representation of the DENV-2 polyprotein and NS2B-NS3pro expression constructs. **(A)** A polyprotein of DENV-2 displaying alongside the cleavage sites by the host-encoded proteases (blue arrows) and the DENV-2-encoded NS2B-NS3pro (red arrows). The NS2B cofactor and the NS3 protease domain (NS3pro) are shaded in gray. **(B)** Overview of the key features of the NS2B and NS3pro domain, which consists of the conserved hydrophobic (blue boxes) and the hydrophilic (open boxes) domains of the NS2B and the 184 amino acids of the NS3pro region that contains the catalytic triad (His51, Asp75, and Ser135). **(C)** The expression construct for autoproteolytically active CF40.NS3pro reported by Clum *et al*. (1997). It is consists of the NS2B hydrophilic regions of both the central 40 amino acid (CF40), and the 10 amino acids (highlighted with a green line) upstream the NS2B-NS3 cleavage site and fused to the NS3pro region. Expression construct for soluble and catalytically active **(D)** CF40.gly.NS3pro reported by Leung *et al*. (2001) which comprises of a Gly4-Ser-Gly4 linker and **(E)** CF40.gly(T).NS3pro reported by Heh *et al*. (2013) that consists of a Gly4-Ser-Gly4 linker.

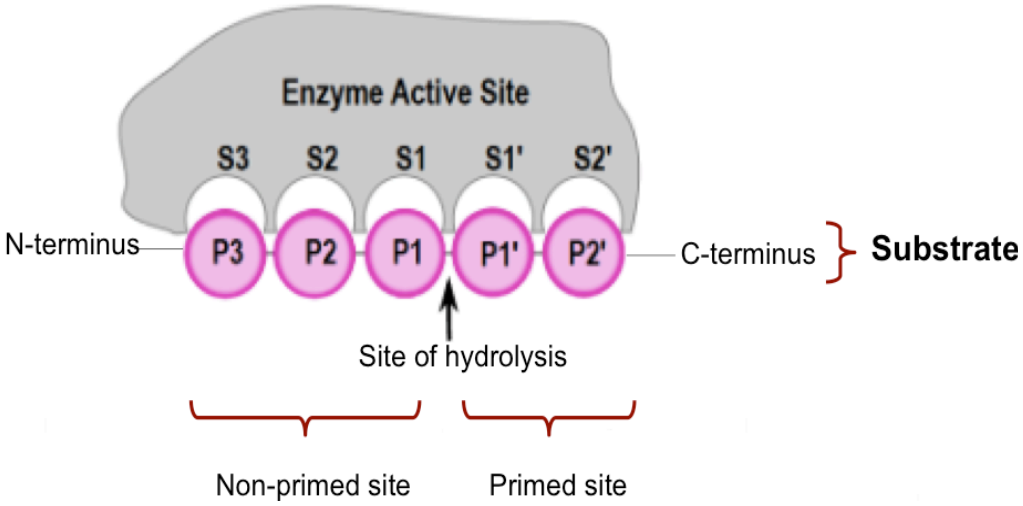

Figure 2.6: Schematic representation of the substrate specificity of the protease. Proteases active site is composed of subsites (S). Each S has an affinity for residues (P) from the substrate. P1, P2, and P3 indicate amino acid residues in the N-terminal of the substrate designated from the cleaved site. Likewise, the residues in C-terminal direction are designated as P1', P2' etc. The proteolysis of the peptide bond is mediated by the protease between P1 and P1'. Excerpt with modification from Schechter & Berger (1967).

NS3pro situated in the first 184 amino acids of the amino-terminal region is responsible for the dengue viral replication by cleaving the viral polyprotein (Figure 2.5B). However, the NS3pro domain without its cofactor (CF) from the 40 amino acids of the hydrophilic region of NS2B (alternately termed as CF40) causes an inefficient protease activity. Previous finding by Clum *et al*. (1997) showed that fusion of CF40 to the NS3pro region further enhances the activation of NS3pro (Figure 2.5C). The co-activity of NS2B is essential in stabilizing the NS3pro by modulating the sequence of the catalytic triad and the substrate-binding pocket contained in the NS3pro (Jan *et al*., 1995). This finding is supported by several *in vivo* (Falgout, Miller, & Lat, 1993) and *in vitro* (Clum *et al*., 1997) studies. An example of this case is the low turnover rate of the small chromogenic substrate N-α-benzoyl-L-Arg-p-nitroanilide (Li *et al*., 2005). However, the expression of this construct is associated with insoluble inclusion bodies and the extracted solubilized protease complex is autoproteolytically active (Yusof *et al*., 2000).

Nevertheless, previous study by Leung *et al*. (2001) showed that by linking CF40 to the NS3pro region via a flexible and noncleavable glycine linker Gly4-Ser-Gly4 (alternately termed as 'gly') lead to the production of soluble and non-proteolytically active NS2B-NS3pro (Figure 2.5D). This linker covalently links both regions (*E*^{125}*VKKQR*-Gly4-Ser-Gly4-AGVLWD^{6}) and consequently, the *cis*-cleavage site is removed by separating the recognition site for *cis*-cleavage at the NS2B-NS3pro junction. Another breakthrough was when a crystal structure of the soluble and enzymatically active NS2B-NS3pro of DENV-2 was produce by Erbel *et al*. (2006).

In this study, NS2B-NS3pro of DENV-2, or shortly termed as the DENV-2 NS2B-NS3pro was used based on the construct provided by Heh *et al*. (2013). The construct was developed according to Erbel *et al*. (2006,) (CF40.gly.NS3pro) based on the template from Yusof *et al*. (2000) (CF40.NS3pro). An additional of 9 nucleotides (A^{5076}GAAAATTG^{5085}) were added to the NS3pro C-terminus to create a reverse primer that avoids the formation of primer dimers as previously observed by Leung *et al*. (2001). Nonetheless, instead of the typical glycine linker Gly4-Ser-Gly4, construct from Heh *et al*. (2013) is linked with Gly4-Thr-Gly4 and henceforth termed as CF40.gly(T).NS3pro (Figure 2.5D). The central residue of serine (Ser) is replaced with threonine (Thr) (nucleotide sequence GGGGGCGGA**GGT*ACC***GGTGGAGGCGGG, with the Thr residue in italics). These would enable the formation of a restriction site for *Kpn*I (bolded residues) to allow a more simplified digestion and ligation of CF40 and NS3pro region at the middle of the linker.

2.2 Surface Plasmon Resonance (SPR)

Surface plasmon resonance (SPR) was first established in 1968 (Otto, 1968), but was only being commercialized for biomolecular interaction analysis (BIA) until early 1990 by Biacore, GE Healthcare (Englebienne *et al*., 2003)**.** SPR is an electromagnetic wave generated when the light is in resonance with the electron in the gold surface (Yakimchuk, 2011). The phenomena will happen when an incident light beam strikes the surface at a fixed angle (Bronner *et al*., 2013). The gold layer is mainly embedded on a surface of the sensor chip, supported by glass. A non-crosslinked carboxymethylated (CM) dextran hydrogel is linked to the gold film, to allow the ligand to bind to the surface of the sensor chip covalently. The schematic view of an SPR biosensor system is illustrated in Figure 2.7.

2.2.1 SPR assay design

In SPR assay, the binding partner immobilized to the sensor chip is called 'ligand', while the interacting molecule is called 'analyte'. The analysis is performed in a continuous flow of buffer, termed as the 'running buffer' (GE Healthcare, 2012). The interaction between a drug and its target protein includes the formation of analyte-ligand complex and dissociation of this complex followed by the analyte removal (Figure 2.7). This whole process causes the changes of wavelength on the gold surface, which is transduced in real time into an optical signal known as the sensorgram**.** SPR is also a precise quantitative method since changes on the sensor surface are proportionally related to the amount of bound molecules (Yakimchuk, 2011).

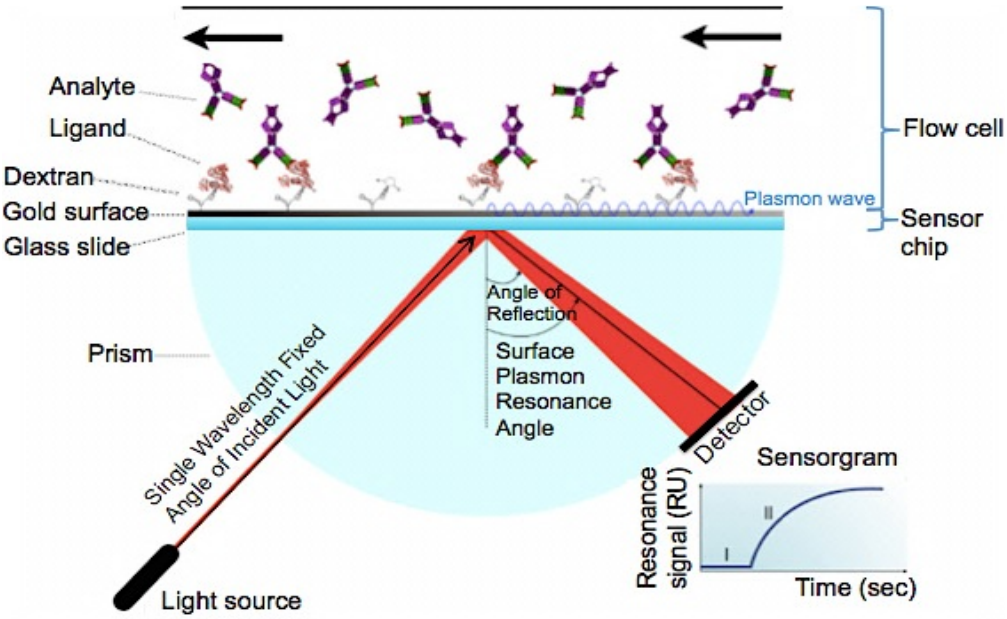

Figure 2.7: Schematic representation of an SPR biosensor system. A polarized wave laser excites the electromagnetic plasmon waves on a thin gold film. The SPR angle shifts when excitation of surface plasmon takes place. Excerpt with modification from Wikipedia (2015).

The fundamental considerations applied in SPR assay are (i) conformation and quality of the ligand and the analyte, (ii) type of interaction involved between the ligand and the sensor matrix, (iii) concentration and duration used for regeneration of the analytes, (iv) flow rates and duration of the association and dissociation phases, and (v) choice of kinetic fitting model to analyze binding data that is often related to the fundamental biological of the system (Lipschultz *et al*., 2000). Figure 2.8 is depicting the typical sensorgram recorded in real time based on the analyte-ligand binding interaction.

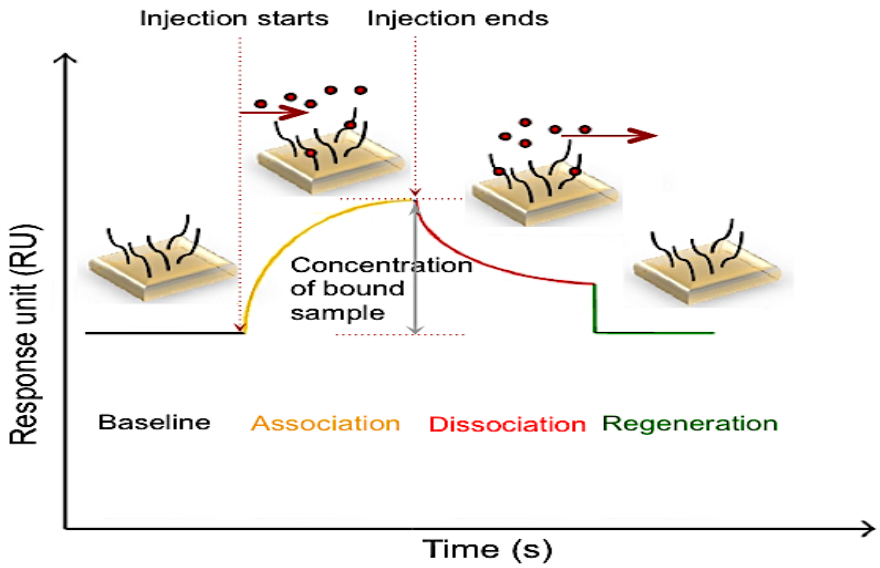

Figure 2.8: Typical SPR sensorgram is depicting four phases of interaction profile. **(1)** Baseline phase: the sensor surface is filled with ligand bound on the surface, **(2)** Association phase: injection of the analyte starts and the response is increasing which correlates with the association of the analyte to the ligand, **(3)** Dissociation phase: a decrease in response during dissociation of the analyte from the ligand and **(4)** Regeneration phase: The analyte is completely removed, leaving only the ligand bound to the surface. Excerpt with modification from Ritzefeld & Sewald (2012).

2.2.2 Applications of SPR

SPR technique allows analysis of the interacting biomolecules to be studied in their native state without labeling. Therefore exposure to experimental artifacts and chemical alteration of the interacting biomolecules could be prevented to avoid the binding site from being occluded (Englebienne *et al*., 2003; Wang & Wang, 2013). SPR can be used for a wide variety of protein and molecules, in assays such as interaction and screening assays, molecular discrimination, determination of binding specificity and its kinetic, measurements of actual (or active) concentration, epitope mapping and thermodynamic parameters (Gopinatha, 2010). Additionally, SPR allows biomarker identification and interaction analysis of RNA, DNA and whole cells (Yakimchuk, 2011).

SPR biosensor can determine the molecular interaction in real time. Only low sample consumption is required for the SPR analysis, within 10- to 1000-fold less than

is needed by other biochemical methods. It is also a highly sensitive biophysical tool as it can detect small molecules with molecular mass as low as 50 Da. Some of its primary functions are to characterize the kinetic parameters based on association rate constant (k_a), dissociation rate constant (k_d) and also the affinity parameters based on the equilibrium association constant (K_A) and the equilibrium dissociation constant (K_D). SPR biosensor can also be used to study weak binding interactions. Other biophysical methods, such as X-ray crystallography and NMR methods can offer high-resolution characteristic about the binding interface, but they have limited throughput, require relatively large amounts of reagents, and often do not provide insight into the strength of a binding interaction (Shepherd *et* al., 2014).

Identification and characterization of small molecules with high binding affinity for their protein targets are important in the drug discovery and development field (Biorad, 2015). However, previous studies showed that low binding affinity of small molecule compounds had been used as a strategy to optimize into high affinity ligands using the structure-based drug design methods. Nevertheless, in the conventional biochemical assay, low affinity compounds often need to be screened at high concentration, which often leads to false positive hit rate. Therefore, secondary biophysical screening such as SPR technique is required to confirm and validate good hits (Shepherd *et al*., 2014). Furthermore, SPR can also be used as the primary screening to analyze hit compounds with slow dissociation rates, which often show superior clinical efficacy (Swinney, 2008).

2.2.3 Immobilization of ligand

Immobilization of ligand to the surface of the sensor chip is one of the most vital and challenging processes in SPR assay. Immobilization may either be directly by covalent

coupling or indirectly by the capturing method (Merwe, 2003). Direct immobilization mainly involves exploitation of the ligand's functional group to bind to the sensor surface with high stability covalently. This method also allows immobilization with high-density level due to the many carboxyl groups such as in the CM5 chip. Macromolecules may contain amine, aldehyde or thiol groups but most of them consist of amine groups. Due to this, 'amine coupling' is considered as one of the most common methods used for direct coupling. Immobilization with amine coupling involves the covalent interaction of free amine groups ($-NH_2$) in the ligand with the esters that are developed during the activation of the sensor surface with EDC/NHS solution (Figure 2.9). Most protein contains many amines and direct immobilization with amine coupling often cause the heterogenous or random orientation of the ligand (Figure 2.10A). As a result, this will decrease the probability for the analyte to reach the active or binding sites of the ligand. Moreover, if the active site is involved in the amine coupling, this will cause the ligand to loss its activity (SPR-pages, 2015a). Other choices for direct immobilization are based on engineered thiol ($-SH_2$) or aldehyde (-COOH) groups in the ligand.

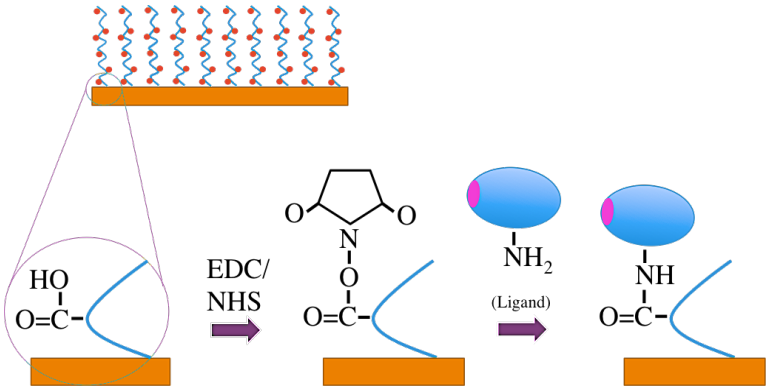

Figure 2.9: Illustration of amine coupling of a ligand to the sensor surface. As highlighted, the sensor surface contains carboxymethyl group (-COOH) attached to the dextran matrix (indicated as blue string). The carboxyl group is activated by the EDC/NHS mixture solution to form into reactive succinimide esters. The ligand is subsequently passed over the activated sensor surface, causing the esters to react spontaneously by covalently link to the primary amine or other nucleophilic groups on the ligand.

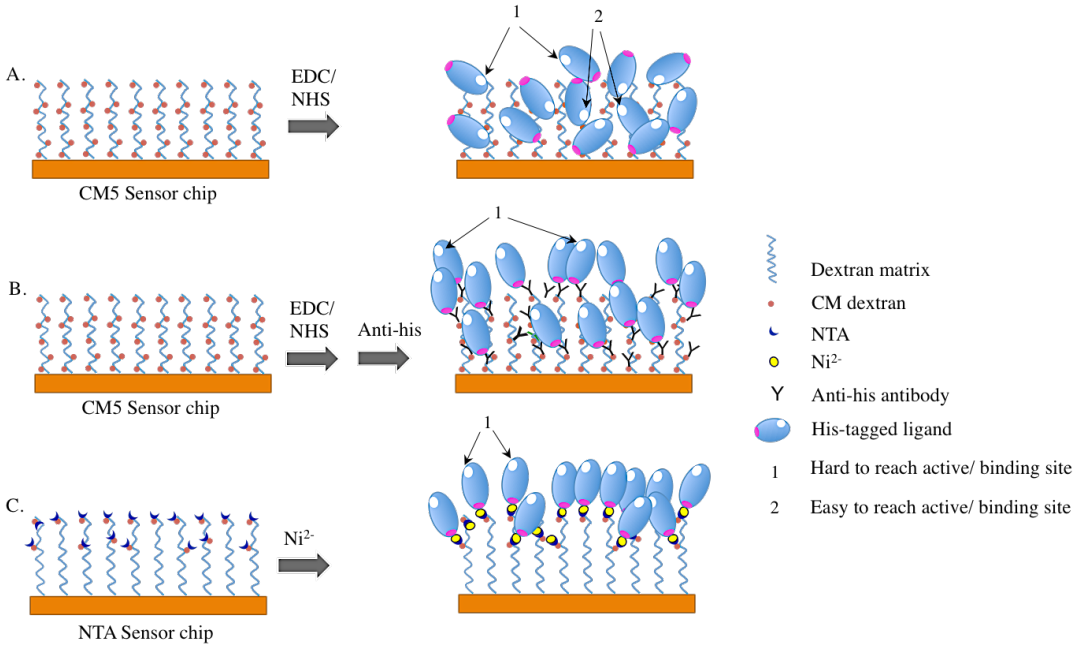

Figure 2.10: Schematic diagrams of methods used for immobilizing ligand. **(A)** Direct immobilization using amine coupling. CM5 chip is activated with the EDC/NHS solution to produce succinimide esters. Ligands are covalently immobilized in a random orientation when free amine groups interact with the esters. **(B)** and **(C)** Indirect immobilizations using capture antibody and Ni-NTA respectively. The antibody is immobilized covalently onto an activated CM5 chip before the ligands are captured by the His-tags. Similarly, these His-tags are captured non-covalently by the Ni-activated NTA sensor surface. Both capturing processes involve oriented immobilization of the ligands.

An alternative is to use an indirect immobilization based on the non-covalent affinity-capturing method between the ligand and the surface of the sensor chip. This approach includes targeted site such as ligands' affinity tags that allows directed structural orientation and a homogeneous immobilization. Compared to amine coupling, the capturing method potentially offers optimal binding site exposure. The active or binding sites of the ligand may not be interfered, which makes the capturing method and ideal option for persevering the ligands' activity (GE Healthcare, 2012). The immobilization includes only the his-tagged proteins captured either by the anti-his antibodies that are immobilized on the CM5 chip (Figure 2.10B) or by the Ni-activated NTA chip (Figure 2.10C). However, the capturing method may cause the ligand to dissociate slowly from the sensor surface, which is less suitable for reliable kinetic studies (Joss *et al*., 1998).

Recently, an improved discovery using 'capture coupling' on NTA chip is developed. This method combines the capturing of the his-tagged ligand and amine coupling, which not only produces a uniform orientation of immobilized ligand but also covalently stabilize the ligand (Willard & Siderovski, 2006). Capture coupling could ease kinetic studies that often demand simplicity during binding evaluations and is beneficial for ligands that become inactive due to direct amine coupling.

2.2.4 Regeneration of analyte

Regeneration of analyte is the process of removing remaining analyte from the sensor surface without affecting the activity of the immobilized ligand. This process is performed when the analyte is not removed sufficiently during the dissociation phase. It is a critical step for accurate analysis to avoid carry over of analytes into the subsequent binding cycle (GE Healthcare, 2012).

2.3 *In silico* study using molecular docking

Understanding the molecular recognition such as small molecule-protein interactions is crucial in therapeutic applications especially for modern structure-based drug design (Huang & Zou, 2010). On that account, it is important to investigate the mechanism of interaction between the constituent molecules and determine the binding mode and the binding energy of the bonding forces of small molecules to the binding site of the target protein (Huang & Zou, 2010; Yuriev *et al*., 2010). Unlike SPR assay (Section 2.2.1), the term ligand is often used in molecular docking to represent small molecules, while the target protein is alternately known as the receptor.

Due to the high cost, difficulties and time-consuming exercise in the laboratory biochemistry, computational and molecular modeling tools have become essential mechanisms towards the understanding of molecular aspects of structure complexes (Huang & Zou, 2010). Several computational approaches have been widely used to discover the novel hits for various therapeutic targets. These approaches are the molecular docking, molecular dynamics, homology modeling and quantitative structure-activity relationships (QSAR) (Kumalo *et al*., 2015). On the other hand, NMR and X-ray crystallography are alternative methods to obtain the experimental structures of these small molecule-protein complexes; or alternately termed as ligand-receptor complexes. But these methods are tedious and time-consuming and therefore, are not suitable for routine study especially when involving the interaction between a receptor and thousands of ligands. Therefore, molecular docking algorithms have been used to overcome this obstacle by predicting the 3D complex structure of the receptor-ligand complex (Pujadas *et al*., 2008). Moreover, molecular docking is also the ultimate computational tool to screen for small molecule compound whenever the three-dimensional structure of a target protein (or receptor) is available (Okimoto *et al*., 2009).

Molecular docking refers to the generation of multiple ligand poses *(*conformations or orientations) after it is docked into the binding site (or binding pocket) of the target protein (or receptor). In the second component, scoring is the prediction of the strength between the target receptor and the ligand for each pose. From here, multiple ligands are ranked according to the calculated binding affinities or docking scores (Okimoto *et al*., 2009). The structure and the database of both the receptor and the ligand must first be prepared before a successful docking process can be performed. A search algorithm is used to compute the two essential components in molecular docking: docking and scoring. The pose with the lowest energy score or free binding energy (E_{bind}) will be predicted as the best binding mode (Huang & Zou, 2010). Figure 2.11 shows the schematic process involved in molecular docking. E_{bind} is referring to the Gibbs free energy (G), which is one of the most important thermodynamic quantities for the characterization of the driving forces. The change in Gibbs free energy (ΔG) of a system that occurs during a reaction is defined as change in enthalpy (H) of the system minus the change in the product of the temperature (T) times the entropy (S) of the system. More clearly, the formula is $\Delta G = \Delta H - T\Delta S$. In analogy with any spontaneous process, protein–ligand binding occurs only when ΔG of the system is negative, which is when the system reaches an equilibrium state at constant pressure and temperature (Du *et al*., 2016).

Autodock, Autodock Vina, GOLD and FlexX are the standard docking software that focuses on docking between the ligand and receptor through non-covalent interactions such as hydrogen bonding, van der Waals interaction and the electrostatics interaction. Nowadays, the conventional method of docking is to use ligands that are bound to a receptor through non-covalent interaction. Most of the current docking process has been focusing on the efficient prediction of the binding modes of non-covalent inhibitors. On

the contrary, docking ligands that involve covalent linkage to the receptor have been considered as a complicated task, due to the reaction involved between the ligand and the receptor that needs to be taken into consideration (Kumalo *et al*., 2015).

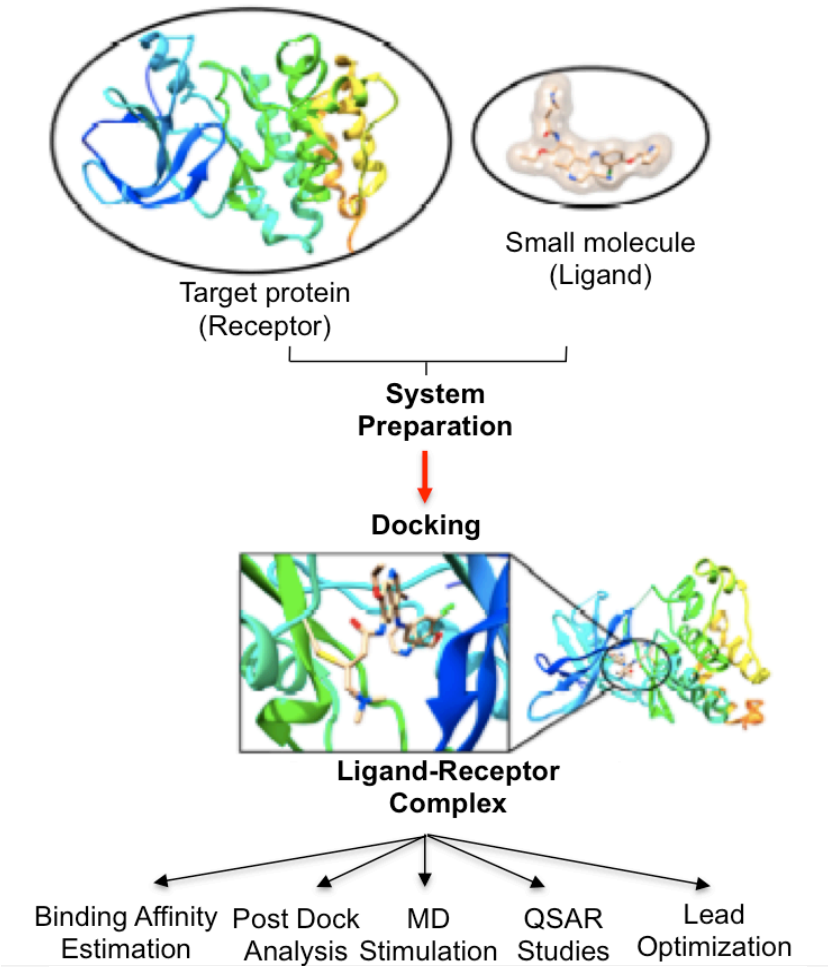

Figure 2.11: General workflow in *in silico* study using molecular docking. The structure of the ligand and receptor must be prepared before the docking process. Once the ligand and receptor are docked, the binding affinity (binding energy) and the distances between the interacting patterns are estimated, and post dock analysis is performed involving predicting the interacted amino acids and types of interaction forces (hydrogen bond, hydrophobic interactions, etc). The docking results could be used in further studies such as molecular dynamic (MD) simulation, Quantitative structure–activity relationship models (QSAR) studies and lead optimization. Excerpt with modification from Kumalo *et al*. (2015).

2.4 Small molecule medicinal drugs as antiviral target for dengue

Dengue is the neglected tropical disease that has been spreading rapidly due to environmental changes, unplanned urbanization and population movements (Centre, 2015). Different strategies have been undertaken to explore for vaccine or antiviral drugs against dengue. One of the promising strategies is to focus on the development of DENV NS2B-NS3pro inhibitors. Numerous studies involving small-molecular-weight compounds have been undertaken (Lescar *et al*., 2008; Melino & Paci, 2007; Oliveira *et al*., 2014; Sampath & Padmanabhan, 2009) as the small molecule is more amenable to the development of a more complex structure by combining molecules that give good binding to different parts of the target protein (Webb, 2013). Several approaches have been implied to search for the DENV-2 NS2B-NS3pro inhibitors involving screening natural products (Frimayanti *et al*., 2011; Kiat *et al*., 2006; Tomlinson *et al*., 2009), structure-based virtual screenings (Knehans *et al*., 2011; Tomlinson & Watowich, 2011; Yang *et al*., 2011), small compound libraries (Sugamoto *et al*., 2008) as well as synthesizing rationally designed based compound (Rahman *et al*., 2006).

There has been ongoing interest in medicinal drugs such as antibiotic for the investigation of antiviral against DENV. A compound derived from the doxorubicin antibiotic showed antiviral activity against the DENV-1, 2, and 3 (EC_{50}: 12 μM, 1.2 μM, and 1.7 μM, respectively). On the contrary, a compound derived from teicoplanin inhibited the DENV-2 at EC_{50}: 6.9 uM, while an antibiotic namely geneticin at EC_{50}: 2 ± 0.1 μg/ml (Rothan *et al*., 2013; Zhang *et al*., 2009).

Tetracycline antibiotics represent one of the most successful classes of pharmaceuticals (Hamad, 2010). Since the 1950s, tetracycline antibiotics have been widely used in human and veterinary medicine to promote animal growth and treat

bacterial infections urinary tract infections, chlamydia, acne, rosacea, and malaria (Chopra *et al*., 1992; Roberts *et al*., 1996). Previously, two types of tetracycline derivatives, doxycycline and rolitetracycline, are shown to inhibit the formation of DENV plaque in BHK-21 cells, with IC_{50} 55 μM and 67 μM respectively. According to an *in silico* docking study, both antibiotics have shown to disrupt the conformational changes in the DENV envelope by exerting hydrophobic interactions against the critical residues in DENV-2 that affected membrane fusion during viral entry (Yang *et al*., 2007). In another inhibition study, at 100 μM, both doxycycline and rolitetraycline shown 53.8 ± 2.8% and 38.9±2.9% of inhibitory effect against the DENV-2 NS2B-NS3pro, with further study showed doxycycline non-competitively inhibited NS2B-NS3pro at K_i value 55.6 ± 5.7 μM (Rothan *et al*., 2013). Furthermore, doxycycline also exhibits inhibition to viral entry and post-infection replication to all four serotypes of the DENVs with higher inhibition to DENV-2 and DENV-4 (Rothan *et al*., 2014c). Based on the consensus *in silico* docking by Gangopadhyay *et al*. (2017), both tetracycline derivatives are predicted to be specific inhibitor against the DENV-2 envelope β-OG pocket, a crucial hinge used for mediating virus-host fusion via conformational changes in the envelope to the fusion-competent form.

Interestingly, researchers have also found that Non-Steroidal Anti-Inflammatory drugs (NSAIDs) can inhibit the replication of the DENV as exhibited by the salicylates (sodium salicylate and aspirin) (Trujillo-Murillo *et al*., 2008a). Meclofenamic acid is the most potent NSAID among the fenamates (the class of N-phenylanthranilic acids) and is known to treat inflammation and chronic pain (Harks *et al*., 2001). Recently, one of the NSAIDs, meclofenamic acid, when used at 100 μM, has shown to inhibit 43.0±1.4% of the DENV-2 NS2B-NS3pro (Rothan *et al*., 2013). Another beneficial property of meclofenamic acid is to inhibit gap junctions in *Aedes aegypti* mosquitoes

that cause an insecticidal effect when injected into the hemolymph of adult female (Calkins *et al*., 2015). Moreover, *in vivo* study on rat shows that meclofenamic acid has anticonvulsive activity against epilepsy (Peretz *et al*., 2005).

Small molecular weight compounds have recently been seen as a potential target for dengue antiviral drugs. Up till now, no related SPR-assays or computational docking studies towards the DENV-2 NS2B-NS3pro have been found for doxycycline, rolitetracycline, and meclofenamic acid. And since obtaining approval for the use of new medicinal agents is a slow and expensive process, a more time- and cost-effective approach is strategically preferred by using known drugs with their ADMET (absorption, distribution, metabolism, and excretion) properties already available. Due to the commercial availability of these medicinal drugs and their functionality in inhibiting the DENV-2 NS2B-NS3, it is hoped that SPR-based kinetic analyses and the computational docking would provide an insight into the binding reaction mechanism that is involved in creating the inhibitory effects of the protease inhibitors.

CHAPTER 3 : MATERIALS AND METHOD

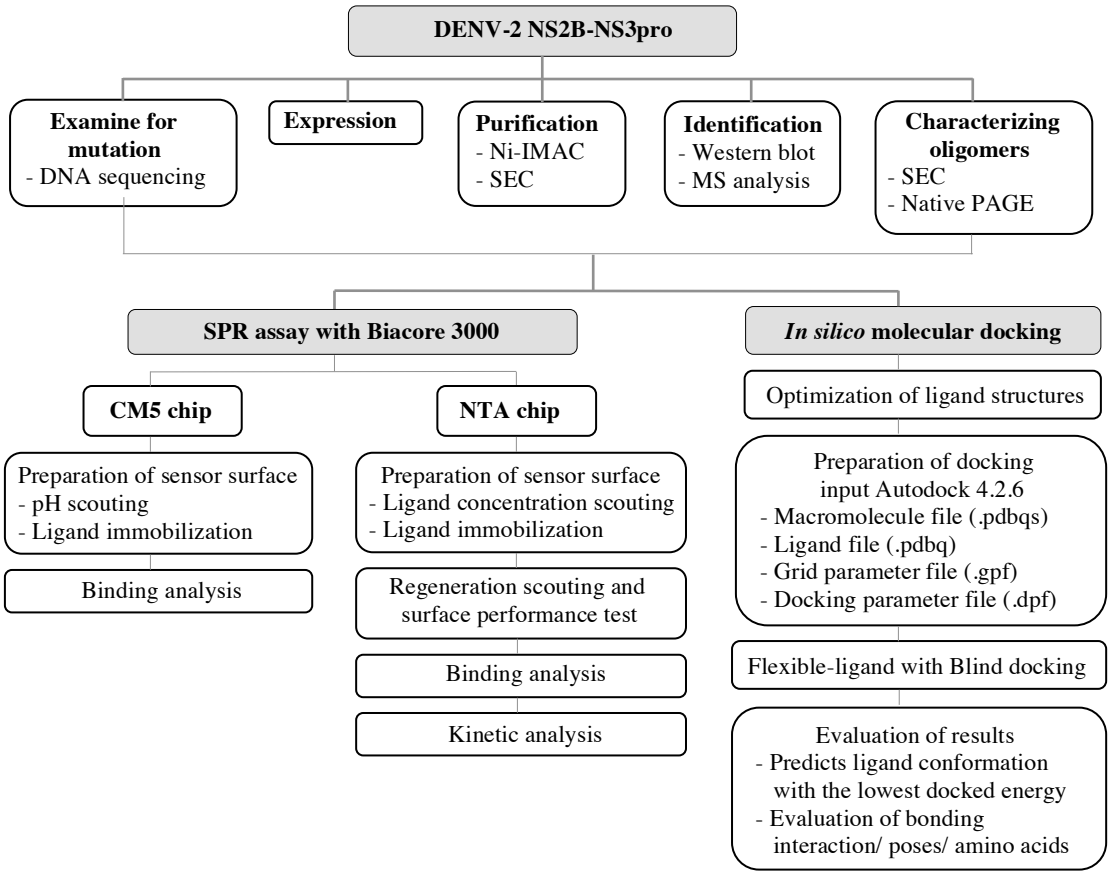

Figure 3.1: Flow chart of research methodology.

3.1 Materials and instrumentations

All reagents and materials were purchased from several brands. Ampicilin from Duchefa Biochemi; yeast extract and bacto-tryptone from Becton, Dickinson and Company; agar, boric acid, imidazole, PBS tablet and nickel chloride from Sigma; NaEDTA from Calbiochem; agarose from Invitrogen; IPTG from Omnipur Calbiochem; HEPES, glycerol, lysozyme, sodium chloride, sodium acetate, lysozyme, acrylamide, bisacrylamide, sodium hydroxide, ammonium bicarbonate, formic acid, acetonitrile, dithiothreitol, iodoacetamide and DMSO from Amresco Inc.; Ni-NTA agarose and QIAamp DNA mini kit from Qiagen; SDS, non-fat dry milk, tween 20 and

nitrocellulose membrane from Biorad ; APS from Bio Basic Inc.; bromophemol blue, coomasie brilliant blue R-250 and TEMED from Merck; hydrochloric acid from Friendemann Schmidt; trypsin gold from Promega; BlueRAY prestained protein ladder (11- 180 kDa) from GeneDirex; O'GeneRuler 100 bp DNA ladder and 6X Orange Loading Dye from Life Technologies; 0.2 and 0.45 μm cellulose acetate membrane syringe filter and Vivaspin Turbo 15 centrifugal concentrator with 10 k MWCO from Sartorius; ZipTip pipette tips from Milipore; UV-transparent 96-well plate from Thermo Fischer Scientific; Kit for Molecular Weights 14 – 500 kDa Non-denaturing PAGE from Sigma; and Hi-Load Superdex 16/600 75 prep grade column, Hi-Trap desalting column, PD-10 column, 10% surfactant P20, CM5 chip, NTA chip, glass vials Ø 16 mm, polypropylene Ø 7mm, regeneration solutions (10 mM Glycine-HCl at pH 3.0, 2.5, 2.0, and 1.5, and 0.05 M NaOH) and amine coupling kit (containing 0.75 g EDC, 0.115 g NHS and 1 M ethanolamine-HCl, pH 8.5) from GE Healthcare.

Instrumentation such as electrophoresis unit from Thermo was used for analyzing DNA. Mini-PROTEAN® electrophoresis system from Biorad was used for SDS-PAGE and native PAGE analysis. Sorval centrifuge fixed angle rotor from Thermo was used during pelletization and concentrating protein solution. AKTA Prime liquid chromatography system from GE Healthcare was used during size exclusion chromatography. Shimadzu UV-visible recorder spectrophotometer (UV-160) was used for protein OD measurement. Benchmark microplate reader from Biorad was used to measure protein concentration in the Bradford assay. Biacore 3000 from GE Healthcare was used for SPR assay.

3.2 The production and characterization of the DENV-2 NS2B-NS3pro

3.2.1 Analyzing the plasmid DNA

3.2.1.1 Bacteria strain

XL1-Blue MRF' *E. coli* strain containing recombinant pQE plasmid with the CF40-$Gly_4ThrGly_4$-NS3pro gene (pQE30.CF40.gly(T).NS3pro); a construct of soluble DENV-2 NS2B-NS3pro gene.

3.2.1.2 Preparation of mixture solutions

100 mg/ml Ampicilin

Ingredient: 1 g Ampicillin.

Preparation: 1 g of ampicillin was solubilized in 10 ml distilled water (dH_2O) and filtered through 0.20 μm syringe filter of cellulose acetate (CA) membrane from Sartorius. The ampicillin solution was aliquoted into 1 ml and stored at -20^oC.

LB (Luria-Bertani) agar

Ingredient: 1 g Yeast Extract; 2 g Bacto-tryptone; 2 g NaCl; 3 g Agar.

Preparation: All ingredients were mixed together and MiliQ water was added to 200 ml. The solution was then sterilized by autoclaving for 15 min at 120^oC. The medium was cooled to 50°C before being supplemented with ampicillin (working concentration 100 μg/ml). Approximately 20 ml of the agar solution was poured into several individual Petri plate and leaved at room temperature to solidify. Once solidified, the petri dishes were sealed with parafilm and stored at 4^oC with the cap placed upside down.

LB medium

Ingredients: 0.05 g Yeast; 0.1 g Bacto-tryptone; 0.1 g NaCl; 10 ml dH_2O; 10 μl 100 mg/ml Ampicillin.

Preparation: The yeast and NaCl was dissolved in 10 ml dH_2O. The medium was sterilized by autoclaving for 15 min at 120^oC. The medium was cooled to room temperature before being supplemented with ampicillin (working concentration 100 µg/ml).

10*X* TBE (Tris-Borate-EDTA) buffer

(0.89 M Tris, 0.89 M Boric Acid, 0.02 M NaEDTA, pH 8.3)

Ingredients: 108 g Tris Base; 55 g Boric acid; 7.5 g NaEDTA.

Preparation: All the ingredients were dissolved in 800 ml dH_2O. The solution was adjusted to pH 8.3 with and the volume was adjusted to 1 L with dH_2O. The solution was stored at room temperature.

1% (w/v) Agarose gel

Ingredients: 0.5 g Agarose; 50 ml TBE buffer.

Preparation: The ingredients were mixed together to a volume of 50 ml and then were heated to melt. The mixture was leaved to cool for 10 min and poured into the gel casting apparatus.

3.2.1.3 Readily prepared mixture solutions

QIAamp DNA mini kit (QIAGEN) containing QIAprep Spin Columns, Buffer P1 with RNase A added, Buffer P2, Buffer N3, Buffer PB, Buffer PE, Buffer EB and 2ml collection Tubes; O'GeneRuler 100 bp DNA ladder and 6X Orange Loading Dye.

3.2.1.4 Growing culture on agar plate

The inoculation on LB agar plate was performed in a sterile laminar airflow chamber. As a start, the inoculating loop was heated until red-hot for sterilization. The loop was

allowed to cool for several seconds before being dipped and gently swirled into a 1 ml glycerol stock solution. By slighly opening the lid of the agar plate, the *E.coli* on the inoculating loop was transferred onto the surface of the LB agar by streaking (Addgene, 2013) to achieve single colonies of *E.coli* carrying only the plasmid DNA pQE30.CF40.gly(T).NS3pro. Once streaked, the LB agar plate was inverted and incubated overnight (12 hours) at 37°C. A single colony grown on the agar plate was used to prepare the glycerol stock and recover the plasmid DNA (Section 3.2.1.5).

3.2.1.5 Preparations for glycerol stock and plasmid DNA

500 ml LB medium prepared in a 1L bottle was autoclaved for 15 min at 121°C. The media was cooled to 50°C before ampicillin was added to a final concentration of 100 µg/ml. The LB medium was transferred to a 1L conflask. A single colony from the LB agar plate was picked using the tip of a sterile pipette and dropped into the LB medium. The opening of the conflask was filled with cotton wool and the conflask was incubated for overnight (16 hours) at 37°C, at a shaking speed of 250 rpm. Once the OD600 nm had reached 0.6, 500 µl of the overnight culture was gently mixed with 500 µl of 50% glycerol that was kept in a 1.5 ml microtube. The glycerol stocks were kept at -80°C until used. Meanwhile, 20 ml of the extra overnight culture was used to prepare for plasmid DNA extraction.

The plasmid DNA (pQE30.CF40.gly(T).NS3pro) was extracted from the cultivated LB media using QIAprep Spin Miniprep Kit. First, 1 ml of the *E.coli* culture was centrifuged at 13,000 rpm for 1 min at room temperature. The supernatant was removed and the pellet containing the *E.coli* was resuspended in 250 µl of Buffer P1 and was then transferred to a 1.5 ml microtube. Next, 250 µl of Buffer P2 was added into the microtube and was gently inverted for 4-6 times to mix. Subsequently, 350 µl of Buffer

N3 was added and was immediately inverted to mix for 4-6 times. Once a cloudy texture was observed, the mixture was taken and centrifuged at 13,000 rpm for 10 min at room temperature. The supernatant developed afterwards was aspirated by pipetting followed by dispensing in into the QIAprep spin column that was placed in a 2 ml collection tube. The column in the tube was centrifuged at 13,000 rpm for 1 min at room temperature. Next, the flow-through was discarded. Subsequently, the QIA-prep spin column was washed with 0.5 ml of Buffer PB and centrifuged at 13,000 rpm for 1 min at room temperature. This process will remove endonucleases to avoid degradation of the plasmid DNA. 0.75 ml of Buffer PE was then added to the QIAprep spin column and was centrifuged at 13,000 rpm for 1 min at room temperature to remove salts. The flow-through was discarded and was centrifuged again at 13,000 rpm for another 1 min at room temperature to remove residual ethanol from Buffer PE. Next, the QIAprep spin column was placed into a clean 1.5 ml microtube. 50 µl of Buffer EB was added to the centre of the QIAprep spin column membrane and was let to stand for 1 min. Next, the column was centrifuged to elute the plasmid DNA at 13,000 rpm for 1 min at room temperature. The extracted plasmid DNA was stored at -20°C for further usage.

3.2.1.6 Evaluation on plasmid DNA

The extracted plasmid DNA was analyzed using 1% (w/v) agarose gel electrophoresis. 5 µl of plasmid DNA was mixed with 2 µl of 6*X* Orange Loading dye and loaded into the wells of the agarose gel. 5 µl of 1 kb DNA ladder was loaded into first lane and used as a marker. The electrophoresis was conducted at 100 V for 1 hour. DNA stained with ethidium bromide contained in the loading dye produced fluorescence under ultraviolet (UV) light and the DNA band was recognized once being separated. The size of the DNA band was estimated by comparing with the DNA ladder. The most prominent DNA band was excised using a gel cutter and sent for DNA

sequencing to First Base Laboratories Sdn Bhd to check for any DNA mutations. Universal primer of pQE-F (5' CCCGAAAAGTGCCACCTG 3' was used during the sequencing analysis. The DNA sequence was verified based on the NCBI database available at www.ncbi.nlm.nih.gov:80/BLAST/. Nucleotide blast (Basic Local Alignment Search Tool) with a blastn algorithm was used for the verification.

3.2.2 Protein expression

3.2.2.1 Preparation of mixture solutions

Preparations for *E.coli* strain and ampicillin are previously mentioned in Section 3.2.1.2.

LB medium

Ingredients: 5 g Yeast; 10 g Bacto-tryptone; 10 g NaCl; 10 ml dH_2O; 1 ml 100 mg/ml Ampicillin.

Preparation: The yeast and NaCl was dissolved in 1 L dH_2O. The medium was sterilized by autoclaving for 15 min at 120^{o}C. The medium was cooled to room temperature before being supplemented with ampicillin (working concentration 100 μg/ml).

IPTG solution

(0.5 M IPTG)

Ingredient: 1.192 g IPTG.

Preparation: IPTG was dissolved in 10 ml of dH_2O and sterile filtered with 0.20 μm CA membrane. The IPTG solution was aliquoted into 1 ml and stored at -20^{o}C, covered with aluminium foil.

Column buffer

(0.05 M HEPES, 0.3 M NaCl, pH 7.5)

Ingredients: 12 g HEPES; 8.78 g NaCl.

Preparation: The ingredients were dissolved in 900 ml dH_2O. The solution was adjusted to pH 7.5 with HCl or NaOH and the volume was made up to 1 L with dH_2O. The solution was sterilized with a 0.20 μm CA membrane and stored at 4^oC.

Lysis buffer

(5% (v/v) Glycerol, 0.1% (w/v) Lysozyme, 0.05 M HEPES, 0.3 M NaCl, pH 7.5)

Ingredients: 5 ml Glycerol, 0.1 g Lysozyme, 95 ml Column buffer.

Preparation: Glycerol and lysozyme were dissolved in 95 ml Column buffer. The pH was again assured to reach 7.5 and stored at 4^oC.

3.2.2.2 Protein expression

1 ml of glycerol stock was thawed and added into 20 ml of sterile LB medium containing 100 μg/ml of ampicillin. The culture was grown overnight at 37°C and 280 rpm. The next day, the overnight culture was inoculated into 1 L of LB medium containing 100 μg/ml of ampicilin and incubated at 37°C and 280 rpm until the OD600 nm reached 0.6. 1 ml of the bacteria culture was taken and centrifuged at 13,000 rpm for 1 min, in which the pellet was kept at -20°C for further analysis with SDS-PAGE as an 'Uninduced Protein'. The rest of the bacteria culture was added with IPTG to a final concentration of 1 mM to induce protein expression. The culture was further incubated for another 3 hours at 37°C and 250 rpm. After the incubation, 1 ml of the culture was taken and centrifuged at 13,000 rpm for 1 min, in which the pellet was kept at -20°C for further analysis with SDS-PAGE as an 'Induced Protein'. The rest of the induced bacteria culture was harvested by centrifugation at 10,000 rpm for 5 min, and the pellet

was stored at -80°C until further used.

The *E.coli* bacteria pellet was thawed at 4°C and resuspended in 5 ml of Lysis buffer for every 1 g of cell pellet. The resuspended pellet was sonicated for 5 pulses on ice, with each pulse for 30 seconds. Then, the sonicated lysate was centrifuged at 10,000 rpm, at 4 °C for 1 hour. The supernatant containing the protein was filtered through a 0.45 µm syringe filter with CA membrane. 0.5 ml of the filtered supernatant was taken and kept -20°C as 'Total Protein' for further analysis with SDS-PAGE.

3.2.3 Purification of NS2B-NS3pro

3.2.3.1 Preparation of mixture solutions

Imidazole solution

(2 M Imidazole, pH 7.5)

Ingredient: 13.615 g of Imidazole.

Preparation: Imidazole was dissolved in 80 ml of dH_2O. The solution was adjusted to pH 7.5 with HCl or NaOH. The solution was brought up to 100 ml and stored at 4^oC with the bottle covered with aluminium foil.

Binding buffer

(0.02 M Imidazole, 0.05 M HEPES, 0.3 M NaCl, pH 7.5)

Ingredients: 1 ml 2 M Imidazole pH 7.5; 99 ml Column buffer;

Preparation: Imidazole and column buffer was added together with a total volume of 100 ml. The buffer was at pH 7.5 and preserved at 4^oC prior usage.

Washing buffer

(0.05 M Imidazole, 0.05 M HEPES, 0.3 M NaCl, pH 7.5)

Ingredients: 2.5 ml 2 M Imidazole pH 7.5; 97.5 ml Column buffer

Preparation: Imidazole and column buffer was added together with a total volume of 100 ml. The buffer was at pH 7.5 and preserved at 4^{o}C prior usage.

Elution buffer

(0.1 M Imidazole, 0.05 M HEPES, 0.3 M NaCl pH 7.5)

Ingredients: 10 ml 2 M Imidazole pH 7.5; 90 ml Column buffer;

Preparation: Imidazole and column buffer was added together with a total volume of 100 ml. The buffer was at pH 7.5 and preserved at 4^{o}C prior usage.

3.2.3.2 Resin and columns

Ni-NTA agarose resin self-packed in P-D10 column was used for purification using Ni-immobilized metal affinity chromatography (Ni-IMAC). Size exclusion chromatography (SEC) was performed using a pre-packed column; the Hi-Load Superdex 16/600 75 prep grades with mean bead size of 34 μm**.**

3.2.3.3 Purification using Ni-IMAC

Ni-IMAC purification was performed at 4°C. Firstly, 2 ml of Ni-NTA agarose resin was loaded into the P-D10 column. The column was let to stand to drain the 20% ethanol out from the resin. Next, the resin was washed with 5 column volume (5 CV) of MiliQ water (10 ml) and equilibrated with 5 CV of binding buffer. The sonicated protein solution together with the equilibrated resin were loaded into a 50 ml eppendorf tube and equilibrated for 1 hour by inversion slowly on a rotator. This is to allow the his-tagged protein to bind to the Ni-NTA resin. After 1 hour, the resin with bound his-tagged protein was allowed to reside onto the bottom of the tube by allowing it to stand for 20 min. 0.5 ml of the supernatant was collected and kept at -20°C as ‘Non-Binding

Protein' for further analysis with SDS-PAGE. The resin with bound protein was resuspended with 20 ml of binding buffer and the whole mixture solution was transferred back into the P-D10 column. The column was allowed to stand to drain out the binding buffer. Immediately without drying the resin, 30 ml of washing buffer was loaded into the column. The first, second and last fractions were collected and kept at -20°C as 'first wash', 'second wash' and 'last wash' for further analysis with SDS-PAGE. Finally, the his-tagged protein bound to the Ni-NTA resin was eluted from the column using the elution buffer and each 1 ml elution was collected into a 1.5 ml microtube. 20 µl from each elution were taken and kept at -20°C as elution 1 to 3 (E1, E2 and E3) for further analysis with SDS-PAGE and Western blot analysis. The rest eluates were pooled and concentrated using the Vivaspin Turbo 15 (10 k MWCO) at 4000 x g, 4°C. The pooled protein was further purified using SEC (Section 3.2.3.3), used to determine its concentration using Bradford assay (3.2.5), identified with Mass Spectrometry (MS) analysis (Section 3.2.7) and further characterized for its oligomeric states with SEC and native PAGE (Section 3.2.8 and 3.2.9).

3.2.3.4 Purification using SEC

Elutions from Ni-IMAC were further purified using the SEC column; the Hi-Load Superdex 16/60 75. The column was clamped to stand onto the AKTA PRIME system and left to equilibrate with the cold temperature, 4°C. Once cooled, the whole purification system was equilibrated with MiliQ water. First, the AKTA PRIME was equilibrated with 75 ml of MiliQ water at high flow rate (50 ml/ min) to wash, and remove any bubbles from the tubing system. Next, 10 ml of MiliQ water was manually injected onto the sample loop using a syringe. By adjusting the system to 'Manual run', the column was allowed to equilibrate with 5 CV (300 ml) of MiliQ water under maximum flow rate of 1 ml/min with the limit pressure set to 0.3 MPa. The system was

set to INJECT mode to allow the MiliQ water to run through the sample loop. The whole AKTA PRIME system and the column was equilibrated with the column buffer by following the same method used during the equilibration with MiliQ water. The next step was the injection of 1 ml of the concentrated protein (elution from Ni-IMAC) into the sample loop of the AKTA PRIME system. Once injected, the system was set to 1 ml/min with an INJECT mode so that the protein solution will be transferred from the sample loop into the system and eventually the column. Protein eluates were monitored at 280 nm and the elution were manually fractionized into 1.5 ml microtube. Once eluted, the protein was immediately kept on ice. Protein fractions from the peak of interest were concentrated with Vivaspin Turbo 15 and spun at 4000 x g, 4°C. The concentrated protein was further used in Bradford assay (3.2.5), MS analysis (Section 3.2.7) and the characterization of oligomeric states with SEC and native PAGE (Section 3.2.8 and 3.2.9).

3.2.4 Protein separation with SDS-PAGE

3.2.4.1 Preparation of mixture solutions

Monomer Solution

(30% (w/v) Acrylamide, 0.8% (w/v) Bis-acrylamide)

Ingredients: 60 g Acrylamide; 1.6 g N,N'-methylene-bis-acrylamide.

Preparation: The acrylamide was dissolved in 150 ml distilled water, followed by the addition of bis-acrylamide. The solution was brought to a final volume of 200 ml with dH_2O, covered the bottle with aluminium foil and stored at 4^oC,

Resolving gel buffer (4*X*)

(1.5 M Tris-HCl, 0.4% (w/v) SDS, pH 8.8)

Ingredients: 18.171 g Tris base; 0.4 g SDS.

Preparation: Tris was dissolved in 450 ml distilled water and the pH was adjusted to 8.8 with HCl. The solution was topped up until 500 ml with dH_2O and stored at 4^oC.

Stacking gel buffer (4*X*)

(0.5 M Tris-HCl, 0.4% (w/v) SDS, pH 6.8)

Ingredients: 6.05 g Tris base; 0.4 g SDS.

Preparation: The ingredients were dissolved in 50 ml dH_2O and the pH was adjusted to 6.8 with HCl. The solution was topped up until 100 ml with dH_2O and stored at 4^oC.

APS solution

(10% (w/v) APS)

Ingredient: 0.1g APS.

Preparation: APS was dissolved in 1 ml dH_2O and aliquoted into 20 µl and stored in 100 µl micorutubes at -20^oC for 1year storage.

Running buffer (5*X*)

(0.125 M Tris base, 0.96 M Glycine)

Ingredients: 7.55 g Tris base; 36.0 g Glycine; 2.5 g SDS.

Preparation: All ingredients were dissolved in 500 ml dH_2O and stored at 4^oC. This stock solution was diluted to 1*X* using dH_2O prior to use.

Sample loading buffer (2*X*)

(0.125 M Tris pH 6.8, 0.5% SDS, 20% Glycerol, 2% (w/v) β-mercaptoethanol, 0.01% (w/v) Bromophemol blue)

Ingredients: 2.5 ml Stacking gel buffer; 4 g SDS, 2 ml Glycerol; 2 µl β-mercaptoethanol; 0.0001 g Bromophenol blue.

Preparation: The ingredients were dissolved in dH_2O and brought to a final volume of 10 ml before being aliquoted into 1 ml and stored at 4^oC.

Coomasie blue staining solution

(0.05% (w/v) Coomasie brilliant blue (CBB) R-250, 50% (v/v) Methanol, 10% (v/v) Acetic acid, 40% (v/v) dH_2O)

Ingredients: 0.25 g CBB R-250; 250 ml Methanol; 50 ml Acetic acid; 200 ml dH_2O.

Preparation: The CBB R-250 was dissolved in methanol before adding acetic acid and dH_2O to a total volume of 500 ml. The solution was stored at room temperature for 6 months.

Destaining solution

(30% (v/v) Methanol, 10% (v/v) Acetic acid, 60% (v/v) dH_2O)

Ingredients: 300 ml Methanol; 100 ml Acetic acid; 600 ml dH_2O.

Preparation: The solution was prepared in volume size of 1 L and stored at room temperature.

Fixing solution

(10% (v/v) Acetic acid, 50% (v/v) Methanol, 40% (v/v) dH_2O)

Ingredients: 100 ml Acetic acid; 500 ml Methanol; 400 ml dH_2O.

Preparation: The solution was prepared in volume size of 1 L and stored at room temperature for 1 month.

Storage solution

(5% (v/v) Acetic acid; 95% (v/v) dH_2O)

Ingredients: 50 ml Acetic acid; 500 ml Methanol; 950 ml dH_2O.

Preparation: The solution was prepared in volume size of 1 L and stored at room temperature for 3 weeks.

3.2.4.2 Readily prepared mixture solutions

BlueRAY prestained protein ladder (11- 180 kDa).

3.2.4.3 Preparation of 12% SDS-PAGE gel

a) Resolving gel solution

Ingredients: 3.75 ml Resolving Gel Buffer (4*X*), 6 ml Monomer Solution; 5.25 ml dH_2O; 10 µl N,N,N',N'-tetramethylethyldiamine (TEMED); 50 µl APS Solution.

Preparation: First, two cleaned glass-plates were assembled together and clipped together before being clipped again on a casting frame. Secondly, a 20 ml beaker was used to mix all the ingredients above, accept for the APS solution, which was added last. Once mixed, instantly the mixture was poured into the sandwiched plates with full care to avoid bubble formation. A layer of methanol (approximately 1 cm in height) was poured on top of the separating solution to compress the solution while casting it into a gel, ensuring an even formation of the gel. The gel was allowed to polymerize for approximately 35 min at room temperature.

b) Stacking gel solution

Ingredients: 1.25 ml Stacking Gel Buffer (4**X**); 650 µl Monomer Solution; 3.05 ml dH_2O; 5 µl TEMED; 25 µl APS Solution.

Preparation: Once the separating gel has polymerized, the methanol layer on top of the separating gel was poured out. All the ingredients above were mixed and APS Solution was added right before casting. A 0.75 mm Teflon comb was inserted onto the stacking solution to form wells and was allowed to polymerize for 35 min at room temperature.

3.2.4.4 Analysis with 12% SDS-PAGE

The purity of NS2B-NS3pro eluted from Ni-IMAC and SEC was analyzed on the 12% SDS-PAGE. 7 µl of the protein sample was mixed with 7 µl of the sample loading buffer (2***X***) and heated at 100°C for 5 min to denature the proteins before being loaded into the wells on the SDS-PAGE. Protein marker (BlueRAY prestained protein ladder, 11 - 180 kDa) was loaded onto one of the well. Protein electrophoresis was at first conducted in the running buffer (1*X*) at 90 V and 25 mA. When the protein had reached the resolving gel, the voltage was increased to 100 V and leaved to run for 1 hour 30 min. Next, the gel was fixed with the fixing solution for 1 hour to prevent the protein from leaking out from the gel during the next staining process. The gel was stained with the heated coomassie blue staining solution for 30 min followed by destaining for overnight under a slow shake. Protein that bound to the CBB R-250 (from the staining solution) appeared as blue bands on the gel. The gel was stored in the storage solution for Western blot (Section 3.2.6) and MS (Section 3.2.7) analyses.

3.2.5 Determination of protein concentration with Bradford Assay

3.2.5.1 Readily prepared mixture solutions

Quick Start™ Bradford Protein Assay Kit (Biorad) containing 2 mg/ ml Bovine Serum Albumin (BSA) Standard and Bradford Dye Reagent.

3.2.5.2 Bradford assay

The reaction mixture was prepared to a total volume of 200 µl in UV-transparent 96-well plate and measured using the Bio-Rad microplate reader. Before measuring the protein concentration, a BSA standard assay consists of five different concentrations of BSA (0.05 - 1.00 mg/mL) was prepared in 10 µl each. 190 µl of Quick Start Bradford Dye Reagent was added to achieve a total volume of 200 µl per mixture. Each

concentration of the BSA standard was prepared in triplicate. The microplate was then incubated for 7 min at room temperature. The absorbance value was measured using the microplate reader at an absorbance wavelength of 595 nm. The output was displayed in a form of absorbance unit, and each triplicate was averaged and plotted into a standard graph to obtain an equation from the straight line. Protein concentration was determined by adding 10 µl of the protein solution into the microplate in triplicate. Each triplicate was added with 190 µl of the Quick Start Bradford Dye Reagent. This was repeated for blanks (the buffer used to elute protein from Ni-IMAC and SEC respectively). The resulted absorbance was added into equation (1) to calculate the concentration of the protein.

Next is an example to calculate the concentration of NS2B-NS3pro eluted from SEC (peak c) using equation (1) developed from the BSA standard curve (Section 4.1.3, Figure 4.8).

Absorbance of NS2B-NS3pro from peak c at 595 nm = 0.522 Au

Absorbance of blank (column buffer) at 595 nm = 0.364 Au

Actual absorbance of NS2B-NS3pro from peak c = (0.522 – 0.364) Au = 0.158 Au

Therefore, the concentration of NS2B-NS3pro from peak c =

y = 0.4904x (y is the absorbance and x is the concentration) ---------- (1)

x = y/ 0.4904

x = 0.158/ 0.4904

x = **0.322 mg/ml**

The size of NS2B-NS3pro as according to the SDS-PAGE analysis is 35kDa. Therefore the concentration of NS2B-NS3pro from peak c as converted into µM is

$$= \frac{0.322 \text{ mg/ ml}}{35000 \text{ kDa}}$$

$$= \frac{0.322 \text{ mg/ ml}}{35000 \text{ g/ mol1111}}$$

$$= \frac{0.322 \text{ mg/ ml}}{35000 \text{ mg/ mmol}}$$

= 0.0000092 mmol/ ml

= 0.0000092 mol/ L

= 0.0000092 M

= **9.2 µM**

3.2.6 Protein identification using Western blot analysis

3.2.6.1 Preparation of mixture solutions

Transfer buffer

(0.025 M Tris base, 0.192 M Glycine/ 10% (v/v) Methanol)

Ingredients: 3 g Tris base; 14.4 g Glycine; 100 ml Methanol.

Preparation: The ingredients were added together and brought to a final volume of 1 L. The solution was stored at 4^{o}C.

TBS (Tris buffered saline) TBS

(0.05 M Tris-HCl, 0.15 M NaCl, pH 7.6)

Ingredients: 3.029 g Tris Base; 4.383 g NaCl.

Preparation: The ingredients were dissolved in 400 ml dH_2O and the pH was adjusted to 7.6 with HCl. The solution was topped up until 500 ml with dH_2O and stored at 4^{o}C.

TBST (Tris buffered saline with Tween)

(0.05 M Tris-HCl, 0.15 M NaCl, 0.05% (v/v) Tween 20, pH 7.6)

Ingredients: 3.029 g Tris Base; 4.383 g NaCl.

Preparation: The ingredients were dissolved in 400 ml dH_2O and the pH was adjusted to 7.6 with HCl. The solution was brought up to 500 ml with dH_2O and stored at 4^oC.

Blocking solution

(5% (w/v) Non-fat Dry Milk in TBS solution)

Ingredients: 2.5 g Non-fat Dry Milk; 50 ml TBS.

Preparation: Non-fat Dry Milk was dissolved in 50 ml TBS solution and was filtered with 0.45 um filter and stored at 4^oC.

3.2.6.2 Western blot analysis

Protein bands from the SDS-PAGE gel was further identified using the western blot analysis. First, a nitrocellulose membrane precisely cut to the size of the whole SDS-PAGE gel was pre-wetted with the transfer buffer. The membrane was attached to one side of the gel and no bubbles were developed during the attachment to avoid the formation of blurry bands. Next, six filter papers were pre-wetted in the transfer buffer with each three were stacked on both sides of the gel (where the other side of the gel had been attached with the membrane). Later, two fiber pads were included into the sandwich, each covering on both sides. Finally, two cassette holders were assembled together with the sandwich set, with the nitrocellulose membrane facing the anode and the gel facing the cathode. The sandwich set was placed into the electrophoretic system. Transfer buffer were added into the tank together with an ice block and left to run at 100 V for 1 hour.

The following step was blocking the nitrocellulose membrane with blocking solution for overnight at 4°C. The nitrocellulose membrane was incubated with primary antibody (the monoclonal anti-his-tag monoclonal antibody, final concentration 1 μg/ml) in the blocking solution for 1 hour at room temperature on a shaker at low speed. Subsequently, the membrane was rinsed with TBS solution followed by washing with TBST solution for 3 times, wherein with every 15 min the membrane was washed with TBS solution. Blocking solution was added to cover the membrane with the secondary antibody (mouse IgG antibody, final concentration 1 μg/ml) and incubated for 1 hour. The membrane was washed again with TBS and TBST solutions using the similar steps mentioned above. Finally, Western blue stabilized substrate for Alkaline phosphatase (Promega) was added just to cover the membrane to allow the detection of the colorimetric bands indicating the NS2B-NS3pro.

3.2.7 In-gel tryptic digestion for Mass Spectrometry (MS) analysis

3.2.7.1 Preparation of mixture solutions to extract protein

All solutions were prepared freshly prior usage and pH adjustment was not required.

0.1 M Ammonium bicarbonate (NH_4HCO_3)

Ingredient: 0.3953 g NH_4HCO_3.

Preparation: NH_4HCO_3 was dissolved in 50 ml dH_2O (the pH was approximately at 8 by default).

Buffer A

(50% (v/v) Acetonitrile (ACN), 0.05 M NH_4HCO_3)

Ingredients: 10 ml 100% ACN; 10 ml 0.1 M NH_4HCO_3.

Preparation: The ingredients were mixed together with a total volume of 20 ml.

Buffer B

(0.01 M Dithiothreitol (DTT), 0.1 M NH_4HCO_3)

Ingredients: 0.077 g DTT; 5 ml 0.1 M NH_4HCO_3.

Preparation: DTT was dissolved in NH_4HCO_3 to a total volume of 5 ml.

Buffer C

(0.055 M IAA, 0.1 M NH_4HCO_3)

Ingredients: 0.051 g IAA; 5 ml 0.1 M NH_4HCO_3.

Preparation: IAA was dissolved in NH_4HCO_3 to a total volume of 5 ml. The preparation was made in dark as IAA is unstable and light-sensitive.

Buffer D

(50% ACN, 0.1 M NH_4HCO_3)

Ingredients: 0.237 g NH_4HCO_3; 30 ml 100% ACN.

Preparation: NH_4HCO_3 was dissolved in ACN to a total volume of 30 ml.

50% (v/v) ACN

Ingredients: 500 µl ACN.

Preparation: ACN was mixed with 500 µl dH_2O to reach a total volume of 1 ml.

3.2.7.2 Preparation of trypsin

a) Preparation of trypsin in acetic acid

Trypsin was constantly kept on ice during the preparation.

0.05 M Acetic acid

Ingredients: 28.62 µl Acetic acid; 9.971 ml dH_2O.

Preparation: The ingredients were mixed together with a total volume of 10 ml.

1µg/µl Trypsin/0.05 M Acetic acid

Ingredients: 100 µg Trypsin; 100 µl 0.05 M Acetic acid.

Preparation: The ingredients were mixed together with a total volume of 100 µl.

b) Preparation of Trypsin/Acetic acid in NH_4HCO_3

10ng/µl Trypsin/Acetic acid, 0.05 M NH_4HCO_3

5 µl 1µg/ µl Trypsin/ 0.05 M Acetic acid; 495 µl 0.05M NH_4HCO_3.

Preparation: The ingredients were mixed together with a total volume of 500 µl.

3.2.7.3 Preparation of mixture solutions to desalt protein

Sample/ Equilibration/ Wash solutions

(0.1% (v/v) Formic Acid (FA)/ 99.9% (v/v) dH_20)

Ingredients: 15 µl FA; 14.985 ml dH_20

Preparation: Both ingredients were mixed to a total volume of 15 ml.

Wetting solution

50% (v/v) ACN

Ingredients: 500 µl ACN

Preparation: ACN was mixed with 500 µl dH_2O to reach a total volume of 1 ml.

Elution solution

(0.1% (v/v) FA/ 50% (v/v) ACN)

Ingredients: 10 µl FA; ml 5 ml 100% ACN; 4.99 ml dH_20.

Preparation: Both ingredients were mixed to a total volume of 10 ml.

3.2.7.4 In-gel digestion with trypsin

The SDS-PAGE gel containing protein band was excised into small sizes. These small gels were transferred into a 1.5 ml microtube. 50 µl of buffer A was added to destain the gel and shook until the blue dye on the gels was cleared off. Buffer A was removed and 150 µl of buffer B was added and shook for 30 min at 60°C. Then it was left to cool at room temperature. Buffer B was removed and changed with 150 µl buffer C for alkylation (incubated in dark for 20 min). Buffer C was removed and the gels were washed with 500 µl buffer D for 20 min, in which was repeated for three times. Buffer D was removed and the gels were dehydrated with 50 µl of 100% ACN, shook for 10 - 15 min. The gels were dried off using a speed vacuum for 10 min at room temperature. Digestion was carried out by adding 25 µl of 10 ng/µl Trypsin/Acetic acid in 0.05 M NH_4HCO_3 for 16 hours at 37°C. Afterwards, the gel-mixture was vortexed for a while and spun for 1 min at 1000 rpm. Digested protein was extracted from the gel by adding 50 µl of 50% ACN and shook for 15 min. The solution was transferred into a new microtube. Then, 50 µl of 100% ACN was added and shook for 15 min. The protein extraction solution was kept at -20°C for further process with desalting.

3.2.7.5 Desalting and spotting

a) Reconstitution of in-gel digested protein solution

Before desalting, the protein extraction solution was dried out using a speed vacuum until all ACN was evaporated. Next, 10 µl of sample solution was added and reconstituted with vortex followed by a brief spin.

b) Preparation of ZipTip

By using a ZipTip, 10 µl of wetting solution was aspirated and discarded on a tissue (repeated for three times). Next, 10 µl of equilibration solution was aspirated and

discarded on a tissue (repeated for three times). Then, the in-gel digested protein solution was aspirated (repeated for ten times). 10 µl of wash solution was aspirated and discarded on a tissue (repeated for three times). Then the digested protein was eluted with 1.5 µl of elution solution into an empty microtube.

c) Spotting onto sample plate

By using a 10 µl pipette tip, 1.5 µl of the elution was mixed with 1.5 µl of matrix in an instant. 0.7 µl of the mixture was spotted on a sample plate.

3.2.8 Determination of the oligomeric states of NS2B-NS3pro using SEC

The column buffer (Section 3.2.2.1) was used for this purpose on the Hi-Load Superdex 16/60 75 pg column.

3.2.8.1 Readily prepared mixture solutions

Gel Filtration Molecular Weight (MW) Markers Kit for MWs 12 – 2,000 kDa (Sigma). Each standard protein was mixed to dissolved in column buffer and 5% (v/v) glycerol to a concentration of 4 mg/ml 200 kDa β-Amylase, 5 mg/ml alcohol dehydrogenase (150 kDa), 10 mg/ml albumin (66 kDa) and 3 mg/ml carbonic anhydrase (29 kDa). 2 mg/ml Blue Dextran (2000 kDa) was prepared separately in the same buffer preparation. All protein solutions were filtered through 0.45 µm and kept on ice prior usage.

3.2.8.2 Determination of the oligomeric states

Instead of purification, SEC was also used to determine the oligomeric states of NS2B-NS3pro. For this purpose, the column was calibrated with the protein MW markers. The void volume (V_O) of the column was determined by injecting 1 ml of blue

dextran. Once eluted, the elution volume (V_e) was determined by injection of 1 ml protein standard mixture containing β-Amylase, alcohol dehydrogenase, albumin and carbonic anhydrase. The calibrations were performed at flow rate of 1 ml/min and the eluates were monitored at 280 nm. The oligomeric states of NS2B-NSpro were determined from the calibration curve based on the $\log_{10}$ MW versus V_e/V_o of the protein MW markers (Section 4.1.4, Figure 4.9).

The equation developed from the calibration curve, y = -0.9575x + 3.2324 was used to determine the size of oligomeric NS2B-NS3pro. As an example, the oligomeric size for NS2B-NS3pro from peak c was calculated by dividing its elution volume (64 ml, Section 4.1.2, Figure 4.7A) by the value of V_o from the blue dextran (45.81 ml, Section 4.1.4, Figure 4.9). The resulted value (1.14) was added to replace the x integer in the calibration equation. With this, the y integer, which is the $\log_{10}$ MW of NS2B-NS3pro was calculated as 1.892. Subsequently, the value in the y integer was antilogged to gain an approximate MW of the oligomer. Finally, the native oligomeric state of NS2B-NS3pro was determined by dividing the MW of the oligomeric NS2B-NS3pro (78 kDa) with the MW observed from the SDS-PAGE (35 kDa) (Section 4.1.3, Table 4.1).

3.2.9 Determination of the oligomeric states of NS2B-NS3pro using native PAGE

3.2.9.1 Preparation of mixture solutions

0.375 M Tris-HCl, pH 8.8

Ingredients: 2.27 g Tris base.

Preparation: Tris base was dissolved in 40 ml dH_2O the pH was adjusted to 8.8 with HCl. The solution was brought up to 50 ml with dH_2O and stored at 4^oC.

0.625 M mM Tris-HCl, pH 6.8

Ingredients: 3.78 g Tris base.

Preparation: Tris base was dissolved in 40 ml dH_2O the pH was adjusted to 6.8 with HCl. The solution was brought up to 50 ml with dH_2O and stored at 4^oC.

Sample loading buffer (2*X*)

(0.625 M Tris-HCl pH 6.8; 25% (v/v) Glycerol; 1% (v/v) Bromophenol blue)

Ingredients: 7.4 ml 0.625 M Tris.Cl pH 6.8; 2.5 ml Glycerol; 100 µl Bromophenol blue.

Preparation: The ingredients were added together and brought to a final volume of 10 ml. The solution was aliquoted into 1 ml and stored at 4^oC.

Running buffer

(0.025 M Tris base/ 0.192 M Glycine)

Ingredients: 4.54 g Tris base; 28.8 g Glycine.

Preparation: The ingredients were added together and brought to a final volume of 2 L. The solution was stored at 4^oC.

Coomasie blue staining solution

(0.3% (w/v) Coomasie brilliant blue (CBB) R-250, 45% (v/v) Methanol, 10% (v/v) Acetic acid, 45% (v/v) dH_2O)

Ingredients: 1.5 g CBB R-250; 225 ml Methanol; 50 ml Acetic acid; 225 ml dH_2O.

Preparation: The CBB R-250 was dissolved in methanol before adding acetic acid and dH_2O to a total volume of 500 ml. The solution was stored at room temperature for 6 months.

Destaining solution

(20% (v/v) Methanol, 10% (v/v) Acetic acid, 70% (v/v) dH_2O)

Ingredients: 200 ml Methanol; 100 ml Acetic acid; 700 ml dH_2O.

Preparation: The solution was prepared in volume size of 1 L and stored at room temperature.

Fixing solution

The same fixing solution used for SDS-PAGE (as in Section 3.1.1.4.1) was prepared.

3.2.9.2 Readily prepared mixture solutions

The kit for Molecular Weights 14 – 500 kDa kDa Non-denaturing PAGE contains albumin from chicken egg white (45 kDa), albumin from bovine serum (66 kDa for monomer and 132 kDa for dimer) and urease from jack bean (272 kDa for trimer and 545 kDa for hexamer). Each of these standard protein was dissolved in 1 ml MiliQ water, except for Urease that was dissolve in a mixture of 0.5 ml MiliQ water and 0.5 ml glycerol.

3.2.9.3 Preparation of 12% native PAGE gel

The method of preparations for both resolving and stacking gel solutions were the same as with that prepared for 12% SDS PAGE-gel (Section 3.2.4.3). The solutions used to prepare both gels are mentioned below.

Resolving gel solution

Ingredients: 5.89 ml 0.375 M Tris-HCl, pH 8.8; 4 ml 30% Acrylamide/ 0.8% Bisacrylamide, 10 µl TEMED, 100 µl 10% APS solution.

Stacking gel solution

Ingredients: 4.275 ml 0.375 M Tris-HCl, pH 8.8; 670 µl 30% Acrylamide/ 0.8% Bisacrylamide, 5 µl TEMED, 50 µl 10% APS solution.

3.2.9.4 Determination of the oligomeric states

The oligomeric state of the DENV-2 NS2B-NS3pro was validated using native PAGE. 7 µl of the eluate from SEC (each from peak a, b and c) was mixed with 7 µl of the sample loading buffer (2***X***) and the mixture was loaded into the wells on the native PAGE. The protein markers were loaded into the wells to an amount of 5 µg for both urease and albumin from chicken egg white and 2.5 µg for albumin from bovine serum. Native PAGE gel was filled with the running buffer and conducted at 100 V and 25 mA in a cold temperature, 4°C. The analysis was conducted until the bromophenol blue dye front reaches the bottom of the gel. Next, the gel was fixed with the fixing solution for 1 hour followed by staining with the coomasie blue staining solution for 30 min. The gel was destained for overnight with the destaining solution under a slow shake. Native proteins that bound to CBB R-250 from the staining solution appeared as blue bands on the gel.

3.3 SPR assay

Buffer solutions were filtered through 0.20 μm CA membrane to remove particles that can clog the IFC (Integrated μ-Fluidic Cartridge) of the sensor chip and were degassed daily in an ultrasonic bath for approximately 10 min to remove air bubbles.

3.3.1 Handling the amine coupling kit and the sensor chips

Amine coupling kit (containing 0.75 g EDC, 0.115 g NHS and 10.5 ml of 1 M ethanolamine-HCl, pH 8.5. NHS and EDC were reconstituted in 10 ml MiliQ water to a final concentration of 0.4 M and 0.1 M respectively, filtered through 0.20 μm CA membrane and aliquoted into 100 μl inside the typical 1.5 ml propylene microtube and stored at -20°C. CM5 and NTA chips were stored at 4°C, with the chips kept constantly dry in an empty 50 ml eppendorf tube.

3.3.2 Readily prepared buffers from GE Healthcare

HBS-EP buffer (Dispenser buffer)

(0.01 M HEPES, 0.15 M NaCl, 0.005% Surfactant P20, 0.003 M EDTA, pH 7.4)

HBS-P buffer

(0.01 M HEPES, 0.15 M NaCl, 0.005% Surfactant P20, pH 7.4)

3.3.3 Preparation of stock solutions

All stock solutions were filtered through 0.20 μm CA membrane before being stored at 4°C for 1 week.

1 M HEPES

Ingredient: 11.915 g HEPES.

Preparation: HEPES was dissolved in 40 ml MiliQ water. The pH was adjusted to 7.4 and the solution was brought up to 50 ml.

1 M NaCl

Ingredient: 2.922 g NaCl.

Preparation: NaCl was dissolved in 40 ml MiliQ water. The pH was adjusted to 7.4 and the solution was brought up to 50 ml.

0.5 M NaEDTA

Ingredients: 18.612 g NaEDTA; 5M NaOH.

Preparation: 18.612 g NaEDTA was dissolved in 50 ml 5M NaOH while adjusting the pH to 8. The solution was brought up to 100 ml with MiliQ water.

0.5 M $NiCl_2$

Ingredients: 0.648 g $NiCl_2$

Preparation: $NiCl_2$ was dissolved in 10 ml MiliQ water.

10*X* PBS

(0.1 M PBS, pH 6.8)

Ingredients: 5 PBS tablets in MiliQ water.

Preparation: PBS tablets were dissolved in 180 ml MiliQ water. The pH was adjusted to 6.8 and the solution was brought up to 200 ml with MiliQ water.

1.01*X* PBS (Sample buffer)

(0.01 M PBS, pH 6.8)

Ingredients: 101 ml 10x PBS; 899 ml MiliQ water.

Preparation: All ingredients were mixed to a total volume of 1 L without the pH being adjusted.

3.3.4 Preparation of buffers

All buffers prepared in-house were made freshly from fresh stock solutions, filtered through 0.20 μm CA membrane and were sonicated before usage.

Running buffer A

(1.01*X* PBS, 1% DMSO, pH 7.4)

Ingredients: 10 ml DMSO, 990 ml 1.01*X* PBS.

Preparation: All ingredients were mixed to a total volume of 1 L and yielded pH 7.4.

Running buffer B

(0.01 M HEPES, 0.15 M NaCl, 0.005% Surfactant P20, 50 μM NaEDTA, pH 7.4)

Preparation: 50 ml NaEDTA was added to 450 ml HBS-P buffer to produce a total volume of 500 ml.

Ni Solution

(0.01 M HEPES, 0.15 M NaCl, 0.005% Surfactant P20, 50 μM NaEDTA, 500 μM $NiCl_2$, pH 7.4)

Ingredients: 3 μl $NiCl_2$ in Running buffer.

Preparation: 3 μl $NiCl_2$ was added to 2997 μl running buffer to produce a total volume of 3 ml.

Regeneration buffer

(0.01 M HEPES, 0.15 M NaCl, 0.005% Surfactant P20, 0.35 M NaEDTA, pH 7.4)

Ingredients: 50 µl HEPES; 750 µl NaCl; 3.5 ml NaEDTA; 2.5 µl 10% Surfactant P20.

Preparation: All the ingredients were mixed and brought to 5 ml by adding 697.5 µl of MiliQ water.

Regeneration solutions

10 mM Glycine-HCl at pH 3.0, 2.5, 2.0, and 1.5, and 0.05 M NaOH purchased from GE Healthcare. 1 M NaCl and 10 mM HCl pH 1 were prepared in house.

3.3.5 Analyte preparation

All analytes were first dissolved in 100% DMSO to a final concentration of 1 M. However, for binding analysis with SPR assay, only 1% of DMSO was used. A sample buffer was added to the stock analyte contained in 100% DMSO so that the constituents of the buffer matched with the running buffer (running buffer A). The DMSO from the analyte stock solution converted the pH of the sample buffer from 6.8 to 7.4, a pH that matched with the running buffer (running buffer A) (Symposium, 2002). Glass vial Ø 9 mm was used during the analyte preparation to avoid adsorption of the analyte to vials. Analyte preparation was performed in a dark area with less aeration to avoid evaporation of DMSO. The vials were kept at room temperature for 24 hours to observe for possible precipitation.

3.3.6 SPR assay on CM5 chip

3.3.6.1 Ligand preparation

The NS2B-NS3pro solution from SEC (peak c) was eluted with the column buffer. The NS2B-NS3pro solution was dialyzed into 10 mM sodium acetate pH 4 and pH 5 respectively using the Hi-Trap desalting column as a preparation for pH scouting.

3.3.6.2 pH scouting

Once the sensor chip was docked, the system was primed for two times using the running buffer (HBS-P) to flush the system and to remove air bubbles (SPR-pages, 2015b). By using the Biacore control software, the wizard for 'Immobilization pH scouting' was selected. 80 µl of 50 µg/ml NS2B-NS3pro in 10 mM sodium acetate at pH 4 and 5 was sequentially injected into the unmodified Fc2 of the CM5 chip for 2 min, with a flow rate of 20 µl/min. Subsequently, the sensor surface was regenerated with 50 mM NaOH to completely remove NS2B-NS3pro.

3.3.6.3 Immobilization with amine coupling

By choosing the 'Aim for immobilized level' wizard, an immobilization level of 6000 RU of NS2B-NS3pro was targeted. Fc1 was treated the same way in Fc2 but omitting the immobilization. At a flow rate of 10 µl/min, both Fc1 and Fc2 were activated with the EDC/NHS solution (mixed by the Biacore system to 1:1 ratio) for 7 min. 50 µg/ml of NS2B-NS3pro reconstituted in 10 mM sodium acetate buffer of pH 4 (as previously optimized during pH scouting) was injected for 5 min into Fc2 for immobilization. Subsequently, both Fc1 and Fc2 were blocked with ethanolamine for 3.5 min to deactivate the remaining surface that was not reacted with NS2B-NS3pro.

3.3.7 SPR assay on NTA chip

3.3.7.1 Ligand preparation

The NS2B-NS3pro was eluted from SEC (peak c) using the column buffer. To match with the running buffer (running buffer B) used for capture coupling, 75 µl of 1 M NaCl and 4 µl of 1M HEPES were added to a 31.25 µl of 9.2 µM NS2B-NS3pro solution (Bradford assay, Section 3.2.5.2). The remaining volume was filled up with running buffer B to a final volume of 200 µl to yield a 50 µg/ml of NS2B-NS3pro.

3.3.7.2 Ligand concentration scouting

Scouting for optimal concentration of NS2B-NS3pro that can reach the target immobilization level of 6000 RU was carried out by capturing 20, 30, 40 and 50 µg/ml of NS2B-NS3pro. The system was primed for two times with the dispenser pump (right pump) immersed into the dispenser buffer and the eluent pump (left pump) into the running buffer (running buffer B). A sequential injection was carried out to activate the NTA chip with Ni solution (40 µl at 40 µl/min), scouting with NS2B-NS3pro (10 µl at 5 µl /min) and the regeneration buffer to regenerate and wash the sensor surface (20 µl at 25 µl/min).

3.3.7.3 Immobilization with capture coupling

NS2B-N3pro was immobilized onto the NTA chip by capture coupling. In sequential injections, NTA surface was activated with Ni solution (40 µl at 40 µl/min) followed by a second activation with EDC/NHS mixture solution (1:1 ratio) (30 µl at 5 µl/min), 50 µg/ml of NS2B-NS3pro was immobilized (25 µl at 5 µl/min), blocked with 1 M ethanolamine (35 µl at 5 µl/min) and finally washed with the regeneration buffer (20 µl at 25 µl/min). Refer to Appendix D for the dialog box for capture coupling.

3.3.7.4 Regeneration scouting and surface performance test

Regeneration scouting was carried out to wash analyte that binds to NS2B-NS3pro. Several regeneration scouting was evaluated using 1M NaCl, 10 mM glycine of pH 3 and 2.5, and 10 mM HCl of pH 1 against 200 µM rolitetracycline. By using the 'Regeneration' wizard, a 'single injection' option was used to enable a sequential injection of analyte and the regeneration solution at 20 µl/min for 1 min, until more than 90% of analyte (rolitetracycline) was regenerated. The best regeneration solution that was able to regenerate the analyte was further verified using the 'Surface

performance test' wizard and examined for its affectivity against the activity of NS2B-NS3pro.

3.3.7.5 Binding analysis

In the binding analysis, a concentration range of analytes between 0 – 500 μM were injected. The concentration range was selected starting from the lowest concentration of analyte that showed measurable binding. The maximum concentration of analyte was selected when the response levels had reached constant values. Sample buffer, or regarded as blank (0 μM), was injected over NS2B-NS3pro prior injection of analytes. This was particularly useful for double referencing. The analyte and sample buffer was injected in triplicate (50 μl/min for 1 min) followed with 5 min of regeneration step with 10 mM HCl of pH 1. Refer to Appendix E for the dialog box for binding analysis.

3.3.7.6 Data evaluation

Data evaluation was performed using the BIAevaluation 4.1. All sensorgrams from Fc2-1 were overlaid. The regeneration curves were removed and all baselines were averaged to zero by y-transformation. Double referencing was implied under the y-transformation by assigning the curve from sample buffer as curve 2. X-transformation was performed to adjust the starting points for association or dissociation. Both phases were highlighted and the concentrations of the analytes were defined. All sensorgrams were globally fitted to the kinetic models using the 1:1 Langmuir and heterogeneous ligand-parallel reaction models provided in the BIAevaluation software. The kinetic fitting was evaluated based on the visual observation on the fitness of the sensorgram with the kinetic models. Verification was made based on the quality of fit by assessing the chi-square (Chi^2) and the residuals values.

3.4 *In silico* molecular docking

In molecular docking, compounds from the small molecule protease inhibitors namely doxycycline, meclofenamic acid, rolitetracycline and the standard compounds, pinostrobin and 4-hydroxypanduratin A are termed as ligands. Meanwhile, the DENV-2 NSB-NS3pro represents the target protein or receptor.

3.4.1 Workstations

Two workstations consisting of four Intel Core 2 Duo E6850 3.00 GHz microprocessors, generated with a random access memory of 8 GB and an Ubuntu 10.04 Linux operating system were utilized to prepare the docking files, run the docking jobs and analyse the output.

3.4.2 Preparation of docking files

3.4.2.1 Preparation for protein structure

The coordinate file of the DENV-2 NS2B-NS3pro 3D homology model, namely DH-1, was retrieved from Heh *et al*. (2013). This model had been previously minimized, water molecules were removed to allow a complete search (docking) of the ligand throughout the protein structure, non-polar hydrogen atoms were merged, Kollman charges were assigned and the solvation parameters were added.

3.4.2.2 Optimization of ligand structure

The ligands' 3D structures were downloaded from the PubChem webpage (http://www.ncbi.nlm.nih.gov/pccompound) (Wang *et al*., 2009). The energy of each structure was minimized using the Hyperchem Pro 6.0 software system by employing the PM3 semiempirical method, where geometrical optimisation was performed using the steepest descent technique, and the operation was terminated at a maximal set of

500 cycles or 0.01 kcal/(Å mol) rms gradient. These processes brought the ligands' energy levels to a minimum and stable structure (Tambunan & Alamudi, 2010). The molecular structures of the standards and target ligands are shown in Figure 3.2.

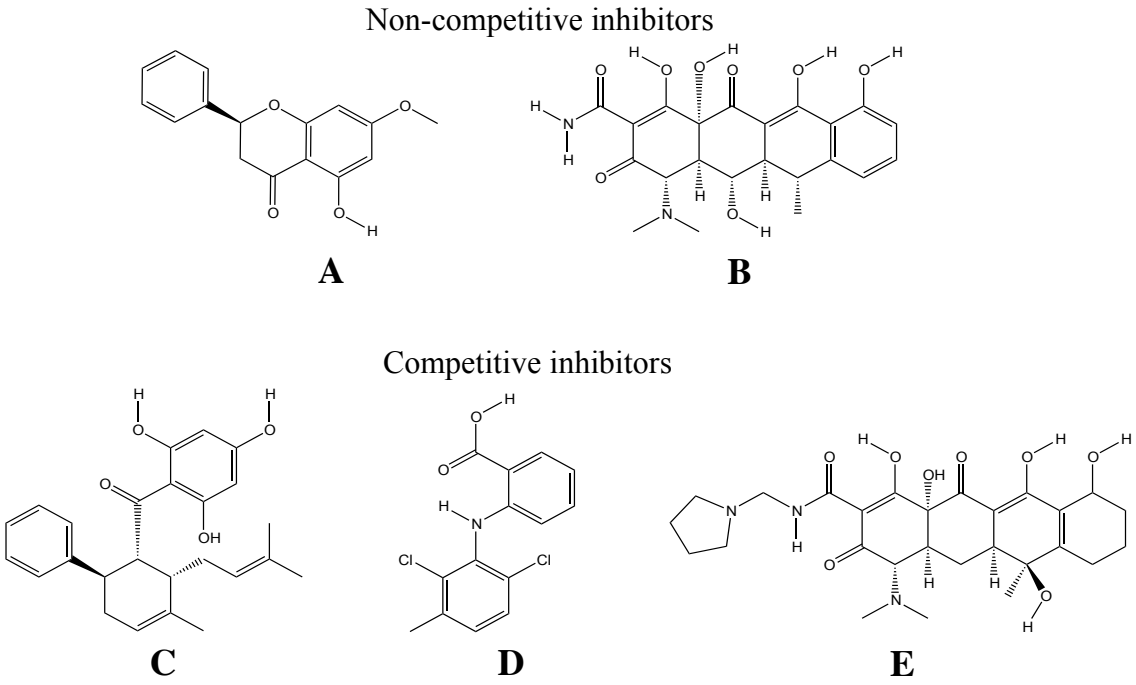

Figure 3.2: Molecular structures of ligands used for molecular docking. Standard ligands are pinostrobin **(A)** (non-competitive inhibitor) and 4-hydroxypanduratin A **(C)** (competitive inhibitor). Target ligands are doxycycline **(B),** meclofenamic acid **(D)** and rolitetracycline **(E)**.

3.4.2.3 Preparation of rigid protein and flexible ligand

By using the AutoDock Tools 1.5.6 software (http://www.mybiosoftware.com/ autodock-4-2-3-autodocktools-1-5-6-suite-automated-docking-tools.html), polar hydrogen atoms were added to the protein structure, while non-polar hydrogen atoms were merged. Kollman charges and solvation parameters were determined by default. Gasteiger charges were added to the minimized ligand structures, and all bonds were made rotatable and flexible by allowing the detection of root torsion.

3.4.2.4 Preparation for blind docking

Blind docking allows the detection of potential modes of ligands and the binding sites by searching the entire surface of protein targets (Heténya & Spoel, 2006). Grid maps were prepared using the AutoDock Tools 1.5.6 software. A grid spacing of 0.41 Å in the x, y and z-dimensions of 126 x 126 x 126 points were set to cover the entire protein and all its binding sites to accommodate free movements of the ligands (Tambunan & Alamudi, 2010). The Lamarckian Genetic Algorithm (LGA) (Atilgan & Hu, 2011) was used to search for the lowest binding energy by implementing local minimization of the genetic algorithm, to enable the modification of the gene population (Atilgan & Hu, 2011; Wang *et al*., 2015). LGA parameters were set as follows: 100 search (docking) runs, population size of 150, 25,000,000 of energy evaluations, 27,000 numbers of generations, mutation rate of 0.02 and crossover rate of 0.8.

3.4.2.5 Blind docking

Molecular docking calculations were performed using the AutoDock 4.2.6 software and the output was clustered based on the root-mean-square deviations (RMSD) tolerance of 2.0 Å.

3.4.2.6 Analysis of docked results

The best-docked models were selected according to the lowest binding energy that comprised the largest clustering number. Two and three-dimensional conformational structures of the ligand-protein complexes were visualized using the Discovery Studio Visualizer 4.5 (http://accelrys.com/products/collaborative-science/biovia-discovery-studio/) to investigate the binding modes, and the type of interactions developed between the ligands and protein binding site. A clearer interpretation of the

hydrophobic interactions was evaluated using the Ligplot program (http://www.ebi.ac.uk/ thornton-srv/software/LigPlus/download.html).

CHAPTER 4 : RESULTS

4.1 DNA verification, protein expression and purification and the characterization of the DENV-2 NS2B-NS3pro

4.1.1 DNA sequencing

The first step of this study was to confirm that the NS2B-NS3pro construct received from Heh *et al*. (2013) is free from possible DNA mutations. The plasmid DNA; pQE30.CF40.gly(T).NS3pro that defines the N-terminal 6xhis-tagged NS2B-NS3pro was extracted and purified from three cultures of *E.coli* strain XL1-Blue MRF'. The integrity of plasmid DNA was examined on 1% agarose gel (Figure 4.1), and each triplicate showed a band consistently at the desired length of 750 bp. The most prominent DNA band as seen in lane 4 was further sent to the First Base Laboratories Sdn. Bhd. for sequence analysis and the results are depicted in Figure 4.2. This sequence was further validated using the NCBI database under the blastn algorithm (http://blast.ncbi.nlm.nih.gov/Blast.cgi). The DNA sequence of the DENV-2 NS2B-NS3pro exhibited 99% identity to the DENV-2 strain BA05i DNA (Figure 4.3). The 1% mismatch nucleotides in the query sequence (DENV-2 strain New Guinea C NS2B-NS3pro) are contributed by the nucleotides located at position 207 (T-A), 249 (G-A), 510 (T-C), 516 (G-A), 586 (T-C), 593 (C-T) and 713 (G-A). A Guanine (G) at location 762 of the query sequence is not detected in the subject sequence, DENV-2 strain BA05i (represent by a "-" symbol).

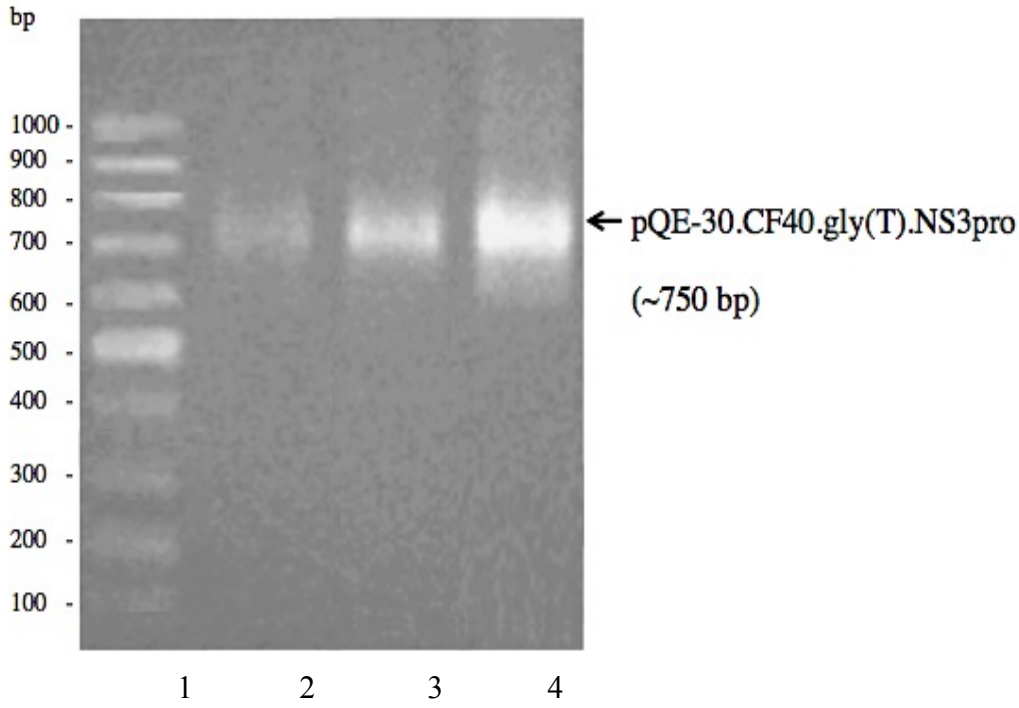

Figure 4.1: The electrophoretic separation of plasmid DNA on 1% agarose gel. Plasmid DNA was extracted from the *E.coli* strain XL1-Blue MRF'. Lane 1, DNA ladder (100 bp); and Lanes 2 – 4, plasmid DNA of pQE30.CF40.gly(T).NS3pro with 750 bp.

```
atgagaggatcgcatcaccatcaccatcacggatccgccgatt
tggaactggagagagctgctgacgtaaggtgggaagaacaggc
agagatatcaggaagtagtccaactctgtcgataaccatatcg
gaagatggtagcatgtcgataaaaaatgaagaggaagaacaga
cactgggggcggaggtaccggtggaggcggggctggagtatt
gtgggatgtcccttcacccccacctgtgggaaaggccgaactg
gaagatggagcctatagaatcaagcagaaagggattctaggat
actcgcagatcggagccggagtttacaaagaaggaacattcca
cacaatgtggcatgtcacacgtggtgctgtcctaatgcataaa
gggaagagaattgaaccatcatgggcggacgtcaagaaagatc
taatatcgtatggaggaggctggaagctagaaggagaatggaa
ggaaggagaagaagtccaggtcctggcattagagcctggaaag
aatccaagagccgtccaaacaaaacccggtctttttaaaacta
acactggaaccataggcgccgtgtctttggacttttctcctgg
aacgtcaggatctccaatcgtcgacaaaaaaggaaaagttgtg
ggcctttatggcaacggtgtcgttacaaggagtggaacatatg
tgagcgctatagcccagactgaaagaagcatcgaagacaatcc
agagattgaagatgacatctttcgaaagagaaaatga
```

Figure 4.2: DNA sequence for plasmid DNA pQE30.CF40.gly(T).NS3pro of the DENV-2 NS2B-NS3pro.This was received from the First Base Laboratories Sdn. Bhd.

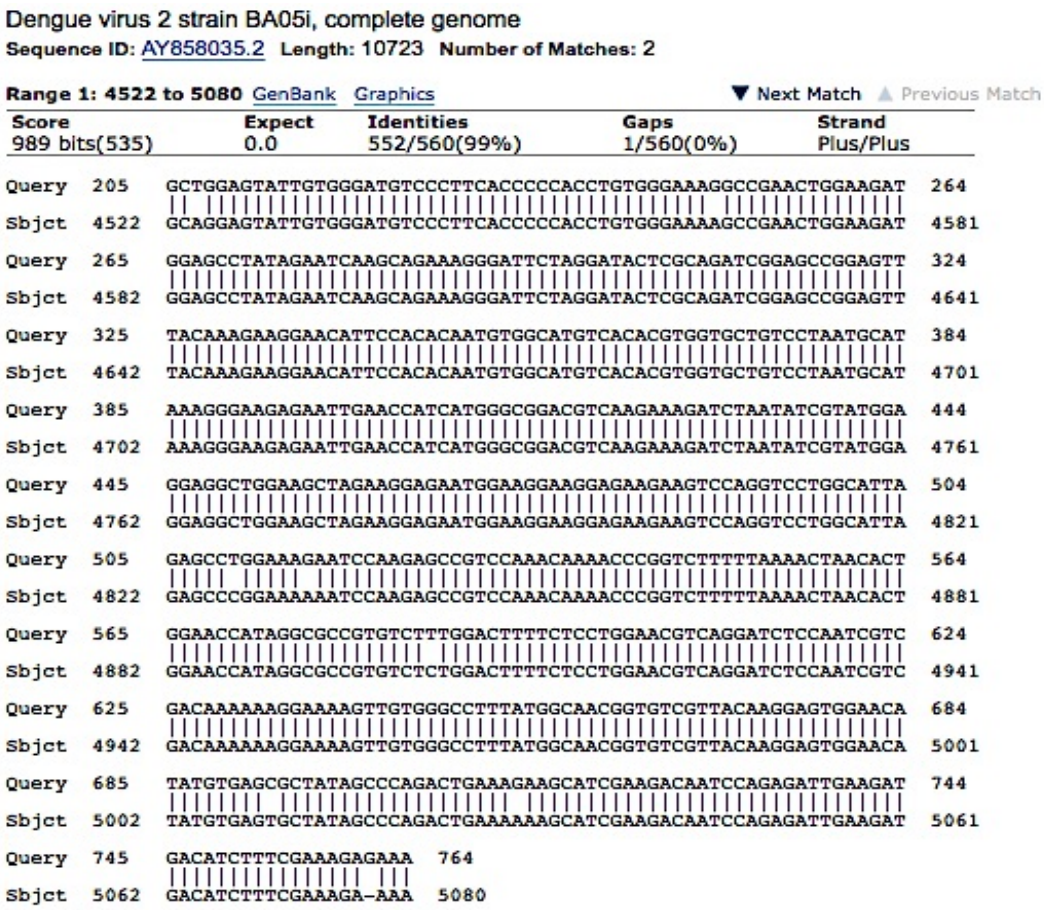

Figure 4.3: Verification of the DNA sequence by NCBI nucleotide BLAST. The DNA sequence shares 99% sequence identity to the DENV-2 strain BA05i.

4.1.2 Protein expression, purification and identification

Following the high sequence identity, we proceed to the expression of NS2B-NS3pro picked from a single colony on the LB agar plate. Figure 4.4 displays the 12% SDS-PAGE analysis on both the protein expression from 5 L LB medium and the purified eluates from Ni-IMAC. The eluates (E1 and E2) were further verified with the Western blot and each protein band was detected by the anti-his antibody at ~35 kDa (Figure 4.5). Identification with Mass Spectrometry (MS) analysis showed that the ~35 kDa protein was indeed NS2B-NS3pro due to its high similarity of 90% with the NS2B-NS3pro from DENV (Figure 4.6). Further purification with SEC using Hi-Load Superdex 16/60 75 prep grade was performed and the results from the chromatogram (Figure 4.7A) indicates a protein separation into three different peaks; peak a, b and c

respectively. Each peak was pooled and examined for purity using 12% SDS-PAGE (Figure 4.7B). It is clearly seen that there are fragments of lower MW protein in peaks a and b with size range similar to that observed in Ni-IMAC eluates. But they are less apparent in peak c, which correlates to its well separated peak profile compared to the overlapping peaks in peaks a and b (Choksupmanee *et al*., 2012).

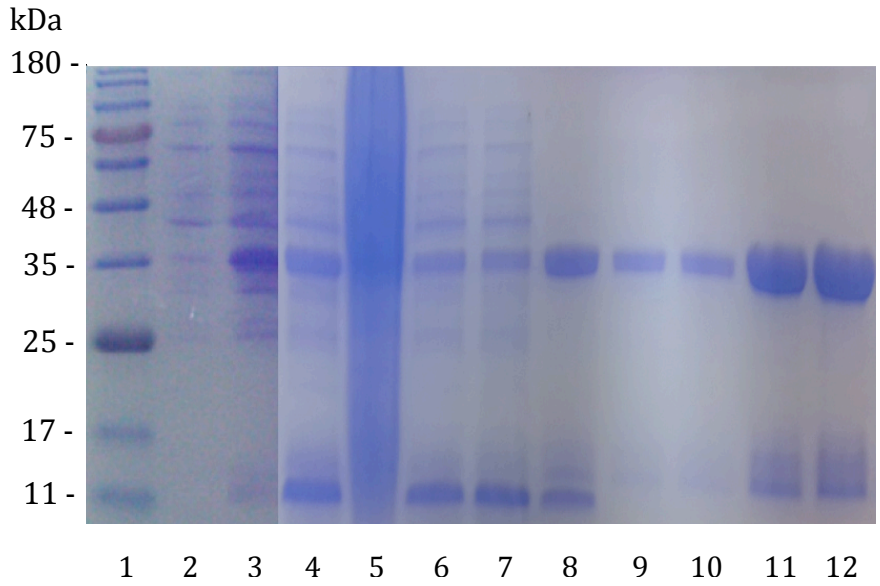

Figure 4.4: SDS-PAGE analysis of the NS2B-NS3pro protein expression and its purification profiles with Ni-IMAC. Protein expression profile: Lane **1**, prestained marker; Lane **2**, total soluble protein expression before induction with IPTG; Lane **3**, total soluble protein expression when induced with IPTG; Lane **4**, unpurified cell lysate; Lane **5**, cell pellet. Ni-IMAC purification profile: Lane **6**, supernatant containing unbound proteins to the Ni-NTA; Lane **7**, non-his-tagged protein contaminants from first wash (W1); Lane **8**, non-his-tagged protein contaminants from second wash (W2); Lane **9**, non-his-tagged protein contaminants from last wash (LW); Lane **10**, first elution of his-tagged proteins (E1); Lane **11**, second elution of his-tagged proteins (E2); and Lane **12**, third elution of his-tagged proteins (E3).

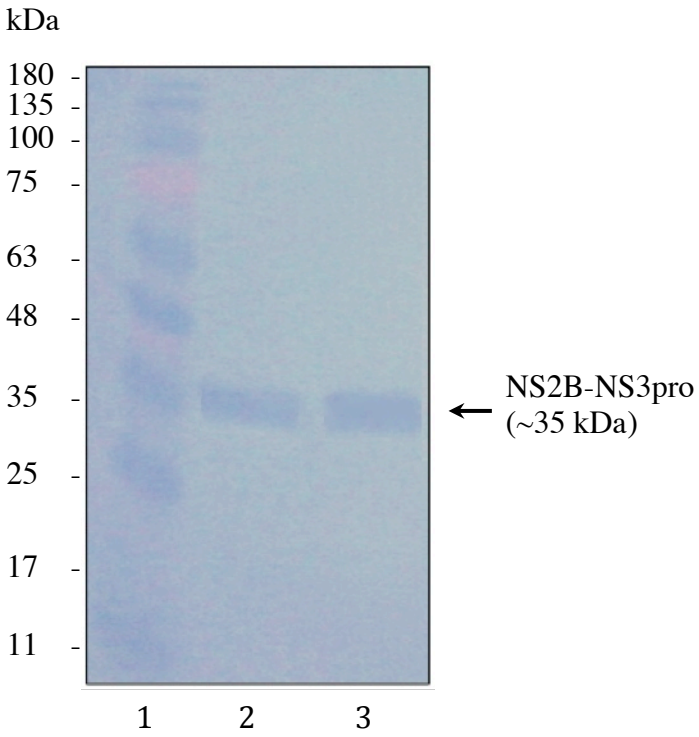

Figure 4.5: Western blot analysis for Ni-IMAC eluates. Lane **1**, prestained protein marker; and Lanes **2** and **3**, protein eluates from E1, E2 and E3.

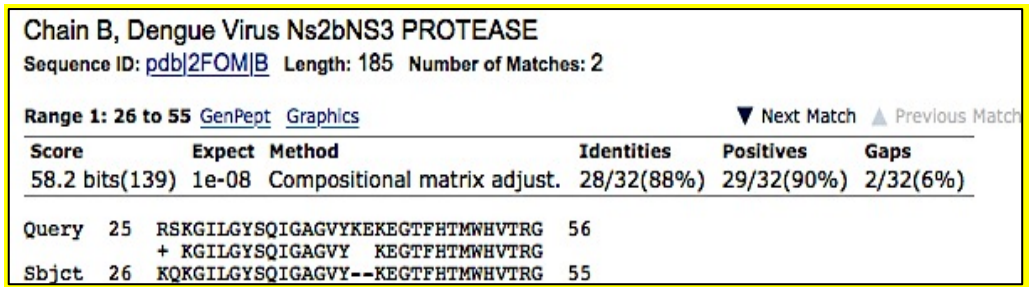

Figure 4.6: Mass Spectrometry (MS) analysis for Ni-IMAC eluate. The eluate (E2) was analyzed and confirmed as NS2B-NS3pro polyprotein from DENV as indicated by the Mascot search engine.

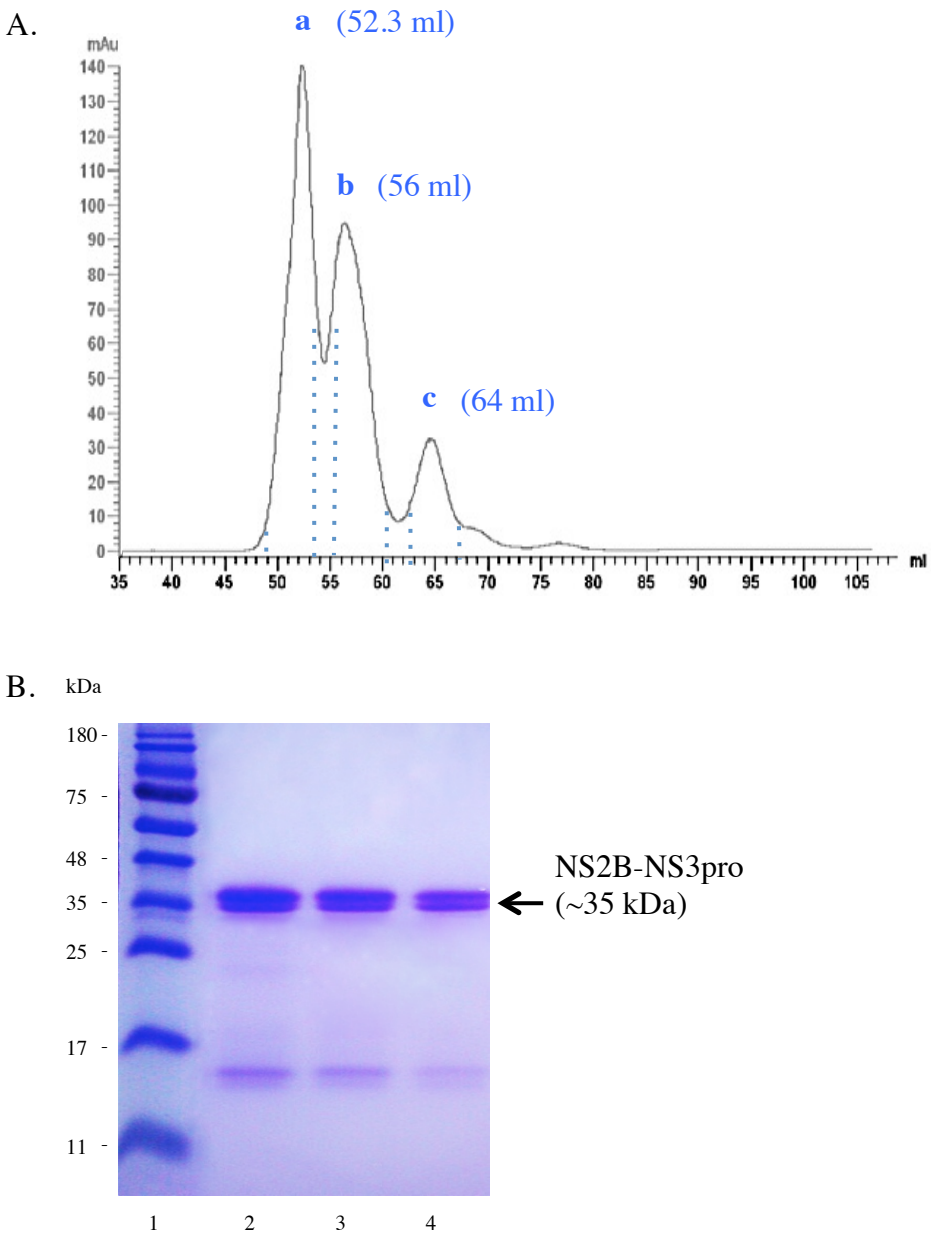

Figure 4.7: Purification of NS2B-NS3pro with SEC. **(A)** Chromatogram eluted from SEC, indicating three different sizes of proteins; peak a, b and c respectively. The elution volume for each peak is indicated as 52.3 ml, 56 ml and 64 ml respectively. **(B)** SDS-PAGE gel for concentrated protein fractionized from SEC. Lanes **1-3**, pooled fractions from peak a, b and c respectively.

4.1.3 Determination of the concentration

Eluates from Ni-IMAC and SEC were quantified based on the BSA standard curve (Figure 4.8) using the Bradford Assay. Calculation for protease concentration is further elaborated in Section 3.2.5.2 and the results are tabulated in Table 4.1.

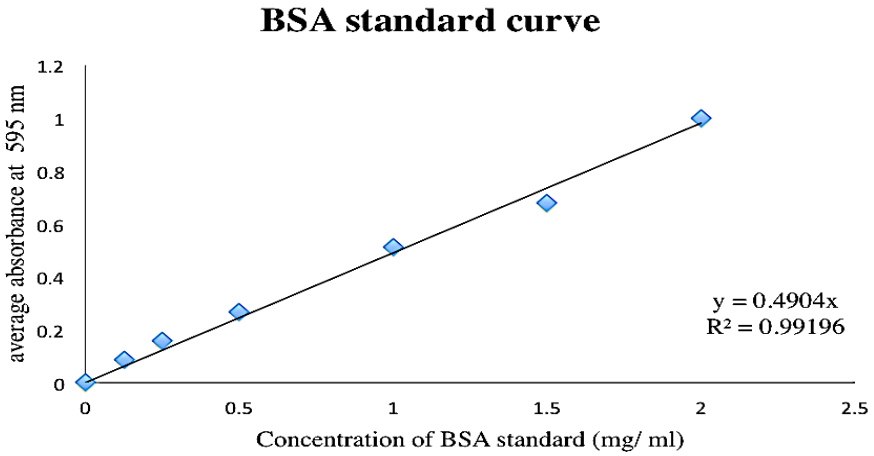

Figure 4.8: Standard curve using dilutions of BSA. The concentration range is 0, 0.125, 0.25, 0.5, 1, 1.5 and 2 mg/ml.

Table 4.1: Total concentration of eluates pooled from Ni-IMAC and SEC, based on the protein expression of 5 L LB medium.

Concentrated eluates	Concentration		Pooled volume (ml)
	(mg/ ml)	(μM)	
Ni-IMAC	3.260	93.1	1
Peak a from SEC	1.564	44.7	1
Peak b from SEC	1.377	45.9	1
Peak c from SEC	0.322	9.2	0.5

4.1.4 Determination of the oligomeric states

Subsequent analysis on the oligomeric state of the NS2B-NS3pro was determined with SEC. Figure 4.9 shows the elution and void volumes of the protein standards; V_e and V_o respectively, and the calibration curve for SEC using Hi-Load Superdex 16/60 75 pg. The sizes of NS2B-NS3pro oligomers were calculated based on equation 1 (Section 3.2.5.2) that was generated based on the calibration curve (Figure 4.9B). The oligomeric states of NS2B-NS3pro eluted from peak a, b and c are listed in Table 4.2. NS2B-NS3pro eluted in peaks a, b and c is determined as a tetramer (138 kDa), trimer

(116 kDa) and dimer (78 kDa) respectively. The oligomeric states of NS2B-NS3pro were further validated with native PAGE (Figure 4.10) and shows correlation with the oligomeric size obtained from SEC.

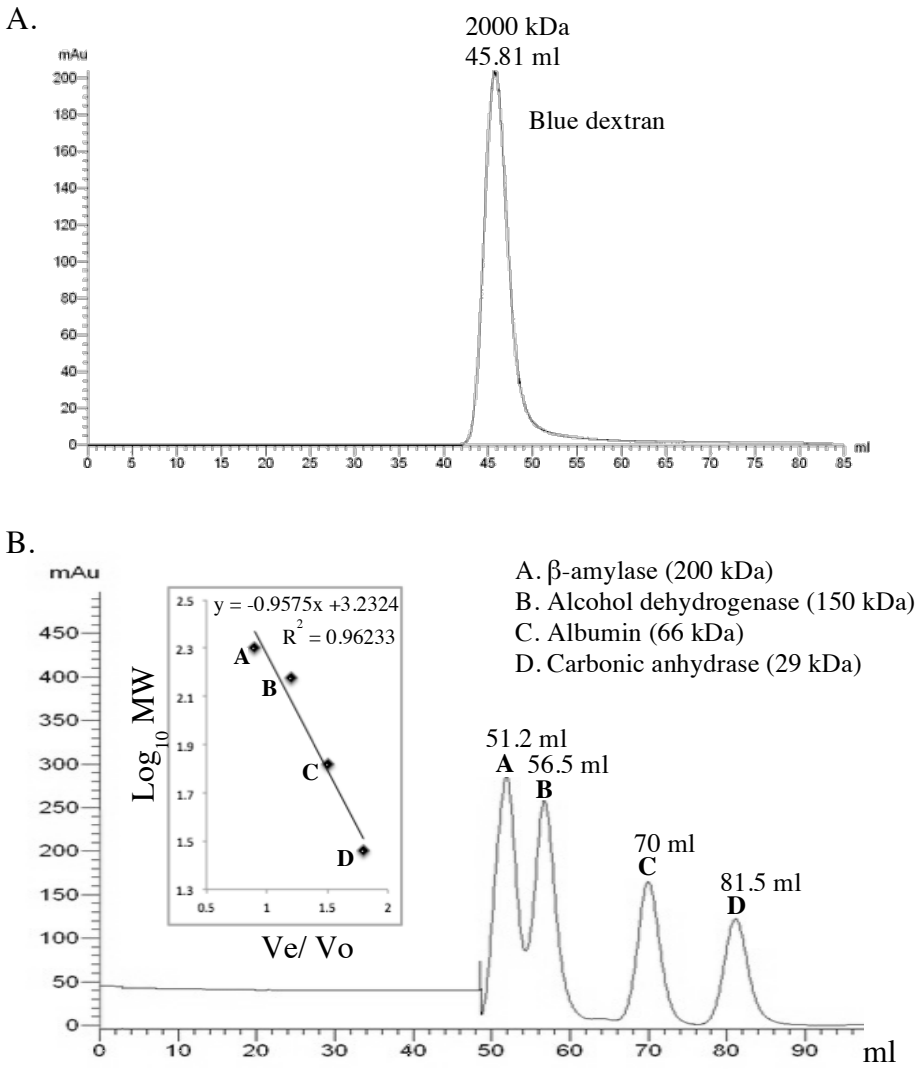

Figure 4.9: Determination of Ve, Vo and the calibration curve for SEC. **(A)** Elution of Blue dextran representing void volume (V_O) at 45.81 ml. **(B)** Elution volume (V_e) of the protein standards at 51.2 ml for β-amylase, 56.5 ml for alcohol dehydrogenase, 70 ml for albumin and 81.5 ml for cabonic anhydrase. The inset shows a linear calibration curve of logarithmic MW of protein standards versus V_e/V_O.

Table 4.2: Oligomeric states of NS2B-NS3pro determined from SEC.

Peak	Ve of NS2B-NS3pro / Vo of blue dextran	Log_{10} MW of	MW (kDa)	Oligomeric state
a	1.14	2.14085	138.3	Tetramer
b	1.22	2.06425	116.0	Trimer
c	1.40	1.8919	78.0	Dimer

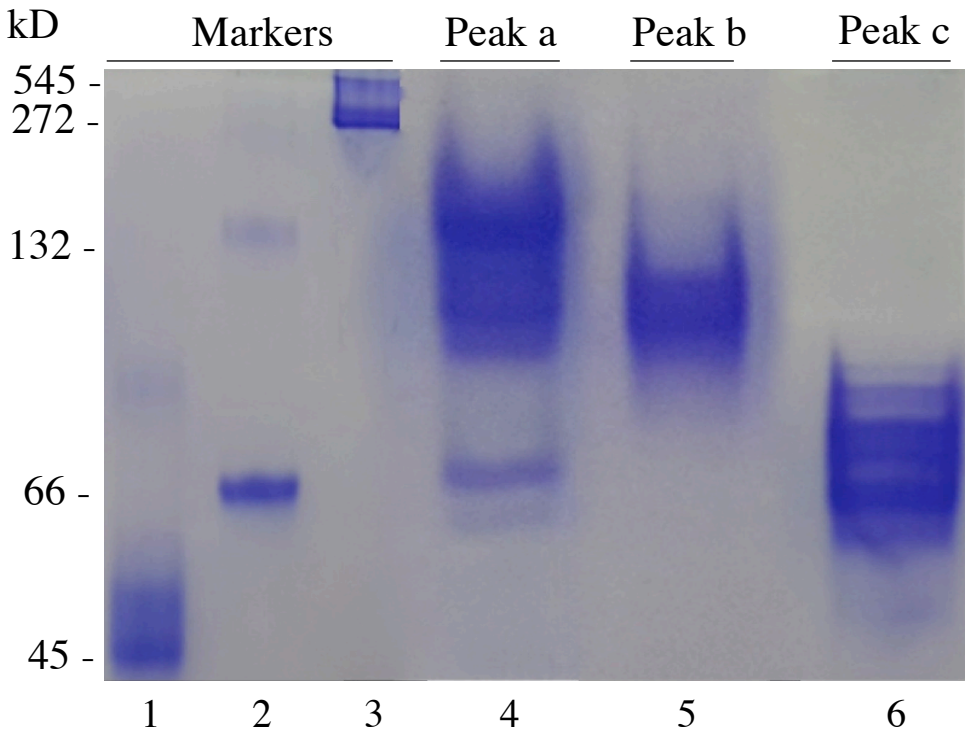

Figure 4.10: Native PAGE analysis for elution profile from SEC. The MW markers are indicated on the left; Lane **1**, albumin from chicken egg white, 45 kDa; Lane **2**, albumin from bovine serum, 66 kDa (monomer) and 132 kDa (dimer); Lane **3**, jack bean urease, 272 kDa (trimer), and 545 kDa (hexamer). The next three lanes in lanes **4**, **5** and **6** correspond to peaks a, b, and c as labeled on chromatogram (Figure 4.7).

4.2 SPR assay

In this study, purified NS2B-NS3pro from SEC, specifically from peak c was chosen for SPR assay as this peak is well separated compared to the overlapping peaks of peaks a and b (Figure 4.7). For SPR assay, NS2B-NS3pro was used as the ligand and immobilized onto the sensor chip. The protease inhibitors from small molecule medicinal drugs namely doxycycline, meclofenamic acid and rolitetracycline were used as the analytes and injected over the immobilized NS2B-NS3pro for binding analysis. SPR assay was performed under continuous flow of running buffer as depicted by the horizontal baselines in the sensorgram. The response data were recorded at report points, which are an average of the slope of the sensorgram over a short time window. The flow cells, Fc1 and Fc2 were used as the reference flow cell and sample flow cell respectively. Both flow cells were treated equally except that NS2B-NS3pro was immobilized on Fc2. Binding analysis was first attempted with CM5 chip before it was found unsuccessful and proceeded with NTA chip.

4.2.1 Initial optimization on binding analysis using CM5 chip

4.2.1.1 Pre-concentration of ligand using pH scouting

The first attempt of this study was to immobilize NS2B-NS3pro onto the CM5 chip via amine coupling. The pH scouting was performed prior immobilization to confirm an ideal concentration of NS2B-NS3pro and to scout suitable pH for immobilization. During this process, NS2B-NS3pro was pre-concentrated onto the non-activated CM dextran based on an electrostatic interaction that is developed at an optimal pH. 50 µg/ml of NS2B-NS3pro reconstituted in 10 mM sodium acetate of both pH 4 and 5 were pre-concentrated onto the CM dextran. Referring to Figure 4.11, pH 4 shows higher pre-concentration level of NS2B-NS3pro compared to pH 5. Therefore, it was concluded that pH 4 is an optimal condition for NS2B-NS3pro immobilization.

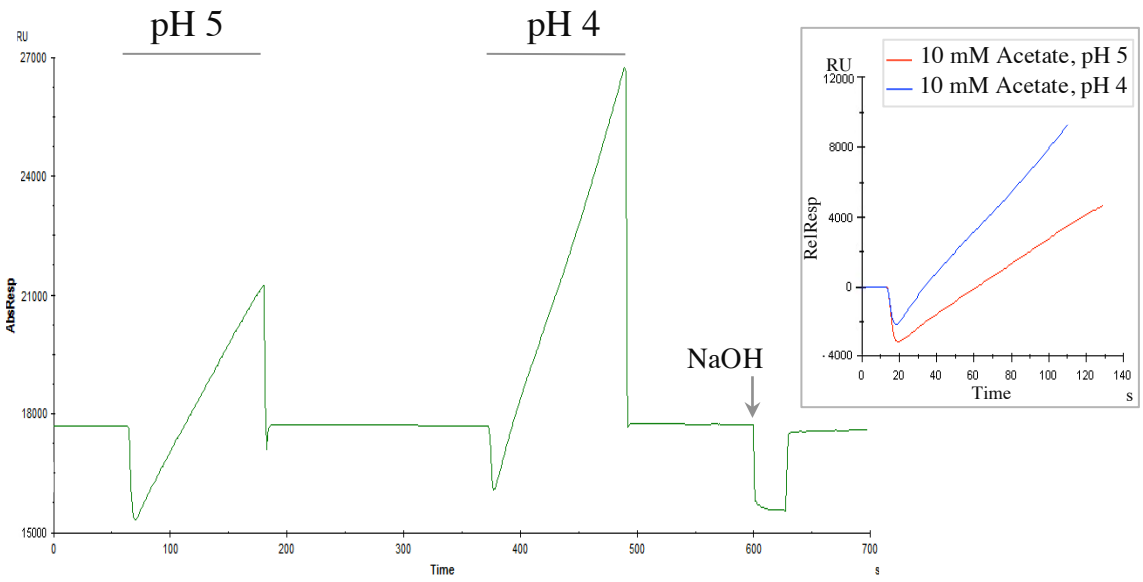

Figure 4.11: The pH scouting to pre-concentrate NS2B-NS3pro onto CM5 chip. 50 µg/ml NS2B-NS3pro reconstituted in 10 mM sodium acetate of both pH 4 and 5 was injected sequentially. This is followed by the injection of 50 mM NaOH to remove the pre-concentrated NS2B-NS3pro. The inset on the right shows RelResp values for NS2B-NS3pro pre-concentrated at pH 4 and 5, precisely at 9302.1 RU and 4765.3 RU respectively.

4.2.1.2 Immobilization using amine coupling

Figure 4.12 shows a sensorgram of NS2B-NS3pro immobilized onto CM5 chip. The sensor surface was first activated with equimolar amounts of EDC and NHS (1:1) to develop succinimide esters, followed by ligand immobilization with 50 µg/ml of NS2B-NS3pro. Ethanolamine was then injected to remove NS2B-NS3pro that were not immobilized and simultaneously blocked unreacted succinimide esters. As a result, a total of 6020.5 RU of NS2B-NS3pro was immobilized onto Fc2 (report point 7), which is acquired from the difference between the amount of bound NS2B-NS3pro during post-ethanolamine and the baseline level.

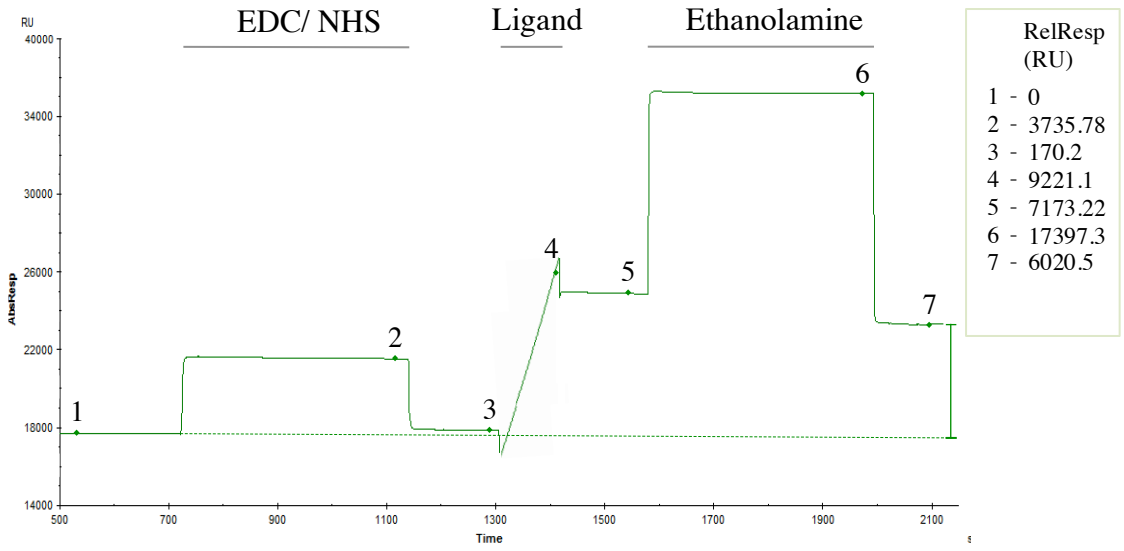

Figure 4.12: The immobilization of NS2B-NS3pro onto CM5 chip via amine coupling. The inset on the right is the ReslResp recorded at respective report points. Report points **(1)** Baseline level, **(2)** Activation of sensor surface with 1:1 EDC/NHS solution to produce reactive succinimide esters, **(3)** Actual amount of activated sensor surface, **(4)** Immobilization of protease via amine coupling, **(5)** Remaining bound protease during post-immobilization, **(6)** Blocking of uncoupled succinimide esters by ethanolamine and **(7)** Actual amount of immobilized protease.

4.2.1.3 Binding analysis

The represantative sensorgram in Figure 4.13 is showing the evaluation of 50 µM meclofenamic acid binding to NS2B-NS3pro. It is clear that the association phase is significantly decreasing during the injection and in each consecutive binding cycle. As good binding event should depict an increment of binding in the association phase, it is concluded that the binding analysis with NS2B-NS3pro immobilized on CM5 chip is an unsuccessful event. Further binding analysis on CM5 chip was halted. Nevertheless, SPR assay still proceeded with an alternative method using NTA chip as further explained in the next section (Section 4.2.2).

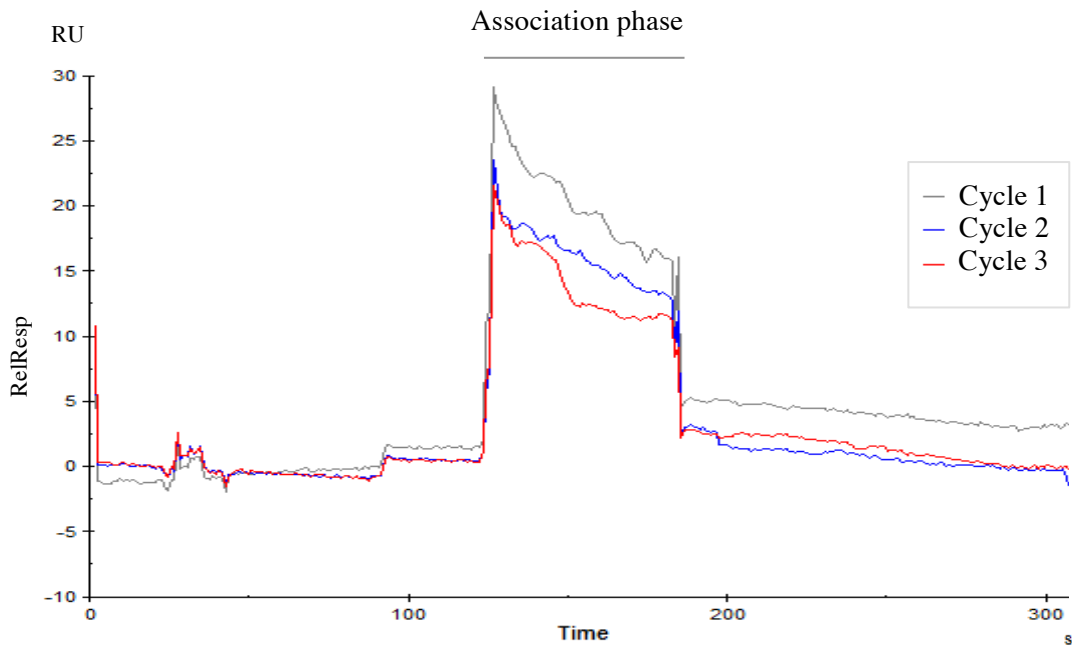

Figure 4.13: Binding analysis of meclofenamic acid with the amine coupled NS2B-NS3pro. A decrement of analyte (50 µM meclofenamic acid) binding is observed in the association phase.

4.2.2 Binding analysis on NTA chip

4.2.2.1 Ligand concentration scouting

Ligand concentration scouting was performed prior the immobilization to observe which concentration of NS2B-NS3pro can reach the target immobilization level of 6000 RU. This process involves scouting of 20, 30, 40 and 50 µg/ml of NS2B-NS3pro that was captured over the Ni-activated NTA chip. Figure 4.14 is showing an overlay of sensorgrams for four consecutive cycles of 'ligand concentration scouting'. Scouting process was initialized with the establishment of the baseline level. By injecting the Ni solution, the NTA chip was activated with 60.5 RU of Ni (Willard & Siderovski, 2006). NS2B-NS3pro was then injected and captured by the Ni moieties before allowed to dissociate by the running buffer (running buffer B, Section 3.3.4). To end the process, the regeneration solution (Section 3.3.4) was injected to wash away both bound NS2B-NS3pro and Ni moieties. A final wash with the running buffer was performed to

remove EDTA particles remained from the regeneration solution. This is to provide a clean sensor surface so that the same NTA chip can be reused. From the ligand concentration scouting, it is evident that with 50 µg/ml, 6001.1 RU of NS2B-NS3pro was captured, which reached the target immobilization level. As a conclusion, 50 µg/ml of NS2B-NS3pro is determined as an optimal concentration for the next immobilization using capture coupling.

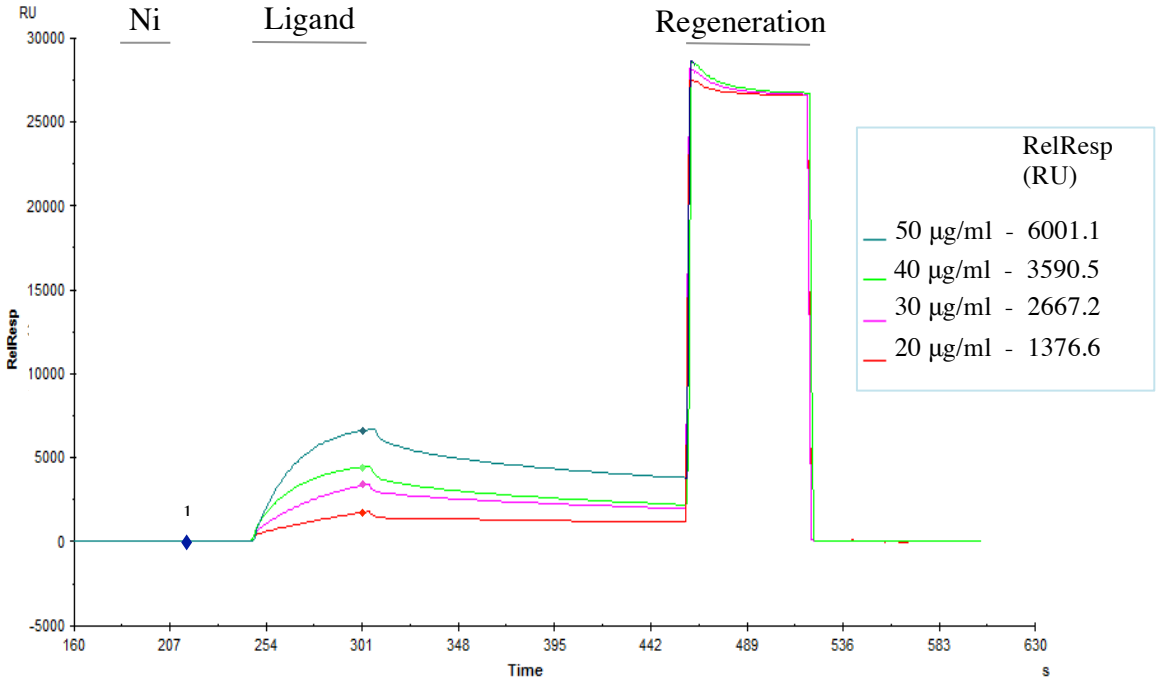

Figure 4.14: The ligand concentration scouting of NS2B-NS3pro on NTA chip. NS2B-NS3pro was scouted at 20, 30, 40 and 50 µg/ml on a Ni-activated NTA chip. Ni activation was recorded as 60.2 RU (report point **1**) and captured level of NS2B-NS3pro was recorded at every 301 seconds.

4.2.2.2 Immobilization using capture coupling

50 µg/ml of NS2B-NS3pro was permanently immobilized onto the same sample flow cell (Fc2) of NTA chip using capture coupling Figure 4.15. Once baseline level was adjusted, NTA chip was activated with 59.3 RU of Ni (report point 2) (Willard & Siderovski, 2006). The carboxyl group of the CM-dextran was then activated with the

EDC/NHS mixture solution (1:1) to form reactive succinimide esters. NS2B-NS3pro was injected for capture coupling, wherein the N-terminal His-tag of NS2B-NS3pro was captured before being immobilized covalently through amine coupling. Non-reacted esters (without bound NS2B-NS3pro) were blocked with ethanolamine. Regeneration buffer (Section 3.3.4) was injected to remove non-covalently bound NS2B-NS3pro and non-bound Ni. As a result, 6064.17 RU of NS2B-NS3pro was capture coupled to the NTA chip. This immobilization level was calculated by the BIAevaluation software based on the difference between the amount of capture coupled NS2B-NS3pro from post-regeneration (report point 10) and the baseline level before Ni-activation (report 1).

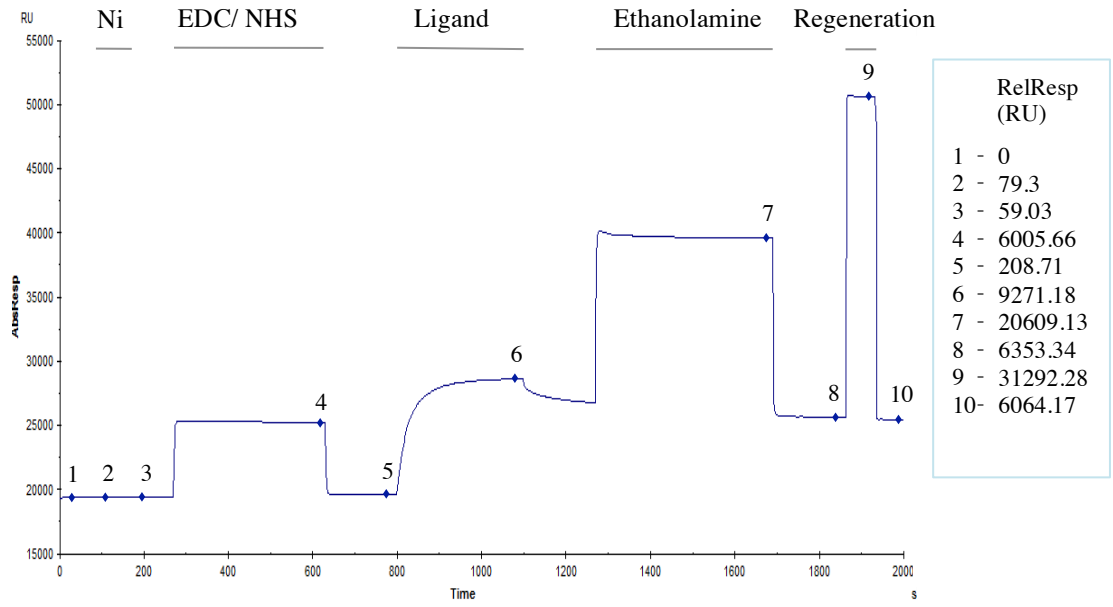

Figure 4.15: Immobilization of NS2B-NS3pro onto NTA chip via capture coupling. The inset on the right is the ReslResp recorded at respective report points. Report points **(1)** Baseline level before surface activation, **(2)** Activation of NTA sensor surface with Ni solution, **(3)** Total amount of bound Ni, **(4)** Second activation of of NTA sensor surface with 1:1 EDC/NHS mixture solution to produce reactive succinimide esters, **(5)** Total amount of developed succinimide esters, **(6)** Capture coupling of NS2B-NS3pro, **(7)** Blocking of non-reacted succinimide esters by ethanolamine **(8)** Remaining amount of capture caoupled NS2B-NS3pro from post-blocking, **(9)** Regeneration phase to wash the NTA sensor surface and **(10)** Total amount of capture coupled NS2B-NS3pro.

4.2.2.3 Processing biosensor data

Figure 4.16 shows the workflow involved in processing the biosensor data. A low concentration of 100 μM rolitetracycline was used for this investigation. The representative sensorgrams in Figure 4.16 are displaying only the association and dissociation phases. The regeneration phase that is required for rolitetracycline was removed prior processing the biosensor data (a full regeneration process is clarified in Section 4.2.2.4). The removal is required since kinetic constant is determined only on the association and dissociation rate constants (K_a and K_d) (GE Healthcare, 2012). The association phase in Fc2 shows increment in analyte binding indicating NS2B-NS3pro is active for binding (Figure 4.16A). Each sensorgram were double referenced by (i) subtraction of response data from the reference flow cell (Fc1) against the response data from the sample flow cell (Fc2) that contains immobilized NS2B-NS3pro to produce response data specifically from the analyte (Fc2-1) (Figure 4.16A) and (ii) subtraction of the average of blanks from the running buffer (0 μM) (Figure 4.16B and C). The running buffer used was running buffer A (Section 3.3.4). Biosensor data were examined for reproducibility based on the triplicates (Figure 4.16D). The results show that the sensorgrams are closely overlaid, indicating high-stability of the biosensor data (Myszka, 1999). However, there is a non-specific binding of rolitetracycline to both Fc1 and Fc2 based on the 'shark's fin' shape sensorgrams. There is also a high bulk refractive index in Fc1, which is also observable in rolitetracycline as well as in doxycycline and meclofenamic acid (Appendix F).

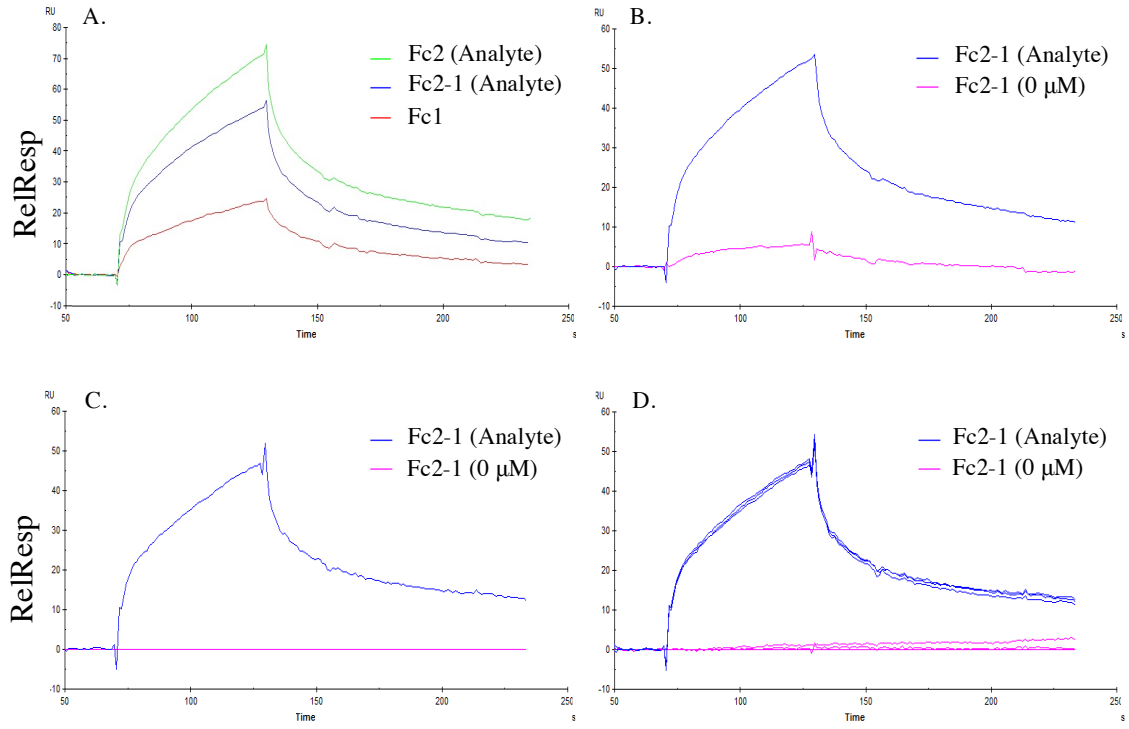

Figure 4.16: Processing biosensor data. **(A)** Overlay of data for 100 µM rolitetracycline (analyte) injected over NS2B-NS3pro from the reaction surface on Fc2 (green) and reference flow cell in Fc1 (red). The specific binding of rolitetracycline was obtained by signal subtraction in Fc2-1 (blue). All data sets were zeroed on the y-axis. **(B)** Overlay of reference subtracted data from Fc2-1 (blue) and running buffer as blank (before double referencing). **(C)** Data from both the sample (Fc2-1) and blank were subtracted from the blank injection (after double referencing). **(D)** Overlay of binding data from 50 µM rolitetracycline and blanks, each injected in triplicates.

4.2.2.4 Regeneration scouting

Regeneration scouting was used to search for potential regeneration conditions that can remove analyte without causing harm to the ligand (GE Healthcare, 2012). It involves sequential injections of analyte followed with the regeneration using the regeneration solution (Section 3.3.4). In this study, only rolitetracycline was requiring regeneration. Therefore, Figure 4.17 shows the regeneration scouting with 10 mM HCl, pH 1 against 200 µM rolitetracycline. The regeneration scouting started off with the determination of the baseline level (report point 1). Rolitetracycline is injected to bind to NS2B-NS3pro followed by its dissociation from NS2B-NS3pro by injecting the

running buffer (running buffer A, Section 3.3.4) (report point 2). During this point, a remaining of 32.2 RU of rolitetracycline is observed, indicating the non-dissociated rolitetracycline and is further removed by the regeneration solution until the baseline level is reached. The whole procedure was repeated for another two cycles to examine for reproducibility. A more comprehensive interpretation of response data collected from regeneration scouting is tabulated in Table 3. It is concluded that 10 mM HCl of pH 1 is able to regenerate (remove) bound analyte at an average of >90%, which further indicate its suitability as the regeneration solution. Nevertheless, its effect towards the activity of NS2B-NS3pro was confirmed using the surface perfomance test (Section 4.2.2.5).

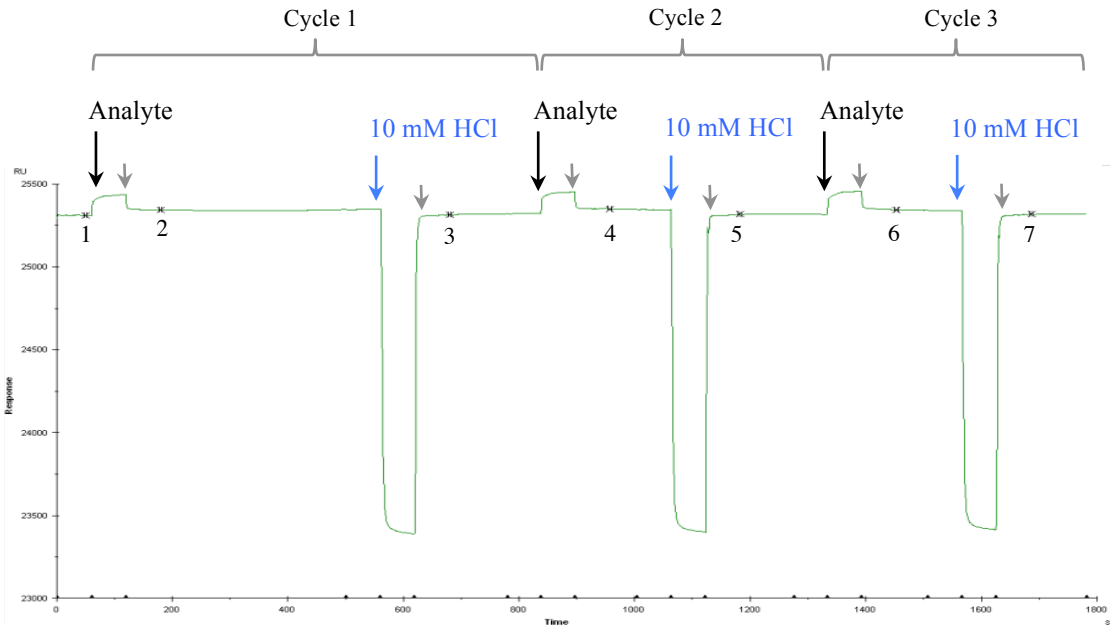

Figure 4.17: Regeneration scouting for rolitetracycline using 10 mM HCl, pH 1. Scouting was performed in three consecutive cycles with 200 µM rolitetracycline as the analyte. Gray arrows are indicating injections of the running buffer (running buffer A, Section 3.3.4) to dissociate analyte. Report point **1**, baseline level with 0 RU; Report points **2**, **4** and **6**, remaining of bound analyte during post-dissociation with 32.2, 37.8 and 33.4 RU respectively; and Report points **3**, **5** and **7**, remaining rolitetracycline during post-regenerations with 3.7, 4.7 and 5.9 RU respectively.

Table 4.3: A comprehensive interpretation of response data collected from regeneration scouting.

Cycles	Solutions	Report points	Changes in RelResp (RU)	Analyte regenerated (%)[a]	Total of remaining analyte	
					(RU)[b]	(%)[c]
1	Anlayte	2	+32.2	-	32.2	-
	10 mM HCl, pH 1	3	-28.5	89	3.7	11
2	Anlayte	4	+34.1	-	37.8	-
	10 mM HCl, pH 1	5	-33.1	97	4.7	12
3	Anlayte	6	+28.6	-	33.4	-
	10 mM HCl, pH 1	7	-27.5	97	5.9	18

\+ Amount of analyte remained after being washed with the running buffer (post-dissociation).

– Amount of analyte being regenerated with 10 mM HCl, pH1.

[a] Percentage of analyte being regenerated was calculated based on the *'Amount of analyte being regenerated with 10 mM HCl, pH1* (RU)' divided by the *'Amount of analyte remained during post-dissociation* (RU)*'*, and multipled by 100%.

[b] Total of remaining analyte (RU) is corresponding to the report points depicted in the regeneration scouting (Figure 4.17).

[c] Percentage of analyte remained bound on the sensor surface was calculated based on the '*Total of remaining of anlayte during post-regeneration* (RU)' divided by the *'Total of remaining of anlayte during post-dissociation* (RU)', multipled by 100%.

4.2.2.5 Surface performance test

A regeneration solution that could remove analyte is still not optimal unless it does not deteriorate the ligand. In surface performance test, this can be monitored based on the consistency in the baseline level, and in the binding response, to ensure that the ligand is active for analyte binding (GE Healthcare, 2012). Figure 4.18 is showing the graphical trend of report points extracted from five consecutive regeneration cycles against 200 μM rolitetracycline. It is observed that both the baseline and response levels are stable, confirming the suitability of 10 mM HCl of pH 1 to regenerate the surface without deteroriating the the acitivity of NS2B-NS3pro.

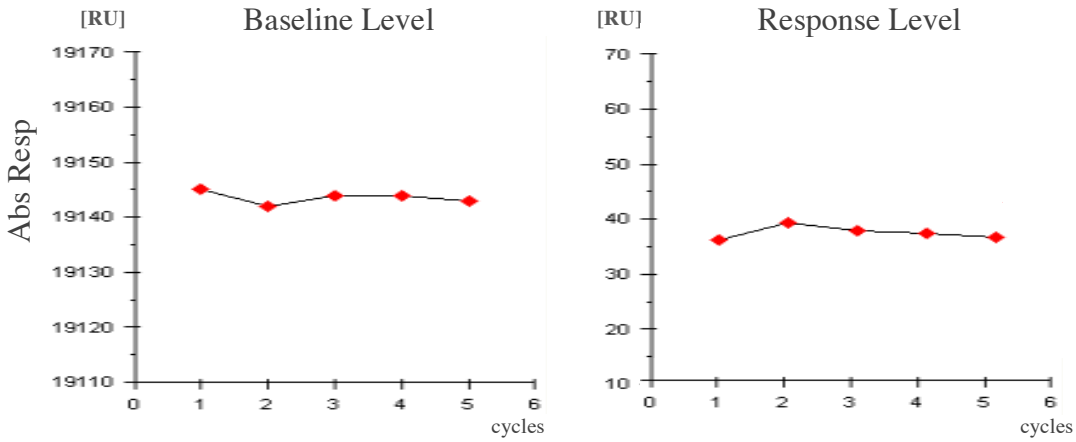

Figure 4.18: Surface performance test with 10 mM HCl, pH1. The analysis was performed in five concecutive cycles of regeneration against 200 µM rolitetracycline. Left and right are the report points in AbsResp for baseline levels and the binding response level. The first cycleindicates the report point prior regeneration. The starting value for post-regeneration is indicated in the second cycle and the following report points are recorded due to the effect of the previous regeneration cycle.

4.2.2.6 Binding analysis

Figure 4.19 shows the double referenced sensorgrams for analytes analyzed in multi-cycle kinetics involving several cycles of alternating analyte injections. These analytes are the protease inhibitors from small molecule medicinal drugs namely doxycycline, meclofenamic acid and rolitetracycline. Each analyte was injected in triplicate within a series of six concentrations between 0 – 500 µM.

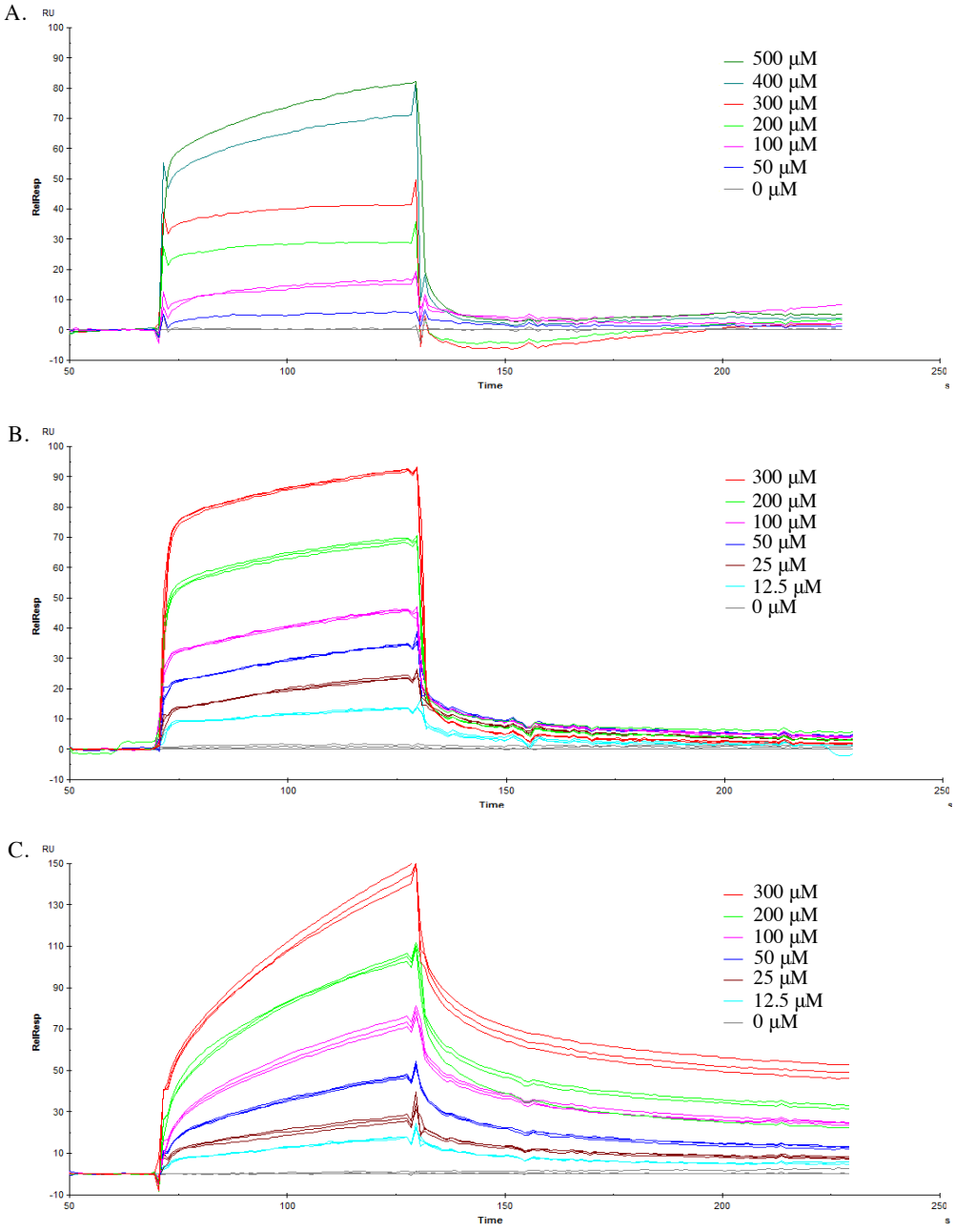

Figure 4.19: Sensorgrams for the binding interaction of protease inhibitors to the capture coupled NS2B-NS3pro. The analytes were injected between **(A)** 0 – 500 µM for doxycycline, **(B)** 0 – 300 µM for meclofenamic acid and **(C)** 0 – 300 µM for rolitetracycline.

4.2.2.7 An attempt for kinetic analysis

Kinetic analysis was performed on the binding sensorgrams from Figure 4.19 as an attempt to determine the rate constants (K_a and K_d). From the sensorgrams, only the average of triplicate was used for kinetic analysis using the global fitting. With global

fitting, the whole sensorgrams from each analyte concentration were simultaneously fit to a kinetic model. In this study, the binding sensorgrams were attempted to fit to both the 1:1 Lagmuir and heterogeneous ligand models for kinetic analysis (Figures 4.20, 4.21 and 4.22). Graphical representations on the residual distribution are also depicted for each sensorgram. The residual and Chi^2 values were also used to determine the quality of kinetic fitting as tabulated in Table 4.4. For each analyte tested, the experimental sensorgrams show poor fitting to both the 1:1 Lagmuir and heterogenous ligand models. The graphical distribution of the residuals are non-randomly distributed along the x-axis (curvilinear), indicating that both kinetic models are following the systemic trend. Additionally, the residual values of all analytes are exceeding the noise level ±2 RU. On the other hand, the Chi^2 values for both doxycycline and meclofenamic acid are lower than 10 RU indicating a relatively good fitting. Meanwhile the range of values rolitetracycline is exceeding the optimal range (> ±2 RU). Despite the acceptable Chi^2 values observed in doxycycline and meclofenamic acid, yet the sensorgrams are depicting a poor state of kinetic fitting.

However, as an attempt to verify these findings, the binding data had been sent for further analysis to Episentec, a biotech company in Sweden that is specialized in the application and development of biosensors (Episentec, 2015). Based on their report, a derivative function, ln(dR/dt), is plotted against time using global fitting (Figure 4.23). The binding data of all analyte concentrations is transformed from the sensorgram based on the derivative function. The main objective is to choose a linear slope within the association and dissociation phases to calculate the rate constants using the 1:1 Langmuir model. A linear slope indicating a Langmuir interaction should follow the dashed lines as highlighted in the figure. However, instead of being linear, the slopes are curvy (black lines) as indicated from the beginning of the analyte injection until

before it reaches equilibrium (in the association phase), and in the dissociation phase. Despite the curvilinearity, there are minor areas near to equilibrium that showed linear slopes in both doxycycline and meclofenamic acid. However, kinetic rate constants could not be extracted due to the accumulative artifacts from the high bulk refractive index and possibly the autoproteolytic activity of NS2B-NS3pro (further clarified in Section 5.3.4).

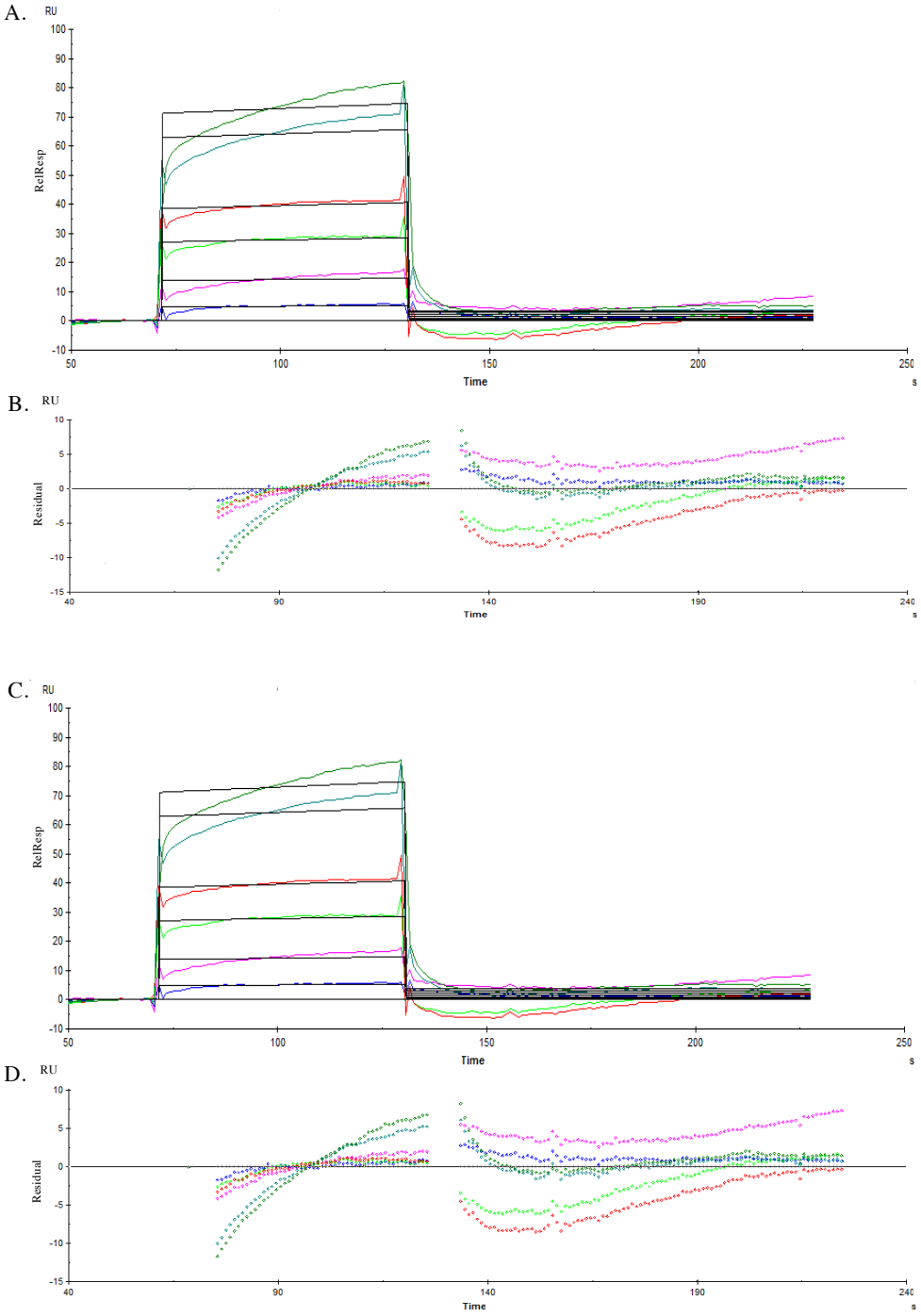

Figure 4.20: Kinetic analysis for doxycycline using 1:1 Langmuir and heterogenous ligand-parallel reaction models **(A** and **C** respectively). The black lines are the fitting sensorgrams and the colorful lines are the experimental sensorgrams. **(B)** and **(D)** Residual plots for each kinetic model.

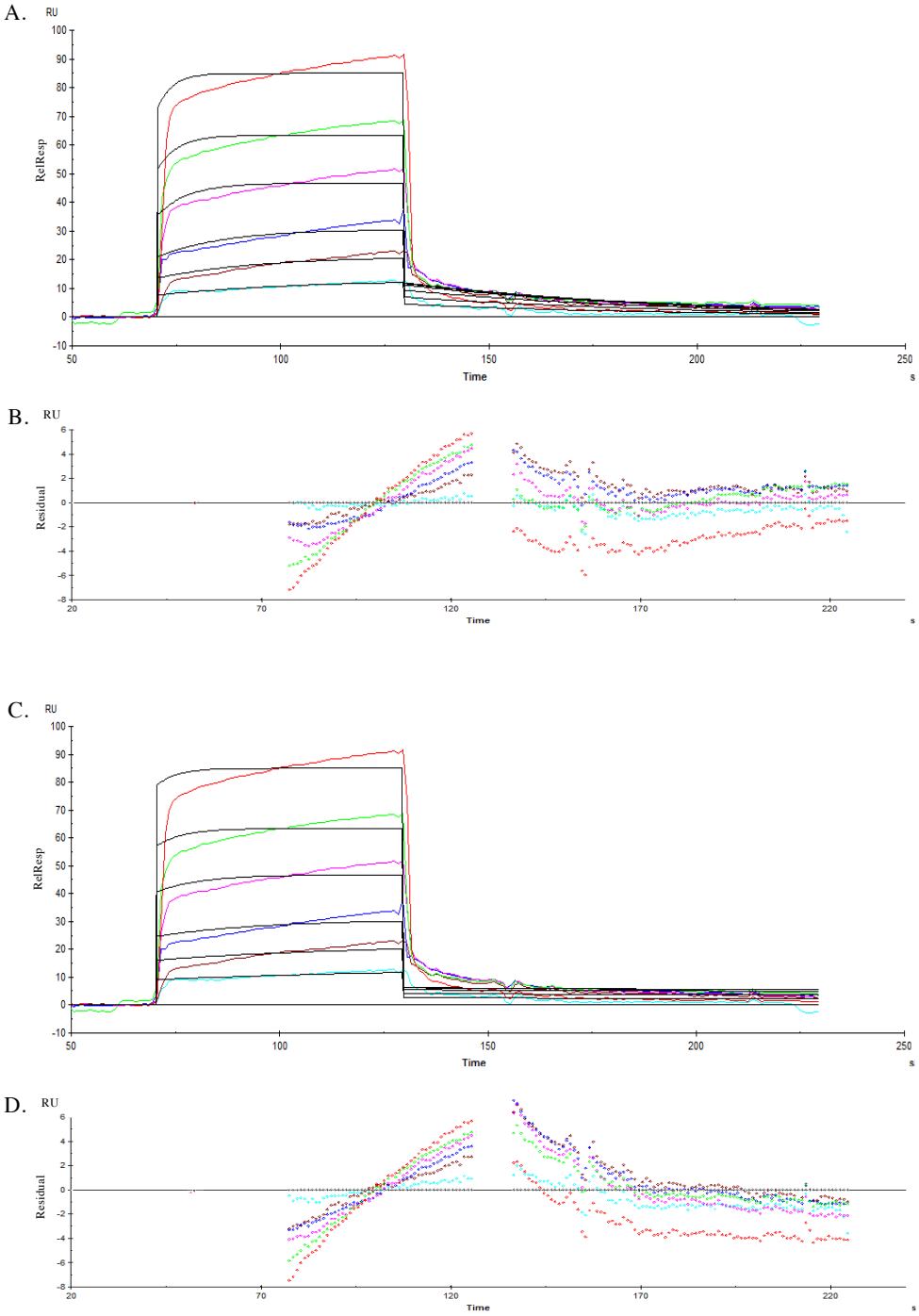

Figure 4.21: Kinetic analysis for meclofenamic acid using 1:1 Langmuir and heterogenous ligand-parallel reaction models (**A** and **C** respectively). The black lines are the fitting sensorgrams and the colorful lines are the experimental sensorgrams. **(B)** and **(D)** Residual plots for each kinetic model.

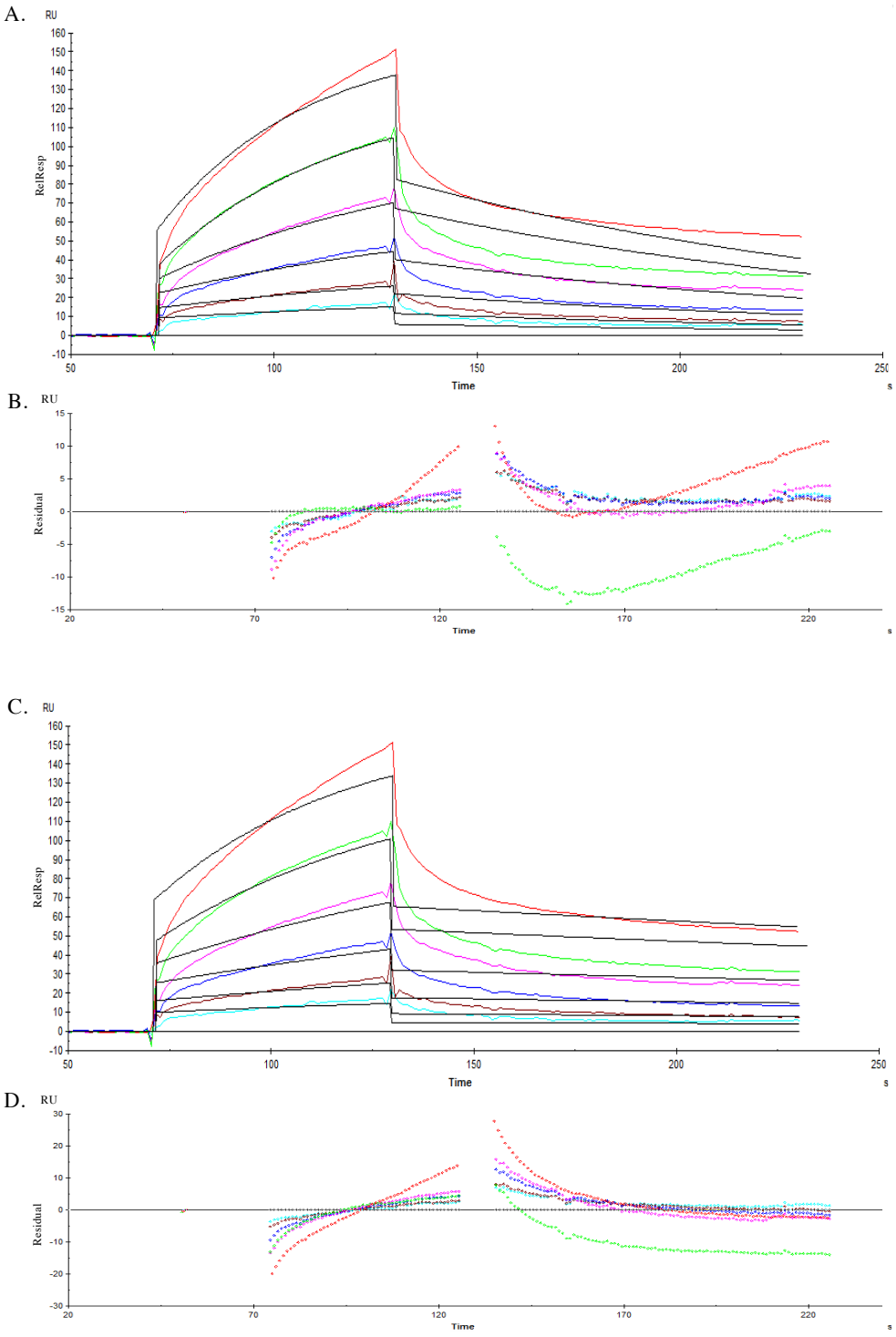

Figure 4.22: Kinetic analysis for rolitetracycline using 1:1 Langmuir and heterogenous ligand-parallel reaction models (**A** and **C** respectively). The black lines are the fitting sensorgrams and the colorful lines are the experimental sensorgrams. **(B)** and **(D)** Residual plots for each kinetic model.

Table 4.4: Quality of fit between the experimental sensorgrams and the 1:1 Langmuir and heterogenous ligand-parallel reaction models.

	Residual (RU)		Chi^2 (RU)	
	Fit 1	Fit 2	Fit 1	Fit 2
Doxycycline	-12.5 – 10	-12.5 – 10	8.83	9.29
Meclofenamic acid	-7 – 6	-7 – 8	3.51	5.05
Rolitetracycline	-15 – 13	-20 – 27.5	15.7	29.1

Fit 1 = 1:1 Lagmuir model; Fit 2 = Heterogeneous ligand-parallel reaction model.

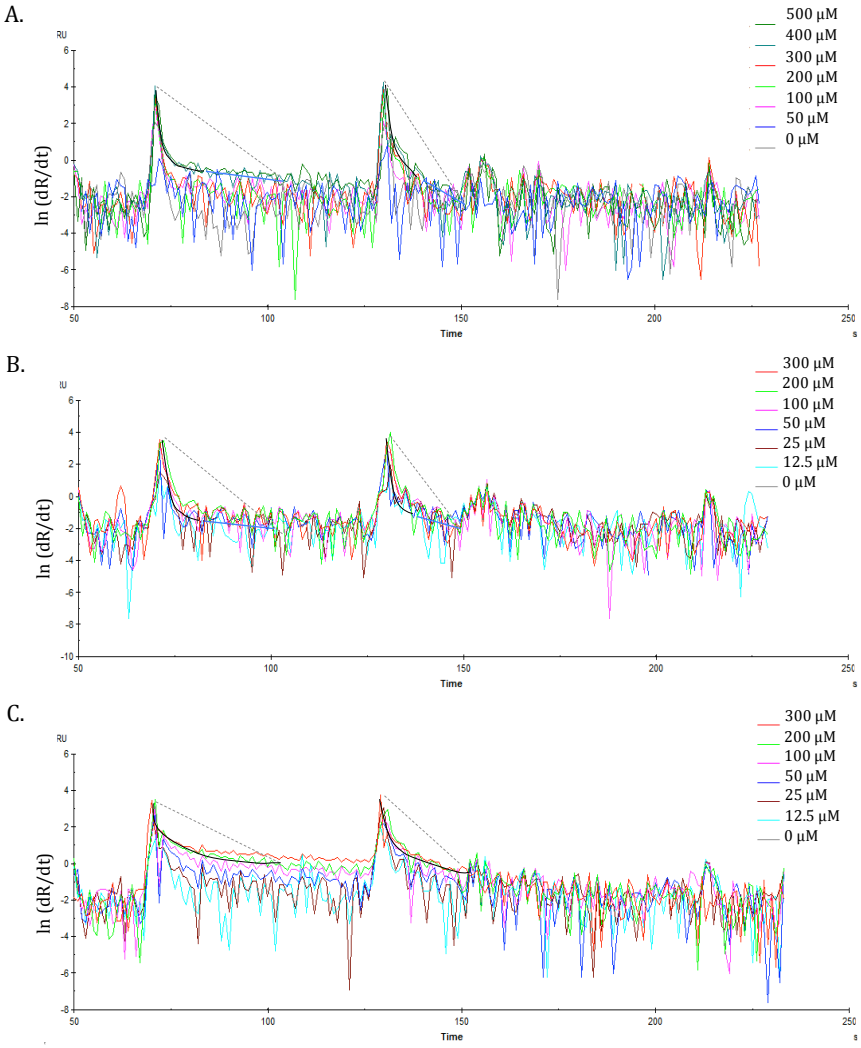

Figure 4.23: Kinetic analysis based on derivative function ln(dR/dt) reported by Episentec. Each is an analysis for **(A)** doxycycline, **(B)** meclofenamic acid and **(C)** rolitetracycline. The binding data from each analyte concentration was translated into the derivative function and plotted against time. The association phase is recorded between 70 – 130 s, while the dissociation phase is between 130 – 230 s. The black curves in the association and dissociation phases are highlighted to show the experimental slopes while the dash lines are highlighted to show how a linear slope should be obtained in a 1:1 Langmuir model.

4.3 *In silico* molecular docking

In silico molecular docking was used to simulate coupling process of three small molecule inhibitors with the homology model of the DENV-2 NS2B-NS3pro, namely DH-1 (Heh *et al*., 2013). According to Heh *et al.* (2013), the protease homology model was developed based on the crystal structure of the DENV-2 NS2B-NS3pro (PDBid: 2FOM) and West Nile Virus (WNV) (PDBid: 2FP7) (Erbel *et al*., 2006). Based on the Ramachandran plots, DH-1 have stereochemical quality, with more than 89% of residues are in the most favored regions, and no residue was detected in the disallowed regions. Verify3D revealed that DH-1 are compatible with the 1D amino acid sequences indicating adequate 3D atomic models. The conformation of the allosteric binding pocket in DH-1 was verified by docking the standard non-competitive ligands (cardamonin, and pinostrobin) (Kiat *et al*., 2006). These ligands interacted with Lys74 from NS3, an essential residue in the protease allosteric site (Othman *et al*., 2008) and the $K_{i\text{dock}}$ values were within the reported $K_{i\text{exp}}$ values (Kiat *et al*., 2006).

According to previous finding, only doxycycline corroborated as non-competitive inhibitor (Rothan *et al*., 2013), while meclofenamic acid and rolitetracycline have shown to inhibit the DENV-2 NS2B-NS3pro but without its inhibitory activity being characterized. Therefore, this study attempts to highlight how these ligands bind and interact with the residues from the binding site of the protease and further categorize the inhibition characteristics of meclofenamic acid and rolitetracyline. Molecular dockings were initialized based on the application of flexible ligands and blind docking to increase the search conformational space (Clark & Ajay, 1995; Hetényi & Spoel, 2006). To validate the docking methodology used in this study, two ligands namely pinostrobin and 4-hydroxypanduratin A were used to represent the standards for non-competitive and competitive inhibitors, respectively.

4.3.1 Non-competitive and competitive inhibitors

Figure 4.24 shows the superimposition of the target and standard ligands with the best binding mode (top ranking docked poses). In this finding, doxycycline was found to superimpose with the standard ligand pinostrobin at an allosteric site, proximal from the catalytic triad (His51, Asp75 and Ser135). This prediction correlates with a previous study that showed doxycycline as a non-competitive inhibitor towards the DENV-2 NS2B-NS3pro (Rothan *et al*., 2013). On the other hand, meclofenamic acid and rolitetracycline are predicted as competitive inhibitors as both are observed to superimpose with the standard ligand, 4-hydroxypanduratin A (competitive inhibitor). Additionally, all competitive ligands, 4-hydroxypanduratin A, meclofenamic acid and rolitetracycline are located close to His51 and Ser135.

4.3.2 Scoring function: Predicted binding energy

The scoring function was determined based on the affinity of the ligands with the residues in the binding site. Table 4.5 shows the comparison of output obtained from molecular docking and the biological activity based on the IC_{50} and K_i values of previous findings. The compounds are arranged accordingly from the strongest to the lowest binding energy value, E_{bind}. Together with the standard ligands, the non-competitive inhibitors (pinostrobin and doxycycline) are ranked among the highest (low E_{bind} values) followed by the competitive compounds (4-hydroxypanduratin A, meclofenamic acid and rolitetracycline). However, the E_{bind} values found in this study do not correlate with the trend in the experimental IC_{50} and K_i values obtained from previous studies. This might be due to the solvation effect that requires the incorporation of molecular descriptors to solve a more accurate interpretation of the conformational energy of ligands (Gupta *et al*., 2015). Therefore, it may not be reasonable to investigate the compound selectivity based on the docking binding energy.

In this case, docking results might not reflect the actual usefulness of pose and the prediction of binding affinity (Li *et al*., 2013). Nevertheless, molecular docking could be used as a tool to study the possible molecular residues and binding interactions that contribute to the ligands' binding conformations (Grinter & Zou, 2014).

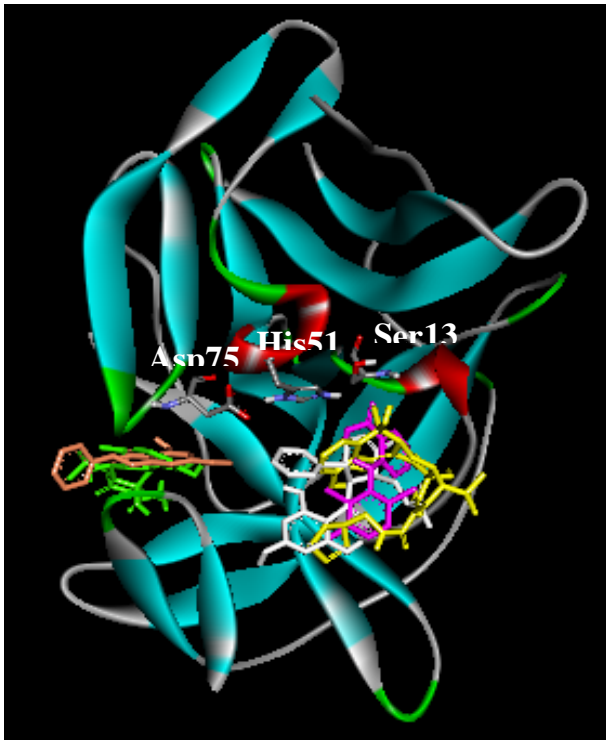

Figure 4.24: Three dimensional structure highlighting the best binding mode of ligands (sticks) in the DENV-2 NS2B-NS3pro (ribbons). NS2B is highlighted in moss green while the rest of the ribbons that are colored elementarily indicate NS3 protease region. Pinostrobin (orange) and 4-hydroxypanduratin A (white) are denoted as the standard ligands, while doxycycline, meclofenamic acid and rolitetracycline are displayed in green, pink and yellow respectively. Residues His51, Asp75 and Ser135 (elementary-colored sticks) are the catalytict riad. The image was generated using the Discovery Studio Visualizer 4.5.

Table 4.5: Relation between the predicted binding energies from docking analysis and the experimental inhibitory activities achieved from previous studies.

Compound	Docking			Experimental			
	No. of atoms	No. of rotatable bonds	E_{bind} [a] (kcal/mol)	IC_{50} [b] (µg/ml)	K_i [c] (µM)	% Inhibition [6] 25 µM	% Inhibition [6] 100 µM
Pinostrobin	34	3	-5.33	90.48 [1]	348 ±70 [4] 345 ± 70 [5]	NA	NA
Doxycycline	56	8	-5.15	52.3 ± 6.2 (at 37°C) [2] 26.7 ± 6.2 (at 40°C) [2] 55.6 [3]	55.6 ± 5.7 [6]	35.6 ± 3.2	53.8 ± 2.8
4-hydroxypanduratin A	57	8	-4.45	40 [5]	21 [5]	NA	NA
Meclofenamic acid	30	4	-3.64	NA	NA	19.4 ± 2.2	43.0 ± 1.4
Rolitetracycline	71	10	-3.21	67.1 [3]	NA	32.8 ± 2.6	38.9 ± 2.9

[a] Lowest binding energy; [b] Half maximal inhibitory concentration; [c] Inhibition constant.

[1] Othman *et al*. (2008); [2] Rothan *et al*. (2014c); [3] Yang *et al*. (2007); [4] Heh *et al*. (2013); [5] Kiat *et al*. (2006); [6] Rothan *et al*. (2013).

NA = Not available.

4.3.3 Binding conformation and interactions

The non-covalent interactions developed between the docked ligands with the residues from the binding site are elaborated further. Figure 4.25 shows the 3D and 2D poses of these ligands in the binding site of the DENV-2 NS2B-NS3pro. Hydrogen bond donors (HBD) and acceptors (HBA), and the length of H-bonds are further clarified in Table 4.6. Obviously, each ligand forms H-bond with the target protein. The (non-competitive) doxycycline involves the most number of H-bonds with Asn167, Trp89, Thr122 and Ile165 in the allosteric site. (Competitive) meclofenamic acid has H-bonding interaction with one of the catalytic triad (His51) and Gly151. Rolitetracycline forms H-bonds with Gly151, in addition to Phe130, Gly153 and Tyr161.

Other non-covalent interactions involving a carbon-oxygen dipole-dipole interaction together with van der Waals and pi effects are clearly demonstrated in the 2D illustrations (Figure 4.25, right). These interactions are further listed in Tables 4.6 and 4.7 together with the standard ligands (pinostrobin and 4-hydroxypanduratin A) for comparison and validation. Based on Table 4.6, doxycycline is involved in a pi-H-bonding with Asn167, a carbon-oxygen dipole-dipole interaction with Glu88. Van der Waals interaction is also observed with Glu91, Thr120, Gly124, Ala164, Ala166 (Table 4.7). For meclofenamic acid and rolitetracycline, both have similirities in incorporating Ser135 (one of the catalytic triad), and other residues Thr134, Tyr150 and Val154 in the van der Waals interactions (Table 4.7). Individually, other residues involved in van der Waals interactions with meclofenamic acid are Phe130, Ser131, Pro132, Asn152 and Gly153, and Asp 129 with rolitetracycline. Among the two competitive compounds, pi effects that are observed only in meclofenamic acid are the alkyl-pi interaction (with Val155 and Tyr161), and a T-shaped pi-pi interaction (between the two benzene rings in meclofenamic acid with Tyr161) (Table 4.7). For rolitetracycline, His51 is observed

to engage in both cation-pi and pi-pi stacking interactions (Table 4.7), which is overlayed to each other based on the 3D structure (Figure 4.25, left).

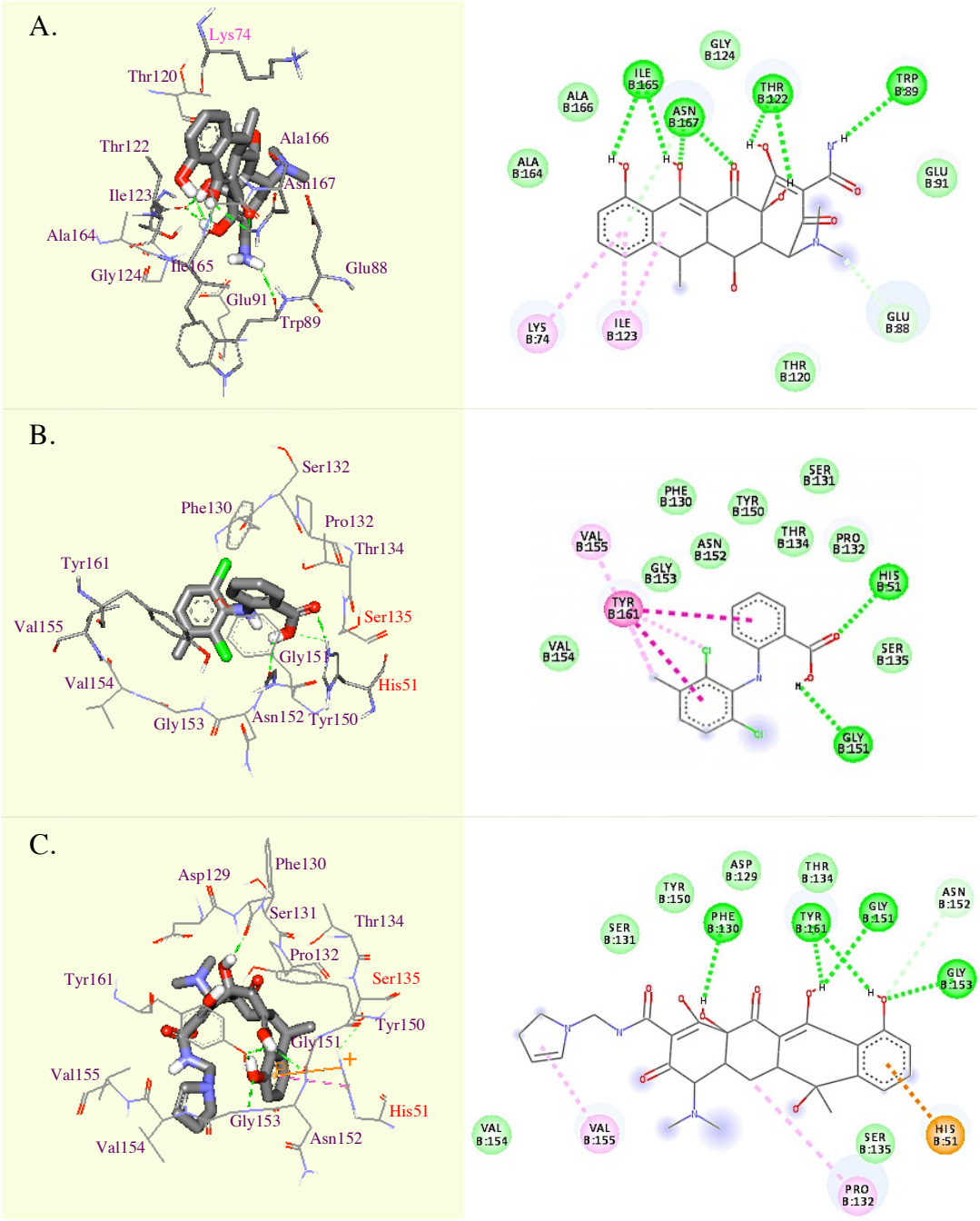

Figure 4.25: The 2D and 3D structural views of ligand-binding site interactions. The ligands are **(A)** doxycycline, **(B)** meclofenamic acid and **(C)** rolitetracycline. The 3D structures display H-bond interactions (green dashed lines) between ligands (sticks) and the binding site (wire frames). A clear observation of cation-pi (orange line) and pi-pi stacking (pink dashed line) are observed only in rolitetracycline. Main residues from both the allosteric site, Lys74 (pink) and the catalytic triad, His51 and Ser135 (orange) are observed. Simplified visualization is illustrated in 2D, which display the H-bonding (dark green circles associated with the green dashed lines); van der Waals forces (medium light green circles); carbon-oxygen dipole-dipole interaction (light green circles with dashed lines); alkyl-pi interactions (light pink circles with dashed lines); T-shaped pi-pi stacking and (parallel) pi-pi stacking (both indicated with dark pink circles); cation-pi interaction (orange circle). The blue halo surrounding the interacting residues represents the solvent accessible surface that is proportional to its diameter. Images were generated using Discovery Studio Visualizer 4.5.

Table 4.6: Residues involved in the H-bonding, pi-H bonding and dipole-dipole interactions in the ligand-protease complex, as determined using Discovery Studio Visualizer 4.5.

ID	H-bond					Pi H-bond	Carbon-Oxygen Dipole-Dipole
	Donors		Acceptors		Distances		
	Atoms	F. groups	Atoms	F.groups	(Å)		
1	B:Asn152:HD21	-NH	O4	-C-O-C-	1.93527	NA	C20 – B:Asn152:O
	B:Asn167:HN	-NH	O3	-OH	1.83825		
	H31	-OH	B:Asn167:O	-C=O	1.90466		
2	B:Asn167:HD22	-NH	O3	-C=O	1.89173	B:Asn167:HN – b	C28 – B:Glu88:OE1
	B:Asn167:HD22	-NH	O5	-OH	2.63800		
	H54	-NH	B:Trp89:O	-C=O	2.38811		
	H50	-OH	B:Thr122:O	-C=O	2.06387		
	H42	-OH	B:Thr122:O	-C=O	1.64877		
	H51	-OH	B:Ile165:O	-C=O	1.90640		
	H56	-OH	B:Ile165:O	-C=O	2.35336		
3	B:Gly153: HN	-NH	O3	-OH	1.85400	NA	A:Ser83:CB– Ob1
	H56	-OH	B:Asn152:OD1	-C=O	1.70581		
	H57	-OH	A:Met84:O	-C=O	2.10307		
4	B: His51:HE2	-NH	O4	-C=O*	2.11584	NA	NA
	B: His51:HE2	-NH	O3	-OH*	2.21816		
	H30	-OH*	B: Gly151:O	-C=O	2.31655		
5	H47	-OH	B:Phe130:O	-C=O	1.78001	NA	B:Asn152:CA – O7
	H57	-OH	B:Gly151:O	-C=O	2.24901		
	H57	-OH	B:Tyr161:OH	-OH	2.18301		
	H71	-OH	B:Tyr161:OH	-OH	2.00355		
	B:Gly153:HN	-NH	O7	-OH	2.72705		

* Carbonyl (-C=O) and hydroxyl (-OH) groups from the same carboxyl (-COOH) functional group.

1 = Pinostrobin; **2** = Doxycycline; **3** = 4-hydroxypanduratin A; **4** = Meclofenamic acid; **5** = Rolitetracycline. F. groups = Functional groups; – = Interacts with.

b1 = Benzene 1; A = NS2B chain in the NS2B-NS3 protease; B = NS3 protease chain in the NS2B-NS3 protease; NA = Not available. For H-bond donors and acceptors; the functional group from where the atom derived is mentioned; and the atoms that are displayed as individuals are indicating contributors from the ligand.

Table 4.7: Residues involved in pi-effects, van der Waals forces and hydrophobic interactions.

Compound	Alkyl-pi	Sigma-pi	Cation-pi	Pi-pi stacking	T-shaped pi-pi	van der Waals	Hydrophobic
Pinostrobin	B:Lys73 – b1 B:Lys74 – b1 B:Lys74 – b2 A:Ile78 – b1 B:Ala164 – b1 B:Ala166 – b2	NA	NA	NA	NA	B:Ile165 B:Asp71 A:Met84	B:Asp71 B:Lys73 B:Lys74 A:Ile78 A:Met84 B:Glu88 B:Ala164 B:Ala166
Doxycycline	NA	NA	NA	NA	NA	B:Glu91 B:Thr120 B:Gly124 B:Ala164 B:Ala166	B:Lys74 A:Ser83 B:Ile123 B:Ala164 B:Ala166
4-hydroxypanduratin A	B:His51 – chy B:Tyr150 – C14 B:Tyr161 – C26	C25 – B:Tyr161	NA	NA	B:His51 – b2	B:Asp75 B:Asp129 B:Phe130 B:Thr134 B:Ser135 B:Gly151 B:Gly153 B:Val155	B:His51 B:Asp75 A:Ser83 B:Asp129 B:Phe130 B:Tyr150 B:Gly151 B:Val155 B:Tyr161
Meclofenamic acid	B:Val155 – C16 B:Tyr161 – Cl1 B:Tyr161 – C16	NA	NA	NA	B:Tyr161 – b1 B:Tyr161 – b2	B:Phe130 B:Ser131 B:Pro132 B:Thr134 B:Ser135 B:Tyr150 B:Asn152 B:Gly153 B:Val154	B:Phe130 B:Ser131 B:Thr134 B:Ser135 B:Tyr150 B:Gly153 B:Val154 B:Val155 B:Tyr161
Rolitetracycline	NA	NA	B:His51:NE2 – b	B:His51 – b	NA	B:Asp129 B:Thr134 B:Ser135 B:Tyr150 B:Val154	B:His51 B:Pro132 B:Ser135 B:Asn152 B:Gly153 B:Val154 B:Val155

– = Interacts with; b = Benzene; b1 = Benzene 1; b2 = Benzene 2; chy = Cyclohexenyl scaffold; cho = Cyclohexanone; chol = Cyclohexenol scaffold; py = Pyrrolidine**;**
A = NS2B chain in the NS2B-NS3 protease; B = NS3pro chain in the NS2B-NS3 protease; NA = Not available. Atoms stated individually are indicating contributors from the ligand.

4.3.4 Hydrophobic interaction

A simplified list of hydrophobic interactions is mentioned in Table 4.7. A visual inspection of the 2D structural view is depicted in Figure 4.26. Based on the 2D structural analysis, the amino acid residues from the non-competitive ligand (doxycycline); Glu88, Ile123, Ala164 and Ala166 are conserved in the hydrophobic binding pocket of the target protein, NS2B-NS3 protease, including Lys74, a key residue in the protease allosteric site (Othman *et al*., 2008), Likewise, the standard ligand (pinostrobin) is observed to have the same hydrophobic interaction with these residues, and additionally with Asp71, Lys73, Ile78 and Met84. In the case of competitive ligands, meclofenamic acid and rolitetracycline, both exhibit hydrophobic interactions with one of the catalytic triads, Ser135, and other residues Gly153, Val155, and Val154. Additionally, meclofenamic acid interacts with Phe130, Ser131, Thr134, Tyr150 and Tyr161. On the other hand, rolitetracycline also interacts with Pro132, Asn152 and another residue from the catalytic triad, His51. Among these residues, Phe130, Tyr150, Val155, Tyr161 and His51 (a catalytic triad) show hydrophobic interactions with the standard competitive inhibitor (4-hydroxypanduratin A). Meanwhile, Asp75, Ser83, Asp129 and Gly151 are other residues found in 4-hydroxypanduratin A but not in meclofenamic acid and rolitetracycline.

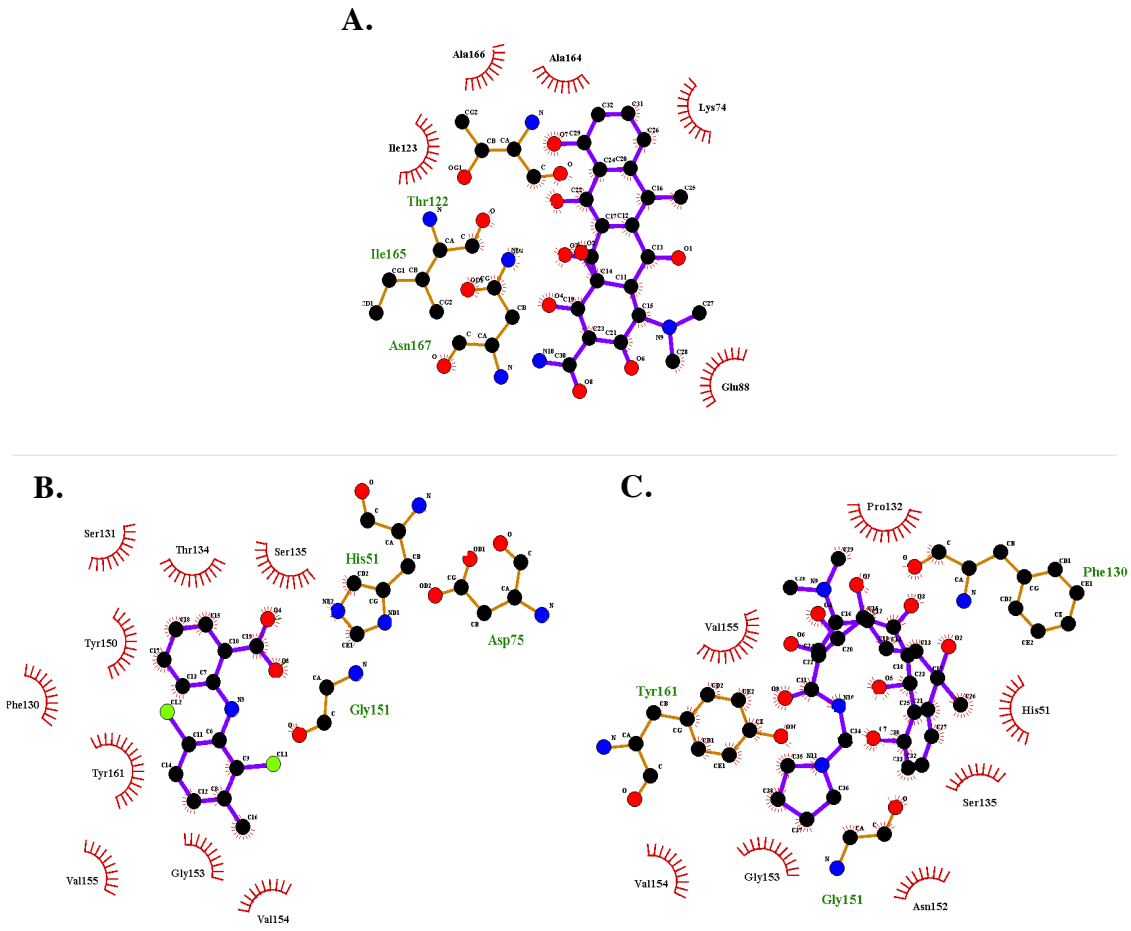

Figure 4.26: Hydrophobic interactions between the ligands and the binding site. The compounds are **(A)** doxycycline, **(B)** meclofenamic acid and **(C)** rolitetracycline. The 2D structures ligand are represented as thick purple sticks. The residues of the binding site are illustrated as brown sticks and those involved in the hydrophobic interactions are depicted as red half-moon lashes. The 2D structural views were generated using the Ligplot program.

4.3.5 Binding pocket and Electrostatic Potential Surface (EPS)

Figure 4.27 shows the different poses of the ligands in the binding pocket. The active site where doxycycline binds is a narrow cleft with a deep hollow, somewhat showing a direct shape complementarity with the structural configuration of the ligand. Relatively, the cleft enclosing the competitive ligands (meclofenamic acid and rolitetracycline) is more exposed and wider. From the top view, it is evident that the shape of the cleft is inclined to the left leaving a more spacious area to the right region of the pocket (Figure 4.27, top). For doxycycline, the cyclohexenone scaffold (with the amide and tertiary amine functional groups) and a tetrahydroquinone scaffold are residing in the left cleft,

while the right cleft is filled with the cyclohexanol and phenolic scaffolds.. For meclofenamic acid, it can be observed that the dichloro toluene ring is occupying the centre of the binding site, while the benzoic acid moiety is seen to reside in the top region of the binding site (Figure 4.27, top). On the contrary, the comparatively extended structure of rolitetracycline is observed to occupy the whole binding pocket with both the terminal pyrrolidine and phenolic rings bent towards the left cleft (Figure 4.27, top). The right cleft of pocket is filled with most part of the 4-methylcyclohexen-1,4-diol moiety and the cyclohexanone, and cyclohexenone scaffolds with the tertiary amine and hydroxyl functional groups. Additionally, the amide group was found situated in the middle of the binding clefts.

The investigation of electrostatic charge distribution revealed variations in surface electrostatic potential at different area of the binding site. Overall, both the binding sites for the non-competitive and the predicted competitive ligands exhibited a mixture of negative (red), positive (blue) and neutral (or hydrophobic; white) surface area. The most prominent area is depicted in bold red demonstrating highly negative potential. For doxycycline, this is more observable on the left side of the binding pocket that is dispersed into two prominent places, which attracts the tertiary amine functional group (the upper region) and the amide side chain (the left region) (Figure 4.27, left and top). This is the opposite of meclofenamic acid and rolitetracycline where the highly positive area is seen on the right side of the binding pocket. As a result, the dichlorotoluene ring in meclofenamic acid could be repelled and bend towards the left side of the cleft (Figure 4.27, all views). But in the case of rolitetracycline, this negative EPS could have attracted the tertiary amine functional group (Figure 4.27, left and top).

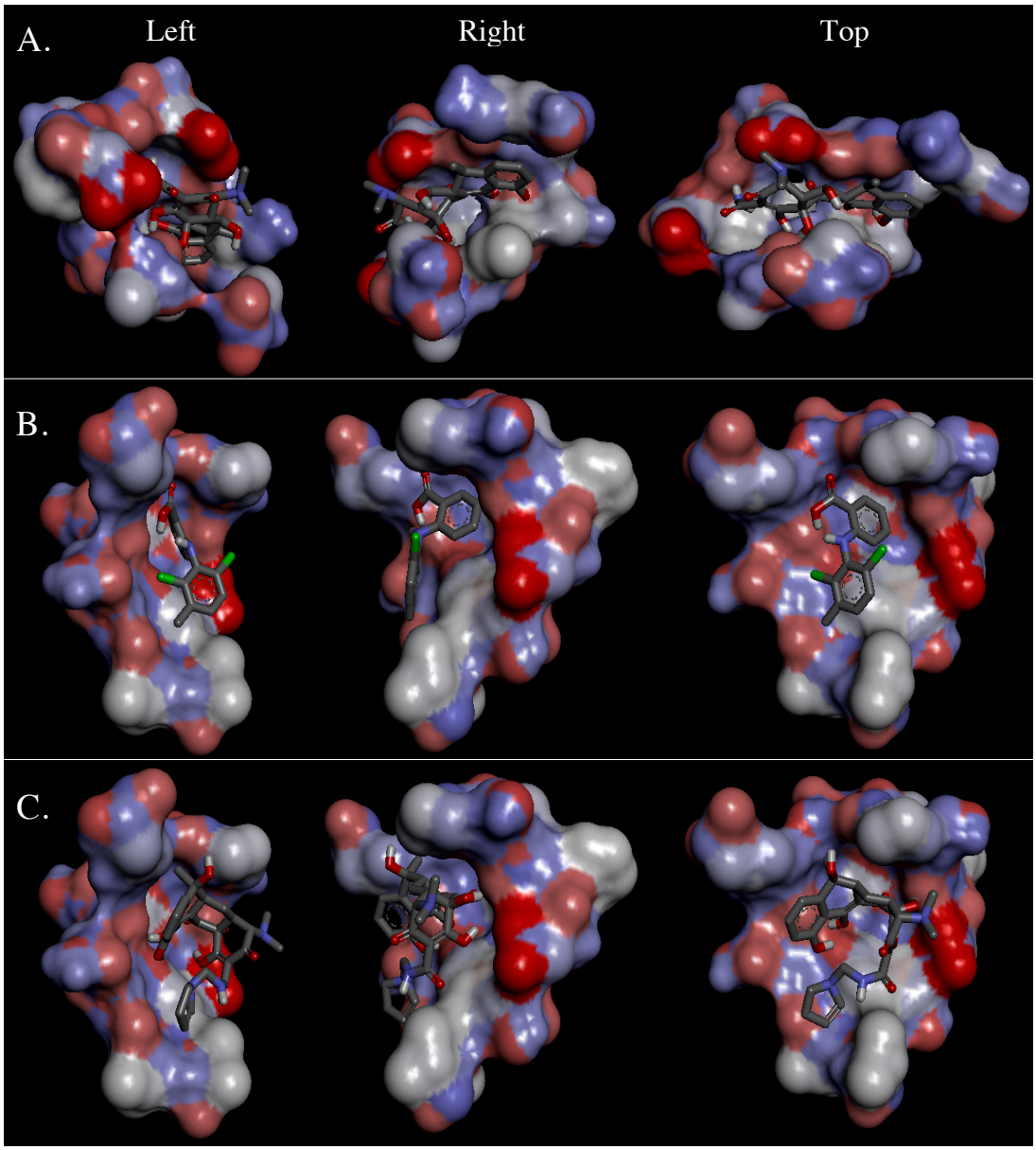

Figure 4.27: Connolly surface representation of the electrostatic potential in the binding pocket of the DENV-2 NS2B-NS3pro complexed with ligands. Each ligand, **(A)** doxycycline, **(B)** meclofenamic acid and **(C)** rolitetracycline are shown as sticks with multiple views from the right, left and top. Connolly surface with red color indicates negative potential, blue surface represents positive potential and white surface for neutral groups. The images were generated using the Discovery Studio Visualizer 4.5.

CHAPTER 2 : DISCUSSION

5.1 DNA validation, expression, purification and the characterization of the DENV-2 NS2B-NS3pro

This study highlights the protease construct from Heh *et al.* (2013) that involves the substitution of residue Ser in the glycine linker, to Trp (Gly4-Trp-Gly4) (Heh *et al*., 2012). This is unlike the typical construct from the previous studies using Gly4-Ser-Gly4 linker (Arakaki *et al*., 2002; Clum *et al*., 1997; Erbel *et al*., 2006; Leung *et al*., 2001). Upon investigations, the protease construct has high similarity with the DENV-2 strain BA05i (Section 4.1.1). The 1% non-mismatched DNA sequence is expected because the protease construct used in this study was from the DENV-2 of the New Guinea C strain (Heh *et al*., 2012; Irie *et al*., 1989). The protease construct was successfully expressed (Section 4.1.2) correlated with findings by Heh *et al*. (2013) and as further validated by the western blot and MS analyses (Section 4.12). Nevertheless, unlike Heh *et al*. (2013), further purification with SEC was performed to exclude the lower MW protein bands (Figure 4.7) but still remained visible, consistent with the purification profile of proteases with typical linker (Arakaki *et al*., 2002; Bera *et al*., 2007; Clum *et al*., 1997; Erbel *et al*., 2006; Kim *et al*., 2013; Leung *et al*., 2001).

According to Arakaki *et al*. (2002), the low MW proteins are not the products of bacterial proteolytic or the autoproteolytic activity of NS2B-NS3pro. This is based on several investigations involving optimizing buffer conditions, extensive purifications (using ion exchange chromatography (IEC), hydrophobic interaction chromatography (HIC), Ni-IMAC and SEC), expression in different cell strains, mutation of the catalytic triad (Ser135 to Ala), implementation of protease inhibitors and several attempts with denaturing and native condition during the purification level, which do not lead to better protein purity. Therefore, they suggest that the low MW proteins may possibly be

the premature translation termination or as a result of frame-shifts and premature termination (resulted from ribosomal slippage at the codons rarely used in *E.coli*).

However, there have been several studies claiming that the lower MW proteins are indeed products of the autoproteolytic cleavage (Bera *et al*., 2007; Bessaud *et al*., 2006; Postarino *et al*., 2007). Choksupmanee *et al*. (2012) also claimed that there is a plausible autoproteolytic site in the DENV-2 NS3pro at the $KQK^{28}\downarrow G^{29}$ site, which closely resembles the NS2B−NS3pro junction. It is ruled out as an uncommon cleavage site as the residue Gln deviates from the common residues for P2 (Arg and Lys) (Yusof *et al*., 2000). Considering these findings, therefore it is possible to say that the low MW proteins found in this study may be the autoproteolytic products of the DENV-2 NS2B-NS3pro.

Protease oligomerization has been determined using SEC (Figure 4.7) and native PAGE (Figure 4.10) analyses with sizes two-fold larger than Arakaki *et al*. (2002). Possibly due to the modification in the glycine linker that could induce the protease's conformational dynamics (Kim *et al*., 2013). The lower MW fragments in the native PAGE is also observed by Arakaki *et al*. (2002). To our knowledge, these may be due to the autoproteolytic products. However, Arakaki *et al*. (2002) has made no clarification upon this issue. As protein activity may or may not be affected by oligomerization, previous studies have shown that the protease construct developed by Heh *et al*. (2013) has been proven active based on several biochemical studies involving *in vitro* protease enzymatic assays (Rothan *et al*., 2013; Rothan *et al*., 2014a; Rothan *et al*., 2014b; Rothan *et al*., 2014c).

In summary, we have purified and homogenized the DENV-2 NS2B-NS3pro using SEC. Upon purifications, peak c showed a comparatively well separated elution profile compared to peaks a and b (Figure 4.7), with the smallest oligomeric size (dimeric) (Figures 4.7 and 410). For this reason, NS2B-NS3pro from peak c was used in the SPR assay (Section 5.2) for kinetic analysis with small molecule protease inhibitors from medicinal drugs.

5.2 SPR assay on CM5 chip

A previous study has shown that NS2B-NS3pro can be immobilized onto CM5 chip using amine coupling (Liu *et al*., 2014). Therefore, our initial attempt was to use the same method for amine coupling to study the kinetic analysis between NS2B-NS3pro and its inhibitors; the small molecule medicinal drugs namely doxycycline, meclofenamic acid and rolitetracycline. In this study, NS2B-NS3pro was used as the ligand while the small molecule compounds act as the analytes.

5.2.1 Pre-concentration and amine coupling

Pre-concentration is a procedure used to allow a high local ligand concentration at the surface of the sensor chip (Merwe, 2003). This process is required only with the CM based sensor chips such as the CM5 chip. Pre-concentration was determined using pH scouting to search for an optimal pH that could efficiently pre-concentrate NS2B-NS3pro to the surface of the sensor chip (GE Healthcare, 2012). Pre-concentration was performed in a standard range between pH 3.5 and the isoelectric point (pI) of NS2B-NS3pro (pI 5.75). At pH above 3.5, the CM-dextran is turned into a negative charged, while pH below the pI value allows the ligand to be positively charged (GE Healthcare, 2007a). Consequently both incidents allow the formation of electrostatic potential interaction between the CM-dextran and the ligand, which in this case is the DENV-2

NS2B-NS3pro. In this study, pH scouting was narrowed into pH 4 and 5 (Bodenreider *et al*., 2009; Liu *et al*., 2014). It was shown the pre-concentration level of 50 µg/ml of NS2B-NS3pro was higher in pH 4 than at pH 5; 9302.1 and 4765.3 RU respectively (Figure 4.11). This further indicates that pH 4 is an optimal pH to pre-concentrate NS2B-NS3pro, consistent with that found by Liu *et al*. (2014). 50 µg/ml of NS2B-NS3pro was also found as a suitable concentration for immobilization since the pre-concentration level was able to reach and exceeded the targeted immobilization level of 6000 RU. This is in accordance to the standard range for ligand immobilization (800 – 7500 RU) (Azmi *et al*., 2010).

50 µg/ml of NS2B-NS3pro was reconstituted in 10 mM sodium acetate, pH 4 for pre-concentration. During this process, the amine groups in NS2B-NS3pro cross reacted with the ester groups on the surface of the CM5 chip (which developed once the surface is activated with EDC/NHS solution, as described in Section 2.2.3). Consequently amine coupling took place and covalently immobilize NS2B-NS3pro. With the 'Aim for immobilization' wizard (Section 3.3.6.3) the immobilization level was able to reach 6020.5 RU (Figure 4.12). Although a higher pre-concentration level is seen during pH scouting (9302.1 RU) (Figure 4.11), the immobilization level is able to maintain within the treshold value (6000 RU) when the 'Aim for immobilization' wizard is implemented (GE Healthcare, 2007a).

5.2.2 Binding analysis

Overall, we have observed poor results from the binding analysis between the small molecule compound-NS2B-NS3pro interactions using CM5 chip. A representative analyte, meclofenamic acid, exhibited a progressively negative binding profile with the association phase dropped significantly (Figure 4.13). This indicates a progressive

dissociation of meclofenamic acid from NS2B-NS3pro, which continues until its injection stopped. Dissociation of NS2B-NS3pro from the sensor surface may cause bound meclofenamic acid to dissociate simultaneously and cause the decreasing binding signal. However, this is impossible since NS2B-NS3pro was covalently immobilized using amine coupling. This is further confirmed based on the constant baseline level depicted from each binding cycle. Furthermore, there was no significant baseline drift to indicate the dissociation of NS2B-NS3pro (Wear *et al*., 2005). Therefore, we presume that the decreasing binding signal may be caused by the deterioration of the biological activity of NS2B-NS3pro due to amine coupling. It is well known that amine coupling causes random orientation of ligand, wherein the binding or the active sites that contain amine group may have been interacted with the CM-dextran and resulted to the inactivation or deterioration of NS2B-NS3pro activity.

This further shows that our finding seems to contradict to that established by previous finding (Liu *et al*., 2014). In their studies, they are able to perform binding analysis and consequently revealed the K_D values for the interactions with small molecule compounds based on the 1:1 Langmuir kinetic model. As it is essential to show how good the sensorgram fit to a kinetic model, Liu *et al*. (2014) however, have not published the kinetically fitted sensorgrams. In other words, it is ambigous to judge the quality of the kinetic analysis based on only the 'bare' sensorgrams (Rich & Myszka, 2000; Rich & Myszka, 2001; Rich & Myszka, 2002; Rich & Myszka, 2005a; Rich & Myszka, 2005b; Rich & Myszka, 2006; Rich & Myszka, 2008; Rich & Myszka, 2010; Rich & Myszka, 2011). Additionally, no residuals or Chi^2 distribution values are exhibited to validate the quality of the kinetic fitting. Meanwhile, another study using ligand–thiol coupling on cysteinated NS2B-NS3pro of the DENV-2 also claimed a 1:1 Langmuir kinetic fitting (Bodenreider *et al*., 2009). However, there is no sensorgram

shown to prove the kinetic values understudied. Therefore, the reliability of these kinetic studies is still difficult to judge, especially with its relation to the biological form of NS2B-NS3pro to interact in a 1:1 binding interaction. Due to these facts, we are unable to relate with the cause of the unsuccessful binding analysis that we encountered with the amine coupling method. Alternatively, we had shifted on using the capture coupling method to immobilize NS2B-NS3pro onto the NTA chip (Section 5.3).

5.3 SPR assay on NTA chip

5.3.1 Optimization for binding analysis

The NTA chip consists of the CM-dextran pre-immobilized with NTA (GE Healthcare, 2013b). For immobilization based on capture coupling, an electrostatic pre-concentration is not required because the ligand is easily captured by the His-tags (SPR-Pages, 2015b). The 'ligand concentration scouting' was performed not only to evaluate the immobilization level but also to examine the potency of the Ni moieties to capture. It also allows the evaluation of the regeneration solution to wash both bound Ni and the captured NS2B-NS3pro, so that the sensor surface can be reused for capture coupling (Figure 4.14).

Capture coupling is a method of immobilization that is superior to capture and amine coupling alone, as it combines the benefits of both. With capture coupling, the ligand is not only captured in a homogenous orientation but also covalently immobilized by amine coupling that it prevents the ligand from being dissociated. Furthermore, oriented immobilization allows a higher specific binding analysis (Guiducci, 2011). In capture coupling, the ligand will first be captured by the Ni on the NTA surface, before being immobilized based on amine coupling. Unprompted amine coupling is unlikely to develop since NS2B-NS3pro requires an acidic condition (pH 4) is required for this

purpose. On the other hand, capture coupling was performed in a neutral condition (pH 7.4), which is impossible to pre-concentrate and immobilize NS2B-NS3pro based on amine coupling unless it is first captured by the His-tags (GE Healthcare, 2007a; Willard & Siderovski, 2006).

Compared to those found with amine coupled NS2B-NS3pro, the analyte showed good binding to the capture coupled NS2B-NS3pro based on the increment of response level during the association phase (Figure 4.16). Although Bodenreider *et al*. (2009) and Liu *et al*. (2014) have successfully use amine coupling on CM5 chip as a mean for binding analysis, looking at another view, this could suggest that oriented immobilization using capture coupling conserves the NS2B-NS3pro activity by persevering its binding or active sites from being modified (GE Healthcare, 2012, Guiducci, 2011).

To determine the optimal analyte concentration range and its injection length, we had scout initially with a vast variety of concentrations in serial dilutions. The analyte was injected with a progressively increasing concentration until a signal was detected and sufficient curvature is seen. From this, an optimal concentration was evaluated and selected. Too low concentration range and too short injection length had resulted in a linear association phase rather than a curvy trend. On the other hand, too a high concentration range and too much time an injection length had caused most of the binding curve to saturate in one side and nearly overlaid each other. As a result, the optimal concentrations range of 0 – 500 μM was chosen for doxycycline while 0 – 300 μM for meclofenamic acid and rolitetracycline (Figure 4.19).

5.3.2 Double referencing

In this study, the binding sensorgrams had been corrected from several artifacts using 'double referencing' to allow accurate and specific binding reactions (Cooper, 2009) to NS2B-NS3pro (Figure 4.16). It involves the first subtraction from the reference cell (Fc1) to remove non-specific binding responses corresponding to rolitetracycline (the representative analyte) bulk refractive index and matrix effect. This is followed by another subtraction from the running buffer (blank) injected into the sample flow cell (Fc2) containing immobilized NSB-NS3pro (Myszka, 1999). The reference flow cell (Fc1) used in this study contained only the activated surface with 1:1 EDC/NHS solution followed by blocking with ethanolamine. The same was applied for Fc2 but with the immobilization of NS2B-NS3pro. The method used for the reference cell not only would remove bulk refractive index and matrix effect but also decrease the negative charge on the sensor surface and reduce non-specific binding (Guiducci, 2011).

For rolitetracycline, the responses in Fc1 and Fc2 showed a 'shark's fin' like shape that indicates binding of non-specific interaction of rolitetracycline to the reference flow cell and the sample flow cell respectively (Figure 4.16A). An effort to remove the non-specific binding response from rolitetracycline through reference subtraction (Fc2-1, or technically termed as Fc2-Fc1) still retain the 'shark's fin' shape sensorgram (Figure 4.16B). Generally, non-specific binding could be corrected simply by reference subtraction although it may not be corrected accurately since the binding in the reference cell (Fc1) is not necessarily identical to that in the sample cell (Fc2) (GE Healthcare, 2013a). It is expected that the non-specific binding is higher in Fc2 due to the cumulative interaction with the immobilized NS2B-NS3pro. Nevertheless, there is no issue of non-specific binding found with doxycycline and meclofenamic acid

(Appendix F).

Another issue that we found is the high bulk refractive index contributed in each analyte binding study. Bulk refractive index is a common occurrence in SPR assay and it is developed due to the difference between the running buffer and sample buffer. In most situations, it can be eliminated by reference subtraction. The bulk refractive index was detected based on the rapid shift of response at the beginning and end of analyte injection. However, the bulk refractive index observed in Fc1 is prominent. The values are beyond the acceptable range (5-10 RU) (GE Healthcare, 2012) and it varies between the different analyte concentrations. Due to the high bulk refractive index, reference subtraction could not remove the whole responses from the bulk refractive index.

In general, this suggests the need to optimize further on a better reference flow cell by immobilizing irrelevant ligands such as BSA to mimic the active surface as closely as possible by approximate the same immobilization level as NS2B-NS3pro. Another method is to simply use an unmodified reference flow cell (without both the activation and immobilization of irrelevant ligand) to inspect for non-specific binding to the dextran matrix (Cooper, 2009).

To complete the data processing, the reference subtracted sensorgrams (Fc2-1) were double referenced by subtracting the average of blank injections (0 μM). This is to remove systemic deviation, baseline drift and noises that could generate false positive or negative responses. These artefacts mainly occur equally during analyte and blank injections (Myszka, 1999). The sensorgrams obtained in this study are of excellent quality in terms of low noise and good repeatability (Figure 4.16 B and C). Consequently, this shows that the level of immobilization is optimum as a low level

could as well cause the noise and baseline drift to be more apparent (Guiducci, 2011). The repeatability (overlaid triplicates) also demonstrates the stability of NS2B-NS3pro and its ability to bind reproducibly the same density of analyte (Rich *et al*., 2002). However, for rolitetracycline, the dissociation did not reach baseline level possibly due to the non-specific binding to the matrix of the sensor chip. Therefore, regeneration was performed, which is explained in the next section (Section 5.3.3).

5.3.3 Regeneration for rolitetracycline

Regeneration is one of the most critical parts of SPR assay, as it affects the reproducibility of interaction data. For rolitetracycline, our first attempt in regeneration scouting began with the mildest regeneration condition to avoid the unnecessary effect on the ligand, started from 1M NaCl and 10 mM glycine pH 3, to a more moderate condition (10 mM glycine pH 2.5 and 2) and finally to a slightly harsher condition (10 mM HCl, pH 1). However the last regeneration solution with 10 mM HCl of pH 1 showed an optimal regeneration condition (Figure 4.17). During the first cycle of its regeneration, 89% of analyte was removed, which later increased to 97% during the next and the following cycles (Table 4.3). On average, >90% of analyte were removed indicating an excellent regeneration achievement (Merwe, 2003).

Based on the surface performance test (Figure (4.18), the baseline levels were constant after each regeneration cycle demonstrating of no accumulation of analyte from the previous cycle. This further suggests that the regeneration condition is sufficient to wash out all bound analyte. The constant analyte binding response also indicates that there is no loss of binding capacity, which means HCl is not harsh and did not deteriorate the biological activity of NS2B-NS3pro. The low pH may prossibly transforms NS2B-NS3pro to become positively charged and partly unfolded

(Andersson *et al*., 1999a). The unfolding process brings the NS2B-NS3pro further apart while the binding sites repel each other. The ability of HCl to remove all bound analyte without causing any irreversible changes to NS2B-NS3pro allows an accurate and reliable binding analysis (Andersson *et al*., 1999b).

5.3.4 An attempt for kinetic determination

From the binding sensorgrams (Figure 4.19), it is clear that the association phase did not saturate to reach steady state, even even at higher analyte concentration. Mostly this could be translated as the deviation from the ideal pseudo-first order binding kinetics (the 1:1 Langmuir interaction model). The non-specific binding and high bulk refractive index may contribute to this deviation. However, other aspects that should also be considered are the heterogeneity in ligand immobilization and binding of analyte under mass transport limitation (MTL). These two are the most common factors that cause the deviation (Zhao, 2010). In this study, ligand heterogeneity could possibly occured due to the autoproteolytic activity of NS2B-NS3pro. However, we had successfully avoided MTL as described thoroughly later. Other possible contribution factors are such as multivalency in the analyte, ligand conformational change upon analyte binding, involvement of a more complex interaction or occlusion of the binding sites due to steric hindrance (crowding effect) (Edward, 2007). But to our knowledge, there is no independent support evidence to claim such findings. In this study, steric hindrance was avoided based on the larger MW of ligand (NS2B-NS3pro) compared to the sizes used for the analytes (the small molecule compounds). The optimal range used to immobilize NS2B-NS3pro (6000 RU) also avoids steric hindrance, as high immobilization level could cause crowding effect to the ligand (Azmi *et al*., 2010; Edward, 2007).

The 1:1 Langmuir model is the simplest kinetic model that could use to describe binding between the small molecule analyte (A) and NS2B-NS3pro (B) to produce single association and dissociation rates ($A + B \leftrightarrow AB$) (GE Healthcare, 2012). In this model, we presume that the dimeric NS2B-NS3pro may interact in a way that only one of the binding sites binds to the analyte. This is possible as the MW of NS2B-NS3pro is larger than the analytes. However, if the larger sized NS2B-NS3pro is used as the analyte, the ligand binding sites will be occluded and will eventually lead to steric hindrance that prevents NS2B-NS3pro to associate (Edward, 2007). Despite the apparent non-Langmuir characteristics, we nevertheless put an attempt to fit the sensorgrams using the 1:1 Langmuir kinetic model to describe the quality of fit. As an effort to describe accurate rate constants, the global fit was used in the kinetic fitting to include the entire set of the association and dissociation phases including all analyte concentrations (GE Healthcare, 2007b). However, as expected, the sensorgrams of all analtes tested fit poorly to the 1:1 interaction model (Figures 4.20A, 4.21A and 4.22A).

Next, we made another attempt to include the autoproteolytic activity of NS2B-NSpro and use the non-Langmuir 2:1 heterogenous ligand-parallel reaction model. This model represents two independent ligands (B_1 and B_2) with each bind to an analyte (A) (**(**$A + B_1 \leftrightarrow AB_1$, $A + B_2 \leftrightarrow AB_2$). The interactions yield two sets of different kinetic properties (k_{a_1} and k_{d_1}, and k_{a_2} and k_{d_2}) (GE Healthcare, 2012). By presuming the autoproteolytic activity of NS2B-N3pro (as previously mentioned in Section 5.1), the protease solution may contain a mixture of intact and truncated fragments (Shiryaev *et al*., 2007) that could cause heterogeneity in ligand population. As a result, this could lead to two different binding sites from both proteases. Nonetheless, as expected, the binding sensorgrams fit poorly to the heterogeneous ligand model (Figures 4.20C, 4.21C and 4.22C).

To find the differences between the experimental and calculated data, and to assess the fitting degree, residual distribution and the Chi^2 values were evaluated for these purposes. Graphical analysis of the residual distributions showed curvilinearity in both 1:1 and 2:1 kinetic models, exceeding the noise level of the detection system (± 2 RU) (Figures 4.20B and C, 4.21B and C and 4.22B and C). The magnitude is greater in rolitetracycline compared to in doxycycline and meclofenamic acid (Table 4.4), indicating the lowest quality of kinetic fitting in rolitetracycline due to the additional artifact of high non-specific binding interactions. These analytes showed a curvilinear trend in the residual distribution (i.e., non-randomly distributed along the x-axis), clearly demonstrating a non-linear relationship between the experimental data and the kinetic fitting models (GE Healthcare, 2012). However, for experimental data that fits the kinetic model, the residual distribution is scattered randomly near 0 RU.

The Chi^2 value, on the other hand, is the averaged of the squared residual per data point, and hence, a global quantification of the residual noise (Nagata, 2000). The Chi^2 value is related to the overall range of the residuals. Nevertheless, the shape of the residual does not affect it. In the Langmuir and heterogenous ligand-parallel reaction models, both doxycycline and meclofenamic acid showed relatively optimal Chi^2 values (< 10 RU) (Nagata, 2000) compared to those found in rolitetracycline (≥ 15 RU) (Table.4.4). Although meclofenamic acid may be showing the lowest range of Chi^2 values (≤ 5 RU), optimally, the values are yet beyond the signal noise (± 2 RU). Nevertheless, the low Chi^2 values may indicate that the experimental data in meclofenamic acid is not far from kinetic accuracy.

The deviation from the pseudo-first (1:1) Langmuir model was however not due to mass transport limitation (MTL). MTL is an occurrence where the transportation of

analyte (mass transportation) from bulk solution to the sensor surface is disturbed due to rapid association of analyte (Zhao, 2010). Consequently, the analyte will be non-uniformly distributed and developed a concentration gradient both in the association and dissociation phases. We had avoided MTL by injecting the analyte at high flow rate (50 µl/min) to reduce diffusion distance and consequently replenish any analyte close to the sensor surface (Zhao, 2010). The acceptably low immobilization level of NS2B-NS3pro (6000 RU) not only could reduce multiphasic behavior (binding to a large number of binding sites) and reduce steric hindrance, but also avoid MTL by allowing less analyte to diffuse and make interaction (SPR-pages, 2015). As a result, the binding sensorgram did not display a linear trend in the association phase to indicate MTL. Nevertheless, the curves are convex indicating of sensorgrams that deviates from 1:1 Langmuir interaction.

To further verify our findings, we had submitted the binding data to Episentec (http://www.episentec.com), a biotech company in Sweden, specialized in the application and development of biosensors. Based on their report (refer to Appendix G), each analyte is of excellent quality with good repeatability in binding and low noise. Nevertheless, as previously described in this report, they also found high bulk refractive index in the binding sensorgrams, with rolitetracycline showed an additional artifact based on its non-specific binding to both Fc1 and Fc2.

According to Episentec, the general equation for association phase of a Langmuir model should follow; $y = A1(1–\exp(-k_{obs} \bullet t))$, where $k_{obs} = k_a \bullet conc + k_d$. And the dissociation phase should follow the general equation $y = A2\exp(-k_d \bullet t)$. In this model, both phases should depict a straight line when plotting a derivative function ln(dR/dt) against time (Figure 4.23), where R is the response and t is the time of analysis. The

slope of the straight line is used to derive rate constants. However, for rolitetracycline it is obvious that a single straight line could not fit neither to the association phase nor the dissociation phase. Both phases are curvy, which confirms that the sensorgrams showed binding of at least two different ligands. For both doxycycline and meclofenamic acid, the curvy slope was only observed in the initial part of the association and dissociation phases. But the extension of each phase showed a roughly monoexponential decay, indicating of a Langmuir component. However, the accumulative response seems to be dominated by high bulk refractive index. The problem is that the linear component together with the high bulk refractive index seems to dominate. On the other hand, k_{obs} can be estimated within the association phase and must always be equal or larger than k_{d}. However, this is obviously not the case in these sensorgrams. To conclude, the sensorgrams did not follow the Langmuir behavior. Nevertheless, the slopes for all analytes tested were not showing a constant horizontal line, demonstrating of an almost negligible effect of MTL.

Overall, further attempts for optimization were halted due to the limited budget, time constraints and the risk to get reproducible data due to the autoproteolytic activity of NS2B-NS3pro.

5.4 *In silico* molecular docking

5.4.1 The structural model for the DENV-2 NS2B-NS3pro

In silico investigation in this study has shown that medicinal drugs can have potential as DENV-2 inhibitors. Computational docking studies highlighted that these drugs can bind tightly to the active and allosteric sites of the DENV-2 NS2B-NS3pro. Structural homology model from Heh *et al.* (2013), namely DH-1, was utilized instead of the crystal structure of the DENV-2 NS2B-NS3pro, due to the observable missing loop between Ile77 and Ser84 of the NS2B region (Erbel *et al*., 2006). DH-1 was previously modelled based on the crystal structure of dengue (2FOM) and West Nile (2FP7) viruses with 89% of its residues were located in the most favored region (Ramachandran plot) (Heh *et al*., 2013). By using 2FP7 as the template, Thr77, Ile78, Ser79, Glu80 Asp81, Gly82, Ser83 and Met84 were added to merge the existing gap. Similar to the study by Heh *et al.* (2013), the current work also utilizes blind docking approach using the algorithm in Autodock. Therefore, a complete structural model of the target protein is essentially required.

5.4.2 The small molecule ligands

Although the *in vitro* inhibitory properties for meclofenamic acid and rolitetracycline have been determined (Table 4.5), the mode of binding to the binding site has yet to be determined. The same goes to doxycycline**,** a notably known non-competitive inhibitor (Rothan *et al*., 2013; Rothan *et al*., 2014c), but to where exactly it binds in the DENV-2 NS3B-NS3pro is still not known. Hence, blind docking technique has been applied in this study to predict the binding sites, based on whether these compounds have an allosteric effect or specifically target the active site. Therefore, a tehcnique based on blind docking was used to maneuver the ligands over the entire surface of the protein to search for the possible binding sites (Hetényi & Spoel, 2006). The prediction of docked

complex using blind docking is an extremely difficult task. However, for docking involving protein-small drug interaction, it can be predicted with a certain degree of confidence (Atkovska *et al*., 2014; Laskowski *et al*., 1996; Peters *et al*., 1996). Blind docking allows the ligand to bind to the actual binding site rather than to the nonspecific and/or energetically unfavorable sites inside the protein (Hetényi & Spoel, 2002). A rigid structure of the target protein was used in the docking process, while only the ligands were made flexibel by allowing rotatable bonds to remain rotatable (Table 4.5) to increase the number of ligands' conformations and the probability to bind to the potential binding site (Atkovska *et al*., 2014; Hetényi & Spoel, 2006).

5.4.3 Scoring function and binding interactions

For the scoring function, the results from the docking studies are presented in the form of free binding energy, E_{bind} (Table 4.5). The more negative values of E_{bind} indicate higher binding affinity towards the binding site (Datar & Jadhav, 2015). Compound doxycycline showed the lowest binding energy, indicating that it has the highest binding affinity towards the DENV-2 NS2B-NS3pro, compared to meclofenamic acid and rolitetracycline. Each showed binding energy of -5.15, -3.64 and -3.21 kcal/mol respectively. However, in general, the computed binding free energy did not correlate with the experimentally determined IC_{50} and K_i values found by Rothan *et al*. (2013), Rothan *et al*. (2014c) and Yang *et al*. (2007). In general, the relative binding energies of ligands bound to the active or binding sites do not often correspond to the experimentally determined IC_{50} and K_i values (Laederach, 2003). It is not possible to state a simple relationship between these parameters with free binding energy (E_{bind}) even with the use of an explicit-solvent molecular dynamics (MD) simulation. This is because the experimental values are dependent on the conditions in which they are measured. (Schrodinger, 2011). In spite of this limitation, this technique

could be used to predict and match the desired binding site, understanding possible conformation and orientation of the compounds and further clarifies the binding interactions in the binding pocket. Therefore, to explain the experimental observation, in depth analyses of the binding interactions have been performed.

By considering the total number of residues that are in contact with the ligands (Tables 4.6 and 4.7), five out of twenty-two residues showed common binding residues with the non-competitive ligands (pinostrobin and doxycycline), which are Lys74, Ala164, Ile165, Ala166 and Asn167. These residues are located at a specific region in the allosteric pocket, proximal to the catalytic triad. Therefore, these findings indeed provide further evidence of the non-competitive inhibitory characteristics of doxycycline. Meanwhile, out of sixteen residues that interact with the standard (4-hydroxypanduratin A) and target (meclofenamic acid and rolitetracycline) ligands, ten residues (Phe130, Thr134, Tyr150, Gly151, Asn152, Gly153, Val155, Tyr161 and two of the catalytic triads His51 and Ser135) interact with all three ligands, emphasizing the feature of competitive inhibitory in meclofenamic acid and rolitetracycline. As a whole, these findings explained the highly superimposed conformation of the target and standard ligands (Figure 4.24), which strongly support the prediction of the ligands to be competitive in their inhibition activity.

Doxycycline which has been predicted to be non-competitive inhibitor, there are seven H-bonds contributed by the HBD from the amino and hydroxyl groups to stabilize and orientate the ligand (Table 4.6 and Figure). The ligand binding affinity is further enhanced by the pi-H-bond, carbon-oxygen dipole-dipole interaction (Table 4.6 and Figure 4.25), van der Waals and hydrophobic interactions (Table 4.6 and Figure 4.25). The pi-H-bonding involves the phenolic ring of doxycycline and Asn167 from

the binding site (specifically the hydrogen atom of the $–NH_2$ group). The pi-donor H-bond is an interaction that involves point to pi-plane interactions, which possess more interaction conformation and larger energy range (2 to 7 k/mol) than the common hydrogen bond and electrostatic interactions. However, only doxycycline exhibits a pi-H-bonding, which is not found in meclofenamic acid and rolitetracycline. This may explain why doxycycline has the lowest binding energy compared to meclofenamic acid and rolitetracycline (Du *et al*., 2013).

Previous studies showed that Lys74 is a crucial residue in the allosteric site of the DENV-2 NS2B-NS3pro (Heh *et al*., 2013; Othman *et al*., 2008). This is due to the backbone carbonyl of Lys74 that is bonded to Asp75, a residue from the catalytic triad. It is presumed that H-bonding with Lys74 may alter the conformational structure of Asp75 and consequently the whole catalytic triad. Eventually this may disrupt the electron transfer required for substrate binding to the active site and decreases the catalytic activity of the target protein (Hedstrom, 2002; Kennepohl *et al*., 2003; Othman *et al*., 2008). However, in this study, both doxycycline and the standard compound (pinostrobin) have a hydrophobic interaction with Lys74, with an additional alkyl-pi interaction with pinostrobin. Nevertheless, involvement of Lys74 in the binding interaction indeed showed that both the standard (pinostrobin) and target (doxycycline) compounds are significant and potential non-competitive inhibitors towards the DENV-2 NS2B-NS3pro (Kiat *et al*., 2006; Othman *et al*., 2008).

For the competitive compounds, comparatively, rolitetracycline shows more favorable H-bonding with four hydroxyls and an amino group**,** while meclofenamic acid forms only three hydrogen bonding interactions (Table 4.6 and Figure 4.25). However, meclofenamic acid showed higher scoring function (lower E_{bind}), which

could be attributable to the two H-bonds that is formed between its carboxyl oxygen atom with the hydrogen atom of the amino group from one of the catalytic triad, His51 (Duax *et al*., 2005) (Table 4.6). The carboxyl group has a greater number of dipoles contributed from the strongly polarized carbonyl and hydroxyl functional groups. Therefore, with the combinatorial interaction of His51 from the catalytic triad and the compound's carboxyl group, as a whole has added to the compound's strong binding affinity (Lifson *et al*., 1979). Contrarily, H-bonding with rolitetracycline involves solely the individual carbonyl and hydroxyl groups respectively (Table 4.6), with which do not involve His51.

5.4.4 Binding pocket

Another critical factor in determining the affinity and the specificity of a drug is the shape complementary with the binding pocket, which is also a hallmark for molecular recognition (Bespamyatnikh *et al*., 2004). It is one of the prime considerations in docking technique where the entire protein molecular surface is taken into account rather than just the active site regions (DesJarlais *et al*., 1988; Norel *et al*., 1999). Shape complementary is important for the target protein to differentiate functional groups in a ligand (Kortagere *et al*., 2009). The affinity of a drug is also dependent on the shape of the ligand-binding pocket (Fukunishi & Nakamura, 2011).

Referring to Figure 4.27, the binding pocket, illustrated in the form of connolly surface, is well-defined for all compounds. The best shape complementary is seen with doxycycline where the binding pocket is narrow and deep, nearly burying doxycycline, which indicates a stronger ligand affinity (Fukunishi & Nakamura 2011). Contrarily, meclofenamic acid and rolitetracycline are enclosed in a more shallow and open binding pocket, demonstrating the relatively weak binding affinity (Fukunishi &

Nakamura, 2011). Looking thoroughly at the connolly surface, the affinity of doxycycline is further enhanced by the large distribution of the negative electrostatic potential surface (EPS) (dark red) (Atkins & Paula 2014) on the left side of the binding pocket (Figure 4.27, left and top). On the contrary, the lower affinity compounds (meclofenamic acid and rolitetracycline**)** have a smaller area of negative EPS towards the right side of the binding pocket (Figure 4.27, left and top). Generally, both the competitive ligands bind to the same pocket, indicating similar core of EPS that could possibly explain their similar values for E_{bind} (Kellenberger *et al*., 2008). However, as discussed above, each compound has its own favourable binding interactions, which when combined with the binding pocket shape complementary, may lead to the different levels of inhibition activity.

CHAPTER 3 : CONCLUSION

6.1 The conclusion

In this study, an *in vitro* method using SPR assay was implemented initially to find the kinetic parameters between medicinal drugs (doxycycline, meclofenamic acid, and rolitetracycline) and the DENV-2 NS2B-NS3pro. However, this attempt was a failure. Nevertheless, *in silico* molecular docking study was added to gain insights into the structural mechanisms of the interaction from the thermodynamic aspect, which was representing binding energy and the different generated conformation of docked ligand.

For SPR assay, amine coupling of NS2B-NS3pro to the CM5 chip has led to random immobilization, which presumably caused the amine group from the binding or active sites of NS2B-NS3pro interacted with the ester groups of the activated sensor chip. Consequently, this led to the inactivation of NS2B-NS3pro based on the decreasing trend in compounds' (medicinal drugs) binding. Nonetheless, with the NTA chip, all compounds showed good binding profiles based on the increasing curve trend in the association phase, indicating the conservation of NS2B-NS3pro activity to bind to each compound. The capture coupling causes the His-tags on NS2B-NS3pro to be captured by the NTA embedded on the chip, producing an orientated immobilization, avoiding the amine group in the binding or active sites from being modified by the ester groups. Even so, a significant bulk refractive index was hindering accurate binding analysis. More concern is on Rolitetracycline, which showed a high degree of non-specific binding, possibly to most of the autoproteolysed NS2B-NS3pro. Overall these artifacts contributed to the failed kinetic analysis, where fitting the 1:1 Langmuir and the 2:1 heterogeneous ligand-parallel reaction models showed approximately the same Chi^2 and residual distributions.

Based on *in silico* molecular docking, doxycycline binds to the allosteric site; proximal to the catalytic triad (His51, Asp75, and Ser135), and had interacted with Lys74 that has a direct covalent linkage with Asp75. With this information, which correlates with the previous finding, further prove the characteristic of doxycycline as a non-competitive compound. Meanwhile, the uncharacterized meclofenamic acid and rolitetracycline was predicted to act as the competitive inhibitors based on their interactions His51 and Ser135. Higher binding affinity in doxycycline matches with its deep binding pocket, while meclofenamic acid and rolitetracycline with lower affinities showed a shallow binding pocket. Moreover, the presence of a pi-H-bond with Asn167, together with the wider distribution of highly negative EPS could explain for the high binding affinity in doxycycline compared to the competitive inhibitors**.** Although both meclofenamic acid and rolitetracycline interact with His51, the carboxyl group from meclofenamic acid involves in a H-bond with this residue, which may explain its higher binding affinity compared to rolitetracycline~~,~~

In conclusion, this study has provided an understanding of the basic knowledge in SPR assay that relates to the small molecule-NS2B-NS3pro interaction. Concurrently, knowledge on the *in silico* molecular docking related to the binding mode and its interactions with the allosteric and active sites of NS2B-NS3pro may be used further for developing potential anti-dengue drugs.

6.2 Future work

Further work on optimizing the reference flow cell is required either by immobilizing irrelevant ligand such as BSA onto the reference flow cell (Fc1) or by leaving the sensor surface being unmodified (without activation or immobilizing any irrelevant ligand). Emphasizing on eliminating the autoproteolytic activity of NS2B-

NS3pro is as well essential to avoid avidity effect due to the complex interaction that may be resulted from the multiple binding sites of NS2B-NS3pro. An *in silico* study using an explicit analysis with molecular dynamics (MD) simulation could be further performed to have an in depth understanding on the nature of atomic and molecular motions involved during the binding complex interaction.

REFERENCES

Abdi, M. M., Abdullah, L. C., Sadrolhosseini, A. R., Yunus, W. M. M., Moksin, M. M., & Tahir, P. M. (2011). Surface plasmon resonance sensing detection of mercury and lead ions based on conducting polymer composite. *PLoS ONE, 6*(9), e24578.

Addgene. (2013). Streaking and isolating bacteria on an LB agar plate. Retrieved 1 February 2015, from https://http://www.addgene.org/plasmid-protocols/streak-plate/

Alen, M. M. F., & Schols, D. (2012). Dengue virus entry as target for antiviral therapy. *Journal of Tropical Medicine*, 1-13.

American Association for the Advancement of Science. (2015). Mixed results for dengue vaccine trial. Retrieved 4 February 2015, from http://news.sciencemag.org/health/2012/09/mixed-results-dengue-vaccine-trial

Andersson, K., Areskoug, D., & Hardenborg, E. (1999a). Exploring buffer space for molecular interactions. *Journal of Molecular Recognition, 12*(5), 310-315.

Andersson, K., Hamalainen, M., & Malmqvist, M. (1999b). Identification and optimization of regeneration conditions for affinity-based biosensor assays. A multivariate cocktail approach. *Analytical Chemistry, 71*(13), 2475-2481.

Amorim, J., Alves, R., Boscardin, S., & Ferreira, L. (2014). The dengue virus non-structural 1 protein: risks and benefits. *Virus Research, 181*(2014), 53-60.

Arakaki, T. L., Fang, N. X., Fairlie, D. P., Young, P. R., & Martin, J. L. (2002). Catalytically active dengue virus NS3 protease forms aggregates that are separable by size exclusion chromatography. *Protein Expression and Purification, 25*(2).

Atilgan, E., & Hu, J. (2011). Improving protein docking using sustainable genetic algorithms. *International Journal of Computational and Information Sciences, 3*, 248-255.

Atkins, P., & Paula, J. d. (2014). Molecular recognition and drug design. *Physical Chemistry*.

Atkovska, K., Samsonov, S. A., Paszkowski-Rogacz, M., & Pisabarro, M. T. (2014). Multipose binding in molecular docking. *International Journal of Molecular Sciences, 15*(2), 2622-2645.

Azmi, A. S., Philip, P. A., Wang, Z., Banerjee, S., Zafar, S. F., Goustin, A. S., . . . Mohammad, R. M. (2010). Reactivation of p53 by novel MDM2 inhibitors: implications for pancreatic cancer therapy. *Current Cancer Drug Targets, 10*(3), 319-331.

Bera, A. K., Kuhn, R. J., & Smith, J. L. (2007). Functional characterization of cis and trans protease activity of the flavivirus NS2B-NS3 protease. *Journal of Biological Chemistry, 282*(17), 12883-12892.

Bespamyatnikh, S., Edelsbrunner, V. C. H., & Rudolph, J. (2004). *Accurate protein docking by shape complementarity alone.* Duke University, NC, Durham.

Bessaud, M. l., Pastorino, B. A. M., Peyrefitte, C. N., Rolland, D., Grandadam, M., & Tolou, H. J. (2006). Functional characterization of the NS2B/NS3 protease complex from seven viruses belonging to different groups inside the genus Flavivirus. *Virus Research, 120*(1-2), 79-90.

Bhatt, S., Gething, P. W., Brady, O. J., Messina, J. P., Farlow, A. W., Moyes, C. L., . . . Hay, S. I. (2013). The global distribution and burden of dengue. *Nature, 496*(7446), 504–507.

Biorad. (2015). Large and small molecule screening by SPR. Retrieved 20 February 2015, from http://www.bio-rad.com/en-sg/applications-technologies/large-small-molecule-screening-spr

Bodenreider, C., Beer, D., Keller, T., Sonntag, S., Wen, D., Yap, L., . . . Lim, S. P. (2009). A fluorescence quenching assay to discriminate between specific and non-specific inhibitors of dengue virus protease. *Analytical Biochemistry, 395*(2), 195-204.

Brady, O. J., Gething, P. W., Bhatt, S., Messina, J. P., Brownstein, J. S., Hoen, A. G., . . . Hay, S. I. (2012). Refining the global spatial limits of dengue virus transmission by evidence-based consensus. *PLoS Neglected Tropical Disease, 6*(8), 1-15.

Bronner, V., Nahshol, O., Schoenemann, A., Bomke, J., & Bravman, T. (2010). Rapid assay development and optimization for small molecule drug discovery. Bio-Rad Laboratories, Inc.

Brooijmans, N., & Kuntz, I. D. (2003). Molecular recognition and docking algorithms. *Annual Review of Biophysics and Biomolecular Structure, 32*(1), 335-373.

Byrd, C. M., Dai, D., Grosenbach, D. W., Berhanu, A., Jones, K. F., Cardwell, K. B., . . . Jordan, R. (2013). A novel Iinhibitor of dengue virus replication that targets the capsid protein. *Antimicrobial Agents Chemotheraphy, 57*(1), 15-25.

Calkins, T. L., & Peter, M. (2015). Piermarini evidence for gap junctions as potential new insecticide targets in the yellow fever mosquito, *Aedes aegypti*, *PLoS ONE, 10*(9), e0137084.

Capeding, M. R., Tran, N. H., Hadinegoro, S. R. S., Ismail, H. I. H. M., Chotpitayasunondh, T., Chua, M. N., . . . Group, C. Y. D. S. (2014). Clinical efficacy and safety of a novel tetravalent dengue vaccine in healthy children in

Asia: a phase 3, randomised, observer-masked, placebo-controlled trial. *Lancet, 384*(9951), 1358-1365.

Centre, U. N. (2015). New UN report urges boosting national-level investment to tackle neglected tropical diseases. Retrieved 1 February 2015, from http://www.un.org/apps/news/story.asp?NewsID=50126 -.VT4wY6YRrNx

Chiu, M., Shih, H., Yang, T., & Yang, Y. (2007). The type 2 dengue virus envelope protein interacts with small ubiquitin-like modifier-1 (SUMO-1) conjugating enzyme 9 (Ubc9). *Journal of Biomedical Sciences, 14*(3), 429-444.

Choksupmanee, O., Hodge, K., Katzenmeier, G., & Chimnaronk, S. (2012). Structural platform for the autolytic activity of an intact NS2B−NS3 protease complex from dengue virus. *Biochemistry, 51*(13), 2840-28451.

Chopra, I., Hawkey, P. M., & Hinton, M. (1992). Tetracyclines, molecular and clinical aspects. *Journal of Antimicrobial Chemotheraphy*, *29*(3), 245–77.

Clark, K. P., & Ajay. (1995). Flexible ligand docking without parameter adjustment across four ligand-receptor complexes. *Journal of Computational Chemistry, 16*(10), 1210-1226.

Clercq, E. D. (2002). Strategies in the design of antiviral drugs. *Nature Review Drug Discovery, 1*(1), 13-25.

Clum, S., Ebner, K. E., & Padmanabhan, R. (1997). Cotranslational membrane insertion of the serine proteinase precursor NS2B-NS3(Pro) of dengue virus type 2 is required for efficient in vitro processing and is mediated through the hydrophobic regions of NS2B. *Journal of Biological Chemistry, 272*(49), 30715-30723.

Cooper, M. A. (2009). *Label-Free Biosensors-Techniques and Applications.* Retrieved from http://assets.cambridge.org/97805218/84532/excerpt/9780521884532_excerpt.pdf

Coulerie, P., Maciuk, A., Eydoux, C. c., Hnawia, E., Lebouvier, N., Figadère, B., . . . Nour, M. (2014). New inhibitors of the DENV-NS5 RdRp from carpolepis laurifolia as potential antiviral drugs for dengue treatment. *Record of Natural Products, 8*(3), 286-289.

DesJarlais, R. L., Sheridan, R. P., Seibel, G. L., Dixon, J. S., Kuntz, I. D., & Venkataraghavant, R. (1988). Using shape complementarity as an initial screen in designing ligands for a receptor binding site of known three-dimensional structure. *Journal of Medicinal Chemistry, 31*(4), 722-729.

Du, Q. S., Wang, Q. Y., Du, L. Q., Chen, D., & Huang, R. B. (2013). Theoretical study on the polar hydrogen-π (Hp-π) interactions between protein side chains.

Chemistry Central Journal, 7(1), 92.

Du, X., Li, Y., Xia, Y., Ai, S., Liang, J., Sang, P., . . . Liu, S. (2016). Insights into Protein–Ligand Interactions: Mechanisms, Models, and Methods. *International Journal of Molecular Sciences*, *17*(22), 144.

Duax, W. L., Thomas, J., Pletnev, V., Addlagatta, A., Huether, R., Habegger, L., & Weeks, C. M. (2005). Determining structure and function of steroid dehydrogenase enzymes by sequence analysis, homology modeling, and rational mutational analysis. *Annals of the New York Academy of Sciences, 1061*, 135–148.

Edwards, D. A. (2007). Steric hindrance effects on surface reactions: applications to BIAcore. *Journal of Mathematical Biology, 55*(4), 517-539.

Englebienne, P., Hoonacker, A. V., & Verhas, M. (2003). Surface plasmon resonance: principles, methods and applications in biomedical sciences. *Spectroscopy, 17*(2-3), 255–273.

Erbel, P., Schiering, N., D'Arcy, A., Renatus, M., Kroemer, M., Lim, S. P., . . . Hommel, U. (2006). Structural basis for the activation of flaviviral NS3 proteases from dengue and West Nile virus. *Nature Structural & Molecular Biology, 13*(4), 372-373.

Fen, Y. W., & Yunus, W. M. M. (2011). Characterization of the optical properties of heavy metal ions using surface plasmon resonance technique. *Optics and Photonics Journal,* 1, 116-123.

Frimayanti, N., Chee, C., Zain, S. M., & Rahman, N. A. (2011). Design of new competitive dengue Ns2b/Ns3 protease inhibitors-A computational approach. *International Jornal of Molecular Sciences, 12*(2), 1089-1100.

Fukunishi, Y., & Nakamura, H. (2011). Prediction of ligand-binding sites of proteins by molecular docking calculation for a random ligand library. *Protein Science, 20*(1), 95-106.

Gangopadhyay, A., Chakraborty, H. J., & Datta, A. (2017). Targeting the dengue β-OG with serotype-specific alkaloid virtual leads. *Journal of Molecular Graphics and Modelling*. *73*, 129-142.

GE Healthcare, (2007a). *Biacore sensor surface handbook.* Retrieved from http://www.helsinki.fi/biosciences/corefacilities/biacore/BR-1005-71AB%20Biacore%20Sensor%20Surface%20Handbook(web).pdf

GE Healthcare. (2007b). *BIAevaluation software handbook.* Retrieved from http://cdn2.hubspot.net/hub/240225/file-352045131-pdf/0-korea_eSupport/Biacore/Software/BR-100229AH_Biacore_3000_BIAevaluation_Software_Handbo

ok(web).pdf

GE Healthcare. (2012). *Biacore assay handbook.* Retrieved from http://www.gelifesciences.com/file_source/GELS/Service%20and%20Support/Documents%20and%20Downloads/Handbooks/pdfs/Biacore%20Assay%20Handbook.pdf

GE Healthcare. (2013a). *Biacore T200 Getting Started.* Retrieved from https://www.gelifesciences.com/gehcls_images/GELS/Related%20Content/Files/1384422145862/litdoc28984098_20131114224511.pdf

GE Healthcare. (2013b). *Sensor Chip NTA*. Retrieved from https://www.g elifesciences.com/gehcls_images/GELS/Related%20Content/Files/1384943366025/litdoc22051997_20131120233727.pdf

Giese, K. C., & Vierling, E. (2002). Changes in oligomerization are essential for the chaperone activity of a small heat shock protein in vivo and in vitro. *Journal of Biological Chemistry, 277*(48), 46310-46318.

Gopinath, S. C. B. (2010). Biosensing applications of surface plasmon resonance-based Biacore technology. *Sensors and Actuators B: Chemical, 150*(2), 722-733.

Grinter, S. Z., & Zou, X. (2014). Challenges, applications, and recent advances of protein-ligand docking in structure-based drug design. *Molecules, 19*(7), 10150-10176.

Gruenberg, A., & Wright, P. J. (1992). Processing of dengue virus type 2 structural proteins containing deletions in hydrophobic domains. *Archieves of Virology, 122*(1), 77-94.

Guiducci, C. (2011). *Surface plasmon resonance based systems. Advanced bioengineering methods laboratory SPR*. Retrieved from http://lben.epfl.ch/files/content/sites/lben/files/users/179705/Surface%20Plasmon%20Resonance%20Handout.pdf

Gupta, A., Chaudhary, N., Kakularam, K. R., Pallu, R. & Polamarasetty, A. (2015). The augmenting effects of desolvation and conformational energy terms on the predictions of docking programs against mPGES-1. *PLoS ONE, 10*(5), e0134472.

Guy, B., Briand, O., Lang, J., Saville, M., & Jackson, N. (2015). Development of the Sanofi pasteur tetravalent dengue vaccine: one more step forward. *Vaccine, 33*(50), 7100–7111.

Hahnefeld, C., Drewianka, S., & Herberg, F., W. (2004) Determination of Kinetic Data Using Surface Plasmon Resonance Biosensors**.** In Decker, & Reischl, U. (Eds.) *Molecular Diagnosis of Infectious Diseases* (pp. 299-320). Totowa, NJ: Humana Press.

Halstead, S. B. (2005). More dengue, more questions. *Emerging Infectious Diseases, 11*(5), 740-741.

Hamad, B. (2010). The antibiotics market. *Nature Reviews Drug Discovery, 9*(9), 675-676.

Harks, E. G. A., de Roos, A. D. G., Peters, P. H. J., de Haan, L. H., Brouwer, A., Ypey, D. L., . . . Theuvenet, A. P. R. (2001). Fenamates: A novel class of reversible gap junction blockers. *The Journal of Pharmacology and Experimental Therapeutics*, *298*(3), 1033-1041.

Hedstrom, L. (2002). Serine Protease Mechanism and Specificity. *Chemical Reviews*, *102*(12), 4501-4524.

Heh, C. H., Othman, R., Buckle, M. J. C., Sharifuddin, Y., Yusof, R., & Rahman, N. A. (2013). Rational discovery of dengue type 2 non-competitive inhibitors. *Chemical Biology & Drug Design, 82*(1), 1-11.

Heilman, J. M., Wolff, J. D., Beards, G. M., & Basden, B. J. (2014). Dengue fever: a Wikipedia clinical review. *8*(4), 105-115.

Herrero, L. J., Zakhary, A., Gahan, M. E., Nelson, M. A., Herring, B. L., Hapel, A. J., . . . Mahalingam, S. (2013). Dengue virus therapeutic intervention strategies based on viral, vector and host factors involved in disease pathogenesis. *Pharmacology & Therapeutics, 137*(2), 266-282.

Hetényi, C. H., & Spoel, D. v. d. (2006). Blind docking of drug-sized compounds to proteins with up to a thousand residues. *FEBS Letters, 580*(5), 1447-1450.

Honari, P., Allaudin, Z. N., Lila, M. A. M., & Mustafa, N. H. B. (2011). An approach towards optimal usage of immobilized sensor chips in surface plasmon resonance based biosensor. *African Journal of Biotechnology, 10*(70), 15795-15800.

Huang, S., & Zou, X. (2010). Advances and challenges in protein-ligand docking. *International Journal of Molecular Sciences, 11*(8), 3016-3034.

Idrees, S., & Ashfaq, U. (2013). RNAi: antiviral therapy against dengue virus. *Asian Pacific Journal of Tropical Biomedicine, 3*(3), 232-236.

Irie, K., Mohan, P. M., Sasaguri, Y., Putnak R., & Padmanabhan, R. (1989). Sequence analysis of cloned dengue virus type 2 genome (New Guinea-C strain). *Gene,* 75: 197-211.

Jan, L., Yang, C., Trent, D., Falgout, B., & Lai, C. (1995). Processing of Japanese encephalitis virus non-structural proteins: NS2B-NS3 complex and heterologous proteases. *Journal of General Virology, 76*(3), 573-580.

Joss, L., Morton, T. A., Doyle, M. L., & Myszka, D. G. (1998). Interpreting kinetic rate constants from optical biosensor data recorded on a decaying surface. *Analytical Biochemistry, 261*(2), 203-210.

Julander, J. G., Perry, S. T., & Shresta, S. (2011). Important advances in the field of anti-dengue virus research. *Antiviral Chemistry and Chemotheraphy, 21*(3), 105–116.

Kadir, S. L. A., Yaakob, H., & Zulkifli, R. M. (2013). Potential anti-dengue medicinal plants: a review. *Journal of Natural Medicines, 67*(4), 677-689.

Kapoor, M., Zhang, L., Ramachandra, M., Kusukawa, J., Ebner, K., & Padmanabhan, R. (1995). Association between NS3 and NS5 proteins of dengue virus type 2 in the putative RNA replicase is linked to differential phosphorylation of NS5. *Journal of Biological Chemistry, 270*(32), 19100-19106.

Kaptein, S. J. F., Burghgraeve, T. D., Froeyen, M., Pastorino, B., Alen, M. M. F., Mondotte, J. A., . . . Neyts, J. (2010). A derivate of the antibiotic doxorubicin is a selective inhibitor of dengue and yellow fever Virus replication in vitro. *Antimicrobial Agents and Chemotheraphy, 54*(12), 5269-5280.

Kellenberger, E., Schalon, C., & Rognan, D. (2008). How to measure the similarity between Protein Ligand-Binding Sites? *Current Computer-Aided Drug Design, 4,* 209-220.

Kennepohl, P., & Solomon, E. I. (2003). Electronic Structure Contributions to Electron-Transfer Reactivity in Iron-Sulfur Active Sites: 3. Kinetics of Electron Transfer. *Inorganic Chemistry*, *42*(3), 696-708.

Kiat, T. S., Pippen, R., Yusof, R., Ibrahim, H., Khalid, N., & Rahman, N. A. (2006). Inhibitory activity of cyclohexenyl chalcone derivatives and flavonoids of fingerroot, Boesenbergia rotunda (L.), towards dengue-2 virus NS3 protease. *Bioorganic & Medicinal Chemistry Letters, 16*(12), 3337-3340.

Kim, Y. M., Gayen, S., Kang, C., Joy, J., Huang, Q., Chen, A. S., . . . Keller, T. H. (2013). NMR Analysis of a novel enzymatically active unlinked dengue NS2B-NS3 protease complex. *Journal of Biological Chemistry, 288*(18), 12891-12900.

Knehans, T., Schüller, A., Doan, D. N., Nacro, K., Hill, J., Güntert, P., . . . Vasudevan, S. G. (2011). Structure-guided fragment-based in silico drug design of dengue protease inhibitors. *Journal of Computer-Aided Molecular Design, 25*(3), 263-274.

Kortagere, S., Krasowski, M. D., & Ekins, S. (2009). The Importance of discerning shape in molecular pharmacology. *Trends in Pharmacological Sciences, 30*(3), 138-147.

Kqueen, C. Y., & Son, R. (2010). Surface plasmon resonance biosensor for real-time detection of genetically modified organisms. *International Food Reseacrh Journal, 17*, 477-483.

Kuhn, R. J., Zhang, W., Rossmann, M. G., Pletnev, S. V., Corver, J., Lenches, E., . . . Strauss, J. H. (2002). Structure of dengue virus: Implications for flavivirus organization, maturation, and fusion. *Cell, 108*(5), 717-725.

Kumalo, H., Bhakat, S., & Soliman, M. (2015). Theory and applications of covalent docking in drug discovery: Merits and pitfalls. *Molecules, 20*(2), 1984-2000.

Kumar, C. V. M. N., Taranath, V., Venkatamuni, A., Vardhan, R. V., Prasad, Y. S., Ravi, U., & Gopal, D. V. R. S. (2015). Therapeutic potential of carica papaya L. leaf extraction in treatment of dengue patients. *International Journal of Applied Biology and Pharmaceutical Technology, 6*(3), 93-98.

Kyle, J., & Harris, E. (2008). Global spread and persistence of dengue. *Annual Review of Microbiology, 62*(1), 71-92.

Laederach, A. T. (2003). *Protein-carbohydrate and protein-protein interactions: Using models to better understand and predict specific molecular recognition* (PhD thesis). Retrieved from http://lib.dr.iastate.edu/cgi/viewcontent.cgi?article=1599&context=rtd

Laskowski, R. A., Luscombe, N. M., Swindells, M. B. & Thornton, J. M. (1996). Protein clefts in molecular recognition and function. *Protein Science, 5*(12): 2438-2452.

Lescar, J., Luo, D., Xu, T., Sampath, A., Lim, S., Canard, B., & Vasudevan, S. (2008). Towards the design of antiviral inhibitors against flaviviruses: The case for the multifunctional NS3 protein from Dengue virus as a target. *Antiviral Research, 80*(2), 94-101.

Leung, D., Schroder, K., White, H., Fang, N.-X., Stoermer, M. J., Abbenante, G., . . . Fairlie, D. P. (2001). Activity of recombinant dengue 2 virus NS3 protease in the presence of a truncated NS2B co-factor, small peptide substrates, and inhibitors. *Journal of Biological Chemistry, 276*(49), 45762-45771.

Li, J., Lim, S., Beer, D., Patel, V., Wen, D., Tumanut, C., . . . Vasudevan, S. (2005). Functional profiling of recombinant NS3 proteases from all four serotypes of dengue virus using tetrapeptide and octapeptide substrate libraries. *Journal of Biological Chemistry, 280*(31), 28766-28774.

Lifson, S., Hagler, A. T., & Dauber, P. (1979). Consistent force field studies of intermolecular forces in hydrogen-bonded crystals. 1. Carboxylic acids, amides, and the C=O-H- hydrogen bonds. *Journal of the American Chemical Society, 101*(11), 5111-5121.

Liu, H., Wu, R., Sun, Y., Ye, Y., Chen, J., Luo, X., . . . Liu, H. (2014). Identification of novel thiadiazoloacrylamide analogues as inhibitors of dengue-2 virus NS2B/NS3 protease. *Bioorganic & Medicinal Chemistry, 22*(22), 6344-6352.

Lipschultz, C. A., Li, Y., & Gill, S. S. (2000). Experimental design for analysis of complex kinetics using surface plasmon resonance. *Method, 20*(3), 310-318.

Low, J. S. Y., Wu, K. X., Chen, K. C., Ng, M. M. L., & Chu, J. J. H. (2011). Narasin, a novel antiviral compound that blocks dengue virus protein expression. *Antiviral Theraphy, 16*(12), 1203-1218.

Ma, L., Jones, C., Groesch, T., Kuhn, R., & Post, C. (2004). Solution structure of dengue virus capsid protein reveals another fold. *Proceedings of the National Academy of Sciences of the United States of America, 101*(10), 3414-3419.

Melino, S., & Paci, M. (2007). Progress for dengue virus diseases. Towards the NS2B-NS3pro inhibition for a therapeutic-based approach. *FEBS Journal, 274*(12), 2986-3002.

Merwe, P. A. v. d. (2003). *Surface plasmon resonance*. Retrieved from https://www.bioch.ox.ac.uk/aspsite/services/equipmentbooking/biophysics/spr.pdf

Miller, S., Sparacio, S., & Bartenschlager, R. (2006). Subcellular localization and membrane topology of the dengue virus type 2 non-structural protein 4B. *Journal of Biological Chemistry, 281*(13), 8854-8863.

Murray, N. E. A., Quam, M. B., & Wilder-Smith, A. (2013). Epidemiology of dengue: Past, present and future prospects. *Journal of Clinical Epidemiology, 5*, 299-309.

Mustafa, L. C. M. S., Rasotgi, C. V., Jain, C. S., & Gupta, L. C. V. (2015). Discovery of fifth serotype of dengue virus (DENV-5): A new public health dilemma in dengue control. *Armed Forces Medical Services, 71*(1), 67-70.

Myszka, D. G. (1999). Improving biosensor analysis. *Journal of Molecular Recognition, 12*(5), 279-284.

Nagata, K. (2000). *Real-Time Analysis of Biomolecular Interactions: Applications of BIACORE.* K. Nagata, & Handa, H. (Eds.).

Navratilova, I., & Hopkins, A. L. (2011). Emerging role of surface plasmon resonance in fragment-based drug discovery. *Future Medicinal Chemistry, 3*(14), 1809-1820.

Norel, R., Petrey, D., Wolfson, H. J., & Nussinov, R. (1999). Examination of Shape Complementarity in Docking of Unbound Proteins. *Proteins: Structure, Function, and Bioinformatics, 36*(3), 307-317.

Okimoto, N., Futatsugi, N., Fuji, H., Suenaga, A., Morimoto, G., Yanai, R. , . . . Taiji, M. (2009). High-performance drug discovery: computational screening by combining docking and molecular dynamics simulations. *PLoS Computational Biology, 5*(10), e1000528.

Oliveira, A. S. d., Silva, M. L. d., Oliveira, A. F. v. C. S., Silva, C. C. d., Teixeirac, R. b. R., & Paula, S. r. O. D. (2014). NS3 and NS5 proteins: Important targets for anti-dengue drug design. *Journal of the Brazilian Chemical Society, 25*(10), 1759-1769.

Othman, R., Kiat, T. S., Khalid, N., Yusof, R., Newhouse, I., Newhouse, J. S., . . . Rahman, N. A. (2008). Docking of noncompetitive inhibitors into dengue virus Type 2 protease: Understanding the interactions with allosteric binding sites. *Journal of Chemical Information and Modelling*, *48*(8), 1582-1591.

Otto, A. (1968). Excitation of nonradiative surface plasma waves in silver by the method of frustrated total reflection. *Zeitschrift für Physik A Hadrons and Nuclei, 216*(4), 398-410.

Panhuis, W. G. v., Gibbons, R. V., Rothman, A. L. T., Srikiatkhachorn, A., Nisalak, A., Burke, D., & Cummings, D. (2010). Inferring the serotype associated with dengue virus infections on the basis of pre- and postinfection neutralizing antibody titers. *The Journal of Infectious Diseases, 202*(7), 1002-1010.

Pasteur, S. (2012). Issue 15 - Spotlight on dengue in southeast asia. Retrieved 28 February 2015, from http://www.denguematters.info/content/issue-15-spotlight-dengue-southeast-asia

Pastorino, B. A. M., Peyrefitte, C. N., Grandadam, M., Lebrun, R., Moinier, D., Rolland, D., . . . Bessaud, M. (2007). Unexpected altered specificity is responsible for St. Louis encephalitis virus recombinant protease autoproteolysis. *Protein & Peptide Letters, 14*(1), 79-82.

Perera, R., & Kuhn, R. J. (2008). Structural proteomics of dengue virus. *Current Opinion on Microbiology, 11*(4), 369–377.

Peretz, A., Degani, N., Nachman, R., Uziyel, Y., Gibor, G., Shabat, D., & Attali, B. (2005). Meclofenamic acid and diclofenac, novel templates of KCNQ2/Q3 potassium channel openers, depress cortical neuron activity and exhibit anticonvulsant properties. *Molecular Pharmacology*, *67*(4), 1053-1066.

Peters, K. P., Fauck, J., & Frömmel, C. (1996). The automatic search for ligand binding sites in proteins of known three-dimensional structure using only geometric criteria. *Journal of Molecular Biology, 256*(1), 201-213.

Pujadas, G., Vaque, M., Ardevol, A., Blade, C., Salvado, M. J., & Blay, M. (2008). Protein-ligand docking: A review of recent advances and future perspectives. *Current Pharmaceutical Analysis, 4*(1), 1-19.

Rahman, N. A., Hadinur, Muliawan, S., Rashid, N. N., Muhamad, M., & Yusof, R. (2006). Studies on Quercus lusitanica extracts on DENV-2 replication. *Dengue Bulletin, 30*.

Ramanan, R. N., Ling, T. C., Tey, B. T., & Ariff, A. B. (2010). A simple method for quantification of interferon-α2b through surface plasmon resonance technique. *African Journal of Biotechnology, 9*(11), 1680-1689.

Raschka, S. (2014). Molecular docking, estimating free energies of binding, and AutoDock's semi-empirical force field. Retrieved 1 March, from http://sebastianraschka.com/Articles/2014_autodock_energycomps.html

Rich, R. L., Hoth, L. R., Geoghegan, K. F., Brown, T. A., LeMotte, P. K., Simons, S. P., . . . Myszka, D. G. (2002). Kinetic analysis of estrogen receptor/ligand interactions. *Proceedings of the National Academy of Sciences of the United States of America, 99*(13), 8562-8567.

Rich, R. L., & Myszka, D. G. (2000). Survey of the 1999 surface plasmon resonance biosensor literature. *Journal of Molecular Recognition, 13*(6), 388-407.

Rich, R. L., & Myszka, D. G. (2001). Survey of the year 2000 commercial optical biosensor literature. *Journal of Molecular Recognition, 14*(5), 273-294.

Rich, R. L., & Myszka, D. G. (2002). Survey of the year 2001 commercial optical biosensor literature. *Journal of Molecular Recognition, 15*(6), 352-376.

Rich, R. L., & Myszka, D. G. (2005a). Survey of the year 2003 commercial optical biosensor literature. *Journal of Molecular Recognition, 18*(1), 1-39.

Rich, R. L., & Myszka, D. G. (2005b). Survey of the year 2004 commercial optical biosensor literature. *Journal of Molecular Recognition, 18*(6), 431-478.

Rich, R. L., & Myszka, D. G. (2006). Survey of the year 2005 commercial optical biosensor literature. *Journal of Molecular Recognition, 19*(6), 478-534.

Rich, R. L., & Myszka, D. G. (2008). Survey of the year 2007 commercial optical biosensor literature. *Journal of Molecular Recognition, 21*(6), 355-400.

Rich, R. L., & Myszka, D. G. (2010). Grading the commercial optical biosensor literature—class of 2008: 'The Mighty Binders'. *Journal of Molecular Recognition, 23*(1), 1-64.

Rich, R. L., & Myszka, D. G. (2011). Survey of the year 2009 commercial optical biosensor literature. *Journal of Molecular Recognition, 24*(6), 892-914.

Ritzefeld, M., & Sewald, N. (2012). Real-time analysis of specific protein-DNA interactions with surface plasmon resonance. *Journal of Amino Acids*, 1-9.

Roberts, C. H., Mongkolsapaya, J., & Screaton, G. (2013). New opportunities for control of dengue virus. *Current Opinion on Infectious Diseases, 26*(6), 567-574.

Roberts, M. C. (1996). Tetracycline resistance determinants: Mechanisms of action, regulation of expression, genetic mobility, and distribution. *FEMS Microbiology Reviews*, *19*(1), 1-24.

Rothan, H. A., Bahrani, H., Mohamed, Z., Rahman, N. A., & Yusof, R. (2014a). Fusion of protegrin-1 and plectasin to MAP30 shows significant inhibition activity against dengue virus replication. *PLoS ONE, 9*(4), e94561.

Rothan, H. A., Buckle, M. J., Ammar, Y. A., Shatrah, P. M., Noorsaadah, A. R., & Rohana, Y. (2013). Study the antiviral activity of some derivatives of tetracycline and non-steroid anti-inflammatory drugs towards dengue virus. *Tropical Biomedicine, 30*(4), 1-10.

Rothan, H. A., Mohamed, Z., Abdulrahman, A. Y., Tan, E. C., Rahman, N. A., & Yusof, R. (2014b). Screening of antiviral activities in medicinal plants extracts against dengue virus using dengue NS2B-NS3 protease assay. *Tropical Biomedicine, 31*(2), 286-296.

Rothan, H. A., Mohamed, Z., Paydar, M., Rahman, N. A., & Yusof, R. (2014c). Inhibitory effect of doxycycline against dengue virus replication in vitro. *Archives of Virology, 159*(4), 711-718.

Sadrolhosseini, A. R., Noor, A. S. M., & Moksin, M. M. (2012). Application of surface plasmon resonance Based on a Metal Nanoparticle. In K. Y. Kim (Ed.), Plasmonics - Principles and Applications.

Sampath, A., & Padmanabhan, R. (2009). Molecular targets for flavivirus drug discovery. *Antiviral Research, 81*(1), 6-15.

Schechter, I., & Berger, A. (1967). On the size of the active site in proteases. I. Papain. *Biochemical and Biophysical Research Communication, 27*(2), 157-162.

Schmitza, J., Roehrigb, J., Barrettc, A., & Hombacha, J. (2011). Next generation dengue vaccines: A review of candidates in preclinical development. *Vaccine, 29*, 7276-7284.

Schrodinger. (2011). Knowledge. Retrieved 2 December 2015, from http://www.schrodinger.com/kb/936

Shepherd, C. A., Hopkins, A. L., & Navratilova, I. (2014). Fragment screening by SPR and advanced application to GPCRs. *Progress in Biophysics and Molecular Biology, 116*(2-3), 113-123.

Shiryaev, S. A., Aleshin, A. E., Ratnikov, B. I., Smith, J. W., Liddington, R. C., & Strongin, A. Y. (2007). Expression and purification of a two-component flaviviral proteinase resistant to autocleavage at the NS2B-NS3 junction region. *Protein Expression and Purification, 52*(2), 334-339.

Simmons, M., Teneza-Mora, N., & Putnak, R. (2012). Advances in the development of vaccines for dengue fever. *Vaccine: Development and Therapy, 2*, 1-14.

SPR-pages. (2015a). Artefacts. Retrieved 5 February 2015, from http://www.sprpages.nl/best-results/artifacts

SPR-Pages. (2015b). Pre-concentration. Retrieved 3 March 2015, from http://www.sprpages.nl/immobilization/ligand-pre-concentration

Sugamoto, K., Kurogi, C., Matsushit, Y.-i., & Matsui, T. (2008). Synthesis of 4-hydroxyderricin and related derivatives. *Tetrahedron Letters, 49*(47), 6639-6641.

Sukupolvi-Petty, S., Austin, S. K., Purtha, W. E., Oliphant, T., Nybakken, G. E., Schlesinger, J. J., . . . Diamond, M. S. (2007). Type- and subcomplex-specific neutralizing antibodies against domain III of dengue virus type 2 envelope protein recognize adjacent epitopes. *Journal Virology, 81*(23), 12816-12826.

Sun, P., & Kochel, T. J. (2013). The battle between infection and host immune responses of dengue virus and its implication in dengue disease pathogenesis. *Scientific World Journal*, 1-11.

Swinney, D. (2008). Applications of binding kinetics to drug discovery: Translation of binding mechanisms to clinically differentiated therapeutic responses. *Pharmaceutical Medicine, 22*(1), 23-34.

Symposium, B. (2002). *Protocol for measuring small molecule interactions using Biacore - A Practical Guide to Experimental Design and Data Evaluation.* Paper presented at the Strategies for Working with Small Molecules, Chicago, Illinois.

Tambunan, U., & Alamudi, S. (2010). Designing cyclic peptide inhibitor of dengue virus NS3-NS2B protease by using molecular docking approach. *Bioinformation, 5*(6), 250-254.

Tanious, F. A., Nguyen, B., & Wilson, W. D. (2008). Biosensor-surface plasmon resonance methods for quantitative analysis of biomolecular interactions. *Methods in Cell Biology, 84*, 53-77.

Thomas, S., & Endy, T. (2013). Current issues in dengue vaccination. *Current Opinion in Infectious Diseases, 26*(5), 429-434.

Tomlinson, S. M., Malmstrom, R. D., Russo, A., Mueller, N., Pang, Y. P., & Watowich, S. J. (2009). Structure-based discovery of dengue virus protease inhibitors. *Antiviral Research, 82*(3), 110-114.

Tomlinson, S. M., & Watowich, S. J. (2011). Anthracene-based inhibitors of dengue virus NS2B-NS3 protease. *Antiviral Research, 89*(2), 127-135.

Trujillo-Murillo, K., Rincón-Sánchez, A. R., Martínez-Rodríguez, H., Bosques-Padilla, F., Ramos-Jiménez, J., Barrera-Saldaña, H. A., . . . Rivas-Estilla, A. M. (2008). Acetylsalicylic acid inhibits hepatitis C virus RNA and protein expression through cyclooxygenase 2 signaling pathways. *Journal of Hepatology, 47*(5), 1462-1472.

Villar, L., Dayan, G. H., Arredondo-Garcia, J. L., Rivera, D. M., Cunha, R., Deseda, C., . . . Group, C. Y. D. S. (2015). Efficacy of a tetravalent dengue vaccine in children in Latin America. *The New England Journal of Medicine, 372*(2), 113-123.

Wang, S., & Wang, R. (2013). DNA biosensor for rapid detection of anticancer drugs. *Biosensors and Bioelectronics, 201,* 359-377.

Wang, Y., Xiao, J., Suzek, T. O., Zhang, J., Wang, J., & Bryant, S. H. (2009). PubChem: A public information system for analyzing bioactivities of small molecules. *Nucleic Acids Research, 37*(Web server), W623-W633.

Wang, Z., Chen, G., Chen, L., Liu, X., Fu, W., Zhang, Y., . . . Cai, Y. (2015). Insights into the binding mode of curcumin to MD-2: studies from molecular docking, molecular dynamics simulations and experimental assessments. *Molecular Biosystems, 11*(7), 1933-1938.

Wear, M. A., Patterson, A., Malone, K., Dunsmore, C., Turner, N. J., & Walkinshaw, M. D. (2005). A surface plasmon resonance-based assay for small molecule inhibitors of human cyclophilin A. *Analytical Biochemistry, 345*(2), 214-226.

Webb, S. (2013). Piece by Piece. A guide to fragment-based drug discovery. Retrieved 4 February 2015, from http://www.the-scientist.com/?articles.view/articleNo/35711/title/Piece-by-Piece/

Wikipedia. (2015). Surface plasmon resonance. Retrieved 19 February 2015, https://en.wikipedia.org/wiki/Surface_plasmon_resonance

Willard, F. S., & Siderovski, D. P. (2006). Covalent immobilization of histidine-tagged proteins for surface plasmon resonance. *Analytical Biochemistry, 353*(1), 147-149.

World Health Organization. (2005). Dengue, dengue haemorrhagic fever and dengue shock syndrome in the context of the integrated management of childhood

illness. Retrieved 5 February 2015, http://whqlibdoc.who.int/hq/2005/WHO_FCH_CAH_05.13_eng.pdf

Xie, X., Wang, Q., Xu, H., Qing, M., Kramer, L., Yuan, Z., & Shi, P. (2011). Inhibition of dengue virus by targeting viral NS4B protein. *Journal of Virology, 85*(21), 11183-11195.

Yakimchuk, K. (2011). Protein receptor-ligand interaction/binding assays. *Materials and Methods, 199*(1).

Yang, J.-M., Chen, Y.-F., Tu, Y.-Y., Yen, K.-R., & Yang, Y.-L. (2007). Combinatorial computational approaches to identify tetracycline derivatives as flavivirus inhibitors. *PLoS ONE, 2*(5), e428.

Yang, C., Hsieh, Y. C., Lee, S. J., Wu, S. H., Liao, C. L., Tsao, C. H., . . . Yueh, A. (2011). Novel dengue virus-specific NS2B/NS3 protease inhibitor, BP2109, discovered by a high-throughput screening assay. *Antimicrobial Agents and Chemotheraphy, 55*(1), 229-238.

Yin, Z., Patel, S. J., Wang, W-L., Wang, G., Chan, W-L., Rao, K. R. R., . . . Keller, T. H. (2006). Peptide inhibitors of dengue virus NS3 protease. Part 1: Warhead. *Bioorganic & Medicinal Chemistry Letters, 16*(1), 36-39.

Yuriev, E., Agostino, M., & Ramsland, P. (2010). Challenges and advances in computational docking: 2009 in review. *Journal of Molecular Recognition, 24*(2), 149-164.

Yusmawati, W. Y. W., Chuah, H. P., & Mahmood, M. Y. W. (2007). Optical properties and sugar content determination of commercial carbonated drinks using surface plasmon resonance. *American Journal of Appled Sciences, 4*(1), 1-4.

Yusof, R., Clum, S., Wetzel, M., Murthy, H. M. K., & Padmanabhan., R. (2000). Purified NS2B/NS3 serine protease of dengue virus type 2 exhibits cofactor NS2B dependence for cleavage of substrates with dibasic amino acids in vitro. *Journal of Biological Chemistry, 275*(14), 9963-9969.

Zhang, X. G., Mason, P. W., Dubovi, E. J., Xu, X., Bourne, N., Renshaw, R. W., . . . Birk, A. V. (2009). Antiviral activity of geneticin against dengue virus. *Antiviral Research, 83*(1), 21-27.

Zhao, P. S. a. H. (2010). The role of mass transport limitation and surface heterogeneity in the biophysical characterization of macromolecular binding processes by SPR biosensing. *Methods in Molecular Biology, 627*(2), 15-54.